LUND UNIVERSITY

Optical Diagnostics with Background Oriented Schlieren

A practical perspective on reactive and non-reactive flow scenarios

Çakir, Bora Orçun

2024

Document Version:
Publisher's PDF, also known as Version of record

Optical Diagnostics with Background Oriented Schlieren

A practical perspective on reactive and non-reactive flow scenarios

BORA O. CAKIR
DEPARTMENT OF ENERGY SCIENCES | FACULTY OF ENGINEERING | LUND UNIVERSITY

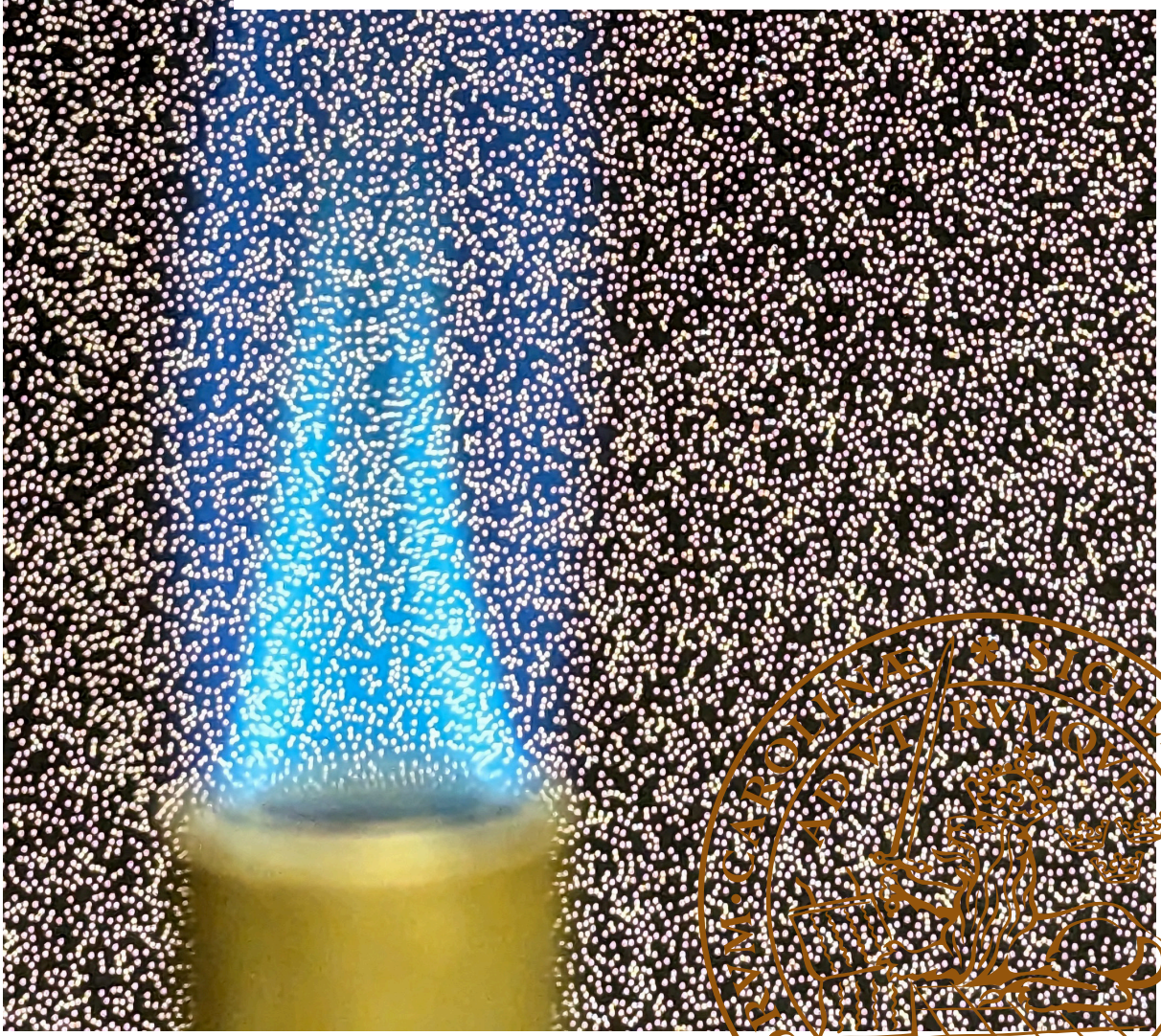

Optical Diagnostics with Background Oriented Schlieren

A practical perspective on reactive and non-reactive flow scenarios

Optical Diagnostics with Background Oriented Schlieren

A practical perspective on reactive and non-reactive flow scenarios

by Bora O. Cakir (ir.)

LUND
UNIVERSITY

Thesis for the degree of PhD
Thesis advisors: Prof. Christer Fureby, Prof. Mattias Richter,
Prof. Sergio Lavagnoli, Dr. Bayindir Saracoglu
Faculty opponent: Dr. Christopher J. Clifford

To be presented, with the permission of the Faculty of Engineering of Lund University, for public criticism at Room M:B, M-Husset (Ole Römers väg 1, Lund) on Friday, the 25th of October 2024 at 10:15.

Organization
LUND UNIVERSITY

Department of Energy Sciences
Box 124
SE–221 00 LUND
Sweden

Author(s)
Bora O. Cakir (ir.)

Document name
DOCTORAL DISSERTATION

Date of disputation
2024-10-25

Sponsoring organizationEU H2020 research and innovation programme, NATO Science for Peace and Security (SPS) programme and Competence cEntre in Sustainable Turbine fuels for Aviation and Power (CESTAP).

Title and subtitle
Optical Diagnostics with Background Oriented Schlieren:A practical perspective on reactive and non-reactive flow scenarios

Abstract
The oldest and without a doubt one of the most versatile non-intrusive measurement approaches is the schlieren imaging technique. Although they have been used over a century for visualization of flow fields, they are associated with certain drawbacks. In this regard, background oriented schlieren (BOS) provides a unique opportunity to quantitatively characterize density varying flows which has a major superiority of adaptability and scalability over a wide range of applications. However, traditionally BOS is referred to lack necessary sensitivity and resolution specifications to compete with classical schlieren. Beyond the many hardware developments that mitigate this weakness, it is shown the application of optical flow (OF) image processing technique can address these issues without altering the complexity level of the measurement setup. Accordingly, the enhanced capabilities of BOS using optical flow is characterized through experimental and numerical assessments. Although optical flow is shown to prevail over the conventional block-matching algorithms, the background patterns employed in BOS were still designed to suit the needs of the prior. Therefore, a dedicated parametric study is performed to unlock the full potential of optical flow, the resolution and sensitivity response of optical flow to different background configurations, in which guideline pattern generation parameters with respect to the flow field of interest are established.

Focusing on exploring the capabilities of BOS in challenging flow visualization applications, qualitative visualizations and quantitative characterizations of density varying features are performed via BOS. In this regard, thermodynamics of a heated swirling subsonic jet, passage and trailing edge flow topology in a turbine cascades, aeroacoustics of dual-stream co-axial supersonic jets, aerodynamics of supersonic objects, dynamics of shock wave transitional and turbulent boundary layer interactions at supersonic and hypersonic speeds are investigated by means of constructing custom BOS experimental setups that are compatible to the specifications and constraints of each facility. Transitioning to reactive flow applications, BOS is demonstrated as an alternative approach for flame visualization in a Bunsen burner and to perform laminar burning velocity measurements of methane/air mixtures. The capability of BOS in terms of providing relevant flow field information in combustion environments is extended to the temperature and heat release characterization of swirl stabilized premixed flames in a model gas turbine combustor.

Key words
optical diagnostics, schlieren, background oriented schlieren, supersonics, hypersonics, aeroacoustics, optical flow, turbomachinery, laminar burning velocity, swirl-stabilized flames

Classification system and/or index terms (if any)

Supplementary bibliographical information

Language
English

ISSN and key title
0282-1990
LUTMDN/TMHP-24/1177-SE

ISBN
978-91-8104-171-2 (print)
978-91-8104-172-9 (pdf)

Recipient's notes

Number of pages
215

Price

Security classification

Signature _____ Date 01.10.2024

Optical Diagnostics with Background Oriented Schlieren

A practical perspective on reactive and non-reactive flow scenarios

by Bora O. Cakir (ir.)

LUND
UNIVERSITY

A doctoral thesis at a university in Sweden takes either the form of a single, cohesive research study (monograph) or a summary of research papers (compilation thesis), which the doctoral student has written alone or together with one or several other author(s).

In the latter case the thesis consists of two parts. An introductory text puts the research work into context and summarizes the main points of the papers. Then, the research publications themselves are reproduced, together with a description of the individual contributions of the authors. The research papers may either have been already published or are manuscripts at various stages (in press, submitted, or in draft).

Cover illustration front: Tomographic BOS setup constructed for partially premixed flames.

Cover illustration back: BOS setup configured in the VKI-S1 wind tunnel.

Funding information: The thesis work was financially supported by the European Union's Horizon 2020 research and innovation programme, MORE & LESS (MDO and REgulations for Low-boom and Environmentally Sustainable Supersonic aviation) project under grant agreement No 101006856, NATO Science for Peace and Security (SPS) programme and the CESTAP (Competence cEntre in Sustainable Turbine fuels for Aviation and Power) supported by the Swedish Energy Agency, industry and academia in collaboration. Computer time was provided by the Swedish National Infrastructure for Computing (SNIC), partially funded by the Swedish Research Council.

Divisin of Heat Transfer
Department of Energy Sciences
Faculty of Engineering
Box 124
SE–221 00 LUND
Sweden

ISBN: 978-91-8104-171-2 (print)
ISBN: 978-91-8104-172-9 (pdf)
ISSN: 0282-1990
ISRN: LUTMDN/TMHP-24/1177-SE

Printed in Sweden by Media-Tryck, Lund University, Lund 2024

Dedicated to my grandparents and to a secure world in peace...

"Yurtta sulh, cihanda sulh."
"Peace at home, peace in the world"
"Fred i hemlandet, fred i världen"

20 April 1931
Mustafa Kemal Ataturk

Contents

Publications included in the thesis

This thesis is based on the following publications, referred to by their Roman numerals:

i **Assessment and Application of Optical Flow in Background-Oriented Schlieren for Compressible Flows**
B.O. Cakir, S. Lavagnoli, B. Saracoglu and C. Fureby
Experiments in Fluids, 2022, 124 (19)

ii **Sensitivity and Resolution Response of Optical Flow Based Background Oriented Schlieren to Speckle Patterns**
B.O. Cakir, S. Lavagnoli, B. Saracoglu and C. Fureby
Measurement Science and Technology, 2024, 35 (075201)

iii **Numerical and Experimental Investigations of Flow Features over a Wedge Exposed to Supersonic Flow at High Reynolds Numbers**
B.O. Cakir, G. Grossir, B. Saracoglu and C. Fureby
Physics of Fluids, 2024, 36 (7)

iv **Application and Assessment of Background Oriented Schlieren for Laminar Burning Velocity Measurements**
B.O. Cakir, D. Sanned, M. Prakash, C. Brackmann, M. Richter, C. Fureby
Under review in Experimental Thermal and Fluid Science

v **On the Application of Background Oriented Schlieren to a Transonic Low-Reynolds Turbine Cascade**
A. Halby, **B.O. Cakir**, L. Da Valle, G. Lopes, M. Okada, S. Lavagnoli
Proceedings of the ASME 2024 International Mechanical Engineering Congress and Exposition GT2024, 24-28 June, 2024, London, United Kingdom (Accepted for publication in ASME Journal of Turbomachinery)

vi **Investigation on Noise and Flow Characteristics of Supersonic Dual-Stream Co-Axial Convergent-Divergent Jets**
A. Zarri, J. De Decker, **B.O. Cakir**, A. Viladegut, G. Grossir, J. Christophe, C. Schram, M. Mancinelli
30th AIAA/CEAS Aeroacoustics Conference, June 4-7, 2024, Rome, Italy (Submitted to AIAA Journal)

Publications not included in the thesis

Journal articles

i **Surface Pressure Reconstruction from LPT Data with Boundary Conforming Grids**
B.O. Cakir, G. Gonzalez and A. Sciacchitano
Measurement Science and Technology, 2024, 35 125303

ii **Reduced Order Computational Methods for the Development of Propulsive Technologies for Supersonic Aviation to Achieve Climate Neutrality**
K. Van den Borre, A.C. Ispir, **B.O. Cakir**, B.H. Saracoglu
Advanced Computational Methods and Design for Greener Aviation. Computational Methods in Applied Sciences, 2024, 59, 95-107

iii **Design Space Investigations of Scramjet Engines Using Reduced-Order Modelling**
A.C. Ispir, **B.O. Cakir** and B. Saracoglu
Acta Astronica, 2024, 217, 349-362

iv **Dense Interpolations of LPT Data in The Presence of Generic Solid Objects**
B.O. Cakir, G. Gonzalez, A. Sciacchitano and B. van Oudheusden
Measurement Science and Technology, 2022, 33 124009

v **Reduced order design and investigation of intakes for high speed propulsion systems**
B.O. Cakir, A.C. Ispir and B. Saracoglu
Acta Astronica, 2022, 199, 259-276

Conference proceedings

i **Flame Dynamics of Sustainable Aviation Fuels in a Swirl-Stabilized Jet Engine Combustor**
B.O. Cakir, D. Sanned, M. Prakash, J.P. Hannappel, A. Subash, M. Richter and C. Fureby
AIAA SCITECH Forum, 6–10 January, 2025, Orlando FL, United States

ii **Large Eddy Simulation of a Model Jet Engine Swirl-Stabilized Flame using Sustainable Aviation Fuels**
P. Vauquelin, **B.O. Cakir**, D. Sanned, M. Prakash, J.P. Hannappel, A. Subash, M. Richter, X.S. Bai and C. Fureby
AIAA SCITECH Forum, 6–10 January, 2025, Orlando FL, United States

iii **Numerical and Experimental Investigations of Flow Dynamics in A Gas Turbine Swirl Combustor**
B.O. Cakir, P. Vauquelin, D. Sanned, M. Prakash, J.P. Hannappel, A. Subash, M. Richter, X.S. and Bai C. Fureby
36th Congress of the International Council of Aeronautical Sciences (ICAS), 9-13 September, 2024 Florence, Italy

iv **Aerodynmic Numerical/Experimental Comparison of a Hypersonic Test Vehicle in More&Less Program**
P. Roncioni, M. Marini, R. Fusaro, N. Viola, D. Pepelea, **B.O. Cakir**, M. Clay
36th Congress of the International Council of Aeronautical Sciences (ICAS), 9-13 September, 2024 Florence, Italy

v **Numerical Investigation on The Fuel Flexibility of a Typical Aero-Engine Swirl-Stabilized Flame**
P. Vauquelin, **B.O. Cakir**, D. Sanned, M. Prakash, J.P. Hannappel, A. Subash, M. Richter, X.S. Bai and C. Fureby
19th International Conference on Numerical Combustion (ICNC2024), May 7-10, 2024, Kyoto City, Japan

vi **Flow Characterization of The Mach 5 Hypersonic Nozzle of VKI-H3 Wind Tunnel**
A. Gyenge, **B.O. Cakir**, G. Grossir, B. Saracoglu and O. Chazot
AIAA SCITECH Forum, 8-12 January, 2024, Orlando FL, United States

xiv **Design Space Exploration for a Scramjet Engine by Using Data Mining and Low-Fidelity Design Techniques**
A.C. Ispir, **B.O. Cakir** and B. Saracoglu
HiSST: 2nd International Conference on High-Speed Vehicle Science & Technology, 12-14 September, 2022, Bruges, Belgium

xv **On the Design of a Mach 5 Axisymmetric Contoured Nozzle for The VKI H3 Hypersonic Tunnel**
B.O. Cakir, G. Grossir, S. Paris and B. Saracoglu
HiSST: 2nd International Conference on High-Speed Vehicle Science & Technology, 12-14 September, 2022, Bruges, Belgium

xvi **Low Fidelity Design and Analysis of Propulsion Systems for High-Supersonic Cruiser Concepts**
B.O. Cakir, S. Lavagnoli, B. Saracoglu and C. Fureby
HiSST: 2nd International Conference on High-Speed Vehicle Science & Technology, 12-14 September, 2022, Bruges, Belgium

xvii **Optical Flow Based Background Oriented Schlieren for Compressible Flows**
B.O. Cakir, S. Lavagnoli, B. Saracoglu and C. Fureby
20th International Symposium on Application of Laser and Imaging Techniques to Fluid Mechanics - LXLASER22, 11 - 14 July, 2022, Lisbon, Portugal

xviii **Dense Flow Field Interpolations from PTV Data in the Presence of Generic Solid Boundaries**
B.O. Cakir, G. Gonzalez, A. Sciacchitano and B. van Oudheusden
14th International Symposium on Particle Image Velocimetry, August 1-4, 2021, Chicago, IL

Acknowledgements

Looking back on this three-year journey to completing my thesis, it's difficult to encapsulate all the emotions and experiences in just a few paragraphs. As I write these words at my final conference as a doctoral candidate, two feelings stand out: pride and gratitude. I am proud not only of my achievements but also of the growth I've undergone—embracing failures, learning from mistakes, pushing beyond my comfort zone, and making decisions with conviction, fully owning their outcomes. When I first began my appointment at the von Karman Institute with an EU project proposal, my PhD topic was far from defined. After eight months of navigating the uncertainty of my research career, I officially began my journey at Lund University. What followed is my love letter to *Background Oriented Schlieren*.

This journey, however, was only possible thanks to the constant support of my family, friends, colleagues, and fellow researchers. Their encouragement has been endless and relentless, and for that, I am deeply grateful.

To my family, I can only express how proud I am to have been raised, nurtured, and educated by you. My gratitude for your unwavering support and the countless efforts you've made throughout my studies and research career grows exponentially every day. This thesis is as much a product of your dedication as it is of mine, and the least I can do is dedicate it to you. To my dearest girlfriend, I want to apologize for making you endure the dark side of my mood throughout these years. From the early days of ambiguity to these final moments, your determined patience and incredible kindness have never failed to amaze me. Every day, you remind me that genuine care and compassion still thrive in a world often consumed by greed and conflict, and for that, I am endlessly grateful.

I would like to express my deepest gratitude to my colleagues and friends at the von Karman Institute. To my office mates, with whom I shared more than just a workspace—your camaraderie and support have made this journey truly rewarding. To my colleagues with whom I spent countless hours testing, your dedication and perseverance have been a constant source of inspiration. I am especially grateful to the facility engineer, test engineers, technicians, and workshop operators, who never hesitated to accommodate my requests. To the senior researchers, it has been an honor to work alongside such accomplished mentors, and to the junior researchers, I am proud to call you my partners in this shared endeavor. A special thanks to all my friends, with whom I have shared a common passion, enthusiasm, and resilience. No symbol could better represent this legacy of over a century of innovation and research than a fine Belgian brew—a fitting testament to the spirit of von Karman that lives on through our collective efforts.

I would like to express my most sincere appreciation to my colleagues and friends at Lund University. To my colleagues at the Department of Energy Sciences: you are an incredibly welcoming and warm crew of researchers at every level of seniority. Your devotion to the endless philosophy of science, coupled with a true sense of companionship, has made my time here unforgettable. Your happiness and positivity are a constant source of inspiration, and I feel privileged to have been part of such a remarkable group. To my colleagues at the Division of Combustion Physics, my dear experimentalists – I owe you a special thanks for giving me the chance to breathe and escape the realm of computations. Senior researchers, your deep involvement with research is a standard that cannot be matched, and your limitless availability and guidance have been invaluable. To the members of our jet engine team, no matter how stressful and challenging our work became, the time we spent together was always a joy. Your commitment, energy, and camaraderie made even the toughest moments memorable. Thank you all for the support and companionship throughout this journey.

To my colleagues and friends in the More & Less project, the immense effort toward establishing a holistic framework for supersonic aviation is beyond measure—it cannot be quantified by hours, weeks, or even years. As an aerospace engineer, I am proud to have been part of this mission from the moment I accepted the role as a researcher on the project. Our consortium's achievements lay the groundwork for bringing faster-than-sound flight back to the skies. I am truly grateful to have met, worked alongside, and spent such meaningful time with you all across Europe. Every gathering, both professionally and socially, has been a joy.

Finally, to everyone I've met, connected with, collaborated with, and shared meals and drinks with along the way—research is driven by people, for people. A testament to this is the wonderful camaraderie and warmth of the research community, which I am proud to be a part of. Every project meeting, every conference was made remarkable by the kindness, generosity, and dedication of people at all levels of seniority. The willingness to engage in deep discussions and embrace collaboration is an invaluable lesson for everyone, both within and beyond the research world. In a world often marked by greed, secrecy, and conflict, sharing knowledge stands as a powerful reminder of how well-educated minds can not only solve complex problems in fluid dynamics but also address global challenges of peace and security with a spirit of connection and cooperation.

Thank you all, for your contributions not only to my thesis, but to the future of humankind.

Popular science summary

Observations of our environment, combined with an insatiable curiosity to understand it, has led to all the scientific discoveries mankind has ever made. Charles Darwin's theory of natural selection, Marie Curie's discovery of radioactivity, Sir Isaac Newton's formulation of the law of universal gravitation are examples of many. The way we understand the behavior of fluids is also through observations we make in nature, and the first observer to document a visual representation was Leonardo da Vinci. Yet while sketching the flow of water in rivers and vortices he had one advantage, the visual cues of the fluid behavior in water were visible to the eye. However, this is very rare in nature. Although we are aware that the wind is blowing, we cannot see it, we feel the heat from a blow-dryer but we cannot observe it. Nonetheless, when the flow we are interested in has variations of properties that would cause the refractivity to change, we might observe it if we now where and how to look since the optical effects are indeed embedded in nature. A distinctive feature of these optical effects is referred to as schlieren which a German word translates as "streaks" of optical inhomogeneities. We experience them every day in the form of heat gazes rising from a hot tarmac or on top of a candle flame. The reason we are able to observe these inhomogeneities is because we have a reference frame in the background so we can distinguish the changes.

The idea of having a reference frame to compare these inhomogeneities in presence of a flow field led to the discovery of a measurement technique called background oriented schlieren (BOS). The name "background-oriented" originates from the use of a pattern in the background of a refractive index variation over which the motion of optical features is traced. It is a relatively new version of schlieren imaging which is one of the oldest measurement techniques ($\sim$160 years). Regardless of age, it has proven itself to be the most versatile and popular optical measurement tool due to its simplicity and non-intrusiveness. However, schlieren has certain disadvantages in terms of cost and complexity, making BOS the superior choice. This led to the ever increasing trend of advancements in BOS. Yet with each advancement, the complexity of the measurement technique is increased while reducing adaptability and increasing cost.

This thesis work takes a few steps back to identify and investigate the constraints of BOS which drives the need for scientists to improve the hardware. It addresses software elements to alleviate these constraints to the extent that it does not alter the basic complexity, prioritizing high adaptability. To do this, an image processing technique referred to as "optical flow" is employed. This approach utilizes the differences in images with and without the flow fields of interest to identify the flow (i.e., the motion) of features in the background patterns. The motion of these features then enable

the characterization of the intensity and orientation of the density varying flow structures within the field of view. Accordingly, the background patterns play a crucial role to identify the displacements with high resolution and sensitivity. Hence, they are optimized through a parametric study composed of numerical and experimental assessments for maximum quality output from the measurement technique.

The high flexibility and adaptability of BOS is utilized to test the simplest form of the hardware configuration to make measurements possible in almost every flow regime. The scalability of the technique allows both small and large scale applications. The explored capability of the image processing tools enabled competition with more complicated and expensive setups. The wide range of applications explored provides a vast spectrum of practical considerations creating a large knowledge base for both industrial and scientific applications. The applications documented in the thesis take on flow characterization for societal challenges of clean and sustainable aviation. Accordingly, measurements of key flow phenomena that determine jet noise specifications, sustainable aviation fuel characteristics, propulsion system performance and future high-speed civil aviation platforms are made. The range of computational and experimental assessments are conducted to evaluate the capabilities of the measurement technique and the associated image processing algorithms. Additionally, a database of recommended practices is composed for each flow scenario. The know-how generated in this thesis is developed into a course of flow visualizations under the title of "making the invisible visible", portraying the power of flow visualization to the next generation of aerospace researchers. So that BOS; a low-cost, highly adaptable, scalable and accessible measurement technique and the developed knowledge base can visualize the currently invisible carbon-free and sustainable future of aviation.

Populärvetenskaplig sammanfattning på svenska

Observationer av vår miljö, kombinerat med en omättlig nyfikenhet att förstå den, har lett till alla vetenskapliga upptäckter mänskligheten någonsin har gjort. Charles Darwins teori om naturligt urval, Marie Curies upptäckt av radioaktivitet, Sir Isaac Newtons formulering av lagen om universell gravitation är exempel på många. Sättet vi förstår vätskors beteende är också genom observationer vi gör i naturen och den första observatören som dokumenterade en visuell representation var Leonardo da Vinci. Genom att skissa flödet av vatten i floder och virvlar hade han en fördel, de visuella ledtrådarna av vätskans beteende i vatten var synliga för ögat. Detta är dock mycket sällsynt i naturen. Även om vi är medvetna om att vinden blåser, kan vi inte se den, vi känner värmen från en hårtork men vi kan inte observera den. Ändå, när flödet vi är intresserade av har variationer i egenskaper som skulle orsaka att brytningsindex förändras, kan vi observera det om vi vet var och hur vi ska titta eftersom de optiska effekterna verkligen är inbäddade i naturen. En särskiljande egenskap hos dessa optiska effekter kallas schlieren vilket är ett tyskt ord som översätts till ”strimmor” av optiska inhomogeniteter. Vi upplever dem varje dag i form av värmeskimrande luften som stiger från en het asfalt eller ovanpå en ljuslåga. Anledningen till att vi kan observera dessa inhomogeniteter är att vi har en referensram i bakgrunden där vi kan urskilja förändringarna.

Idén att ha en referensram för att jämföra dessa inhomogeniteter i närvaro av ett flödesfält leder till upptäckten av en mätteknik kallad Background Oriented Schlieren (BOS). Namnet ”background-oriented” kommer från användningen av ett mönster i bakgrunden av en variation i brytningsindex över vilket rörelsen av optiska funktioner spåras. Det är en relativt ny version av schlieren-avbildning som är en av de äldsta mätteknikerna (cirka 160 år). Oavsett ålder har den visat sig vara det mest mångsidiga och populära optiska mätverktyget på grund av sin enkelhet och icke-intrusivitet. Men schlieren har vissa nackdelar när det gäller kostnad och komplexitet, vilket gör BOS till det överlägsna valet. Detta ledde till en ständigt ökande trend av framsteg inom BOS. Men med varje framsteg ökade tekniken i komplexitet, vilket också var förknippat med ökande kostnader och minskad anpassningsförmåga.

Detta avhandlingsarbete tar några steg tillbaka för att identifiera och undersöka begränsningarna av BOS som driver behovet av att förbättra hårdvaran. Det tar upp mjukvaruelement för att lindra dessa begränsningar till den grad att det inte förändrar den grundläggande komplexiteten, med prioritet på hög anpassningsförmåga. För att göra detta används en bildbehandlingsteknik kallad ”optisk flöde”. Denna metod använder skillnaderna i bilder med och utan de flödesfält av intresse för att identifiera flödet (d.v.s. rörelsen) av funktioner i bakgrundsmönstren. Rörelsen av dessa funktioner möjliggör sedan karakterisering av intensiteten och orienteringen av de täthetsva-

rierande flödesfunktionerna inom synfältet. Bakgrundsmönstren spelar en avgörande roll för att identifiera förskjutningarna med hög upplösning och känslighet. Därför genomförs en studie både beräkningsmässigt och experimentellt för att optimera bakgrundsmönstren för maximal kvalitetsutgång från mättekniken.

Den höga flexibiliteten och anpassningsförmågan hos BOS används för att testa den enklaste formen av hårdvarukonfiguration för att göra mätningar möjliga i nästan alla flödesregimer. Teknikens skalbarhet möjliggör både små och stora applikationer. Den utforskade kapaciteten hos bildbehandlingsverktygen möjliggjorde konkurrens med mycket mer komplicerade och dyra uppsättningar. Det breda utbudet av utforskade tillämpningar ger ett stort spektrum av praktiska överväganden och skapar en stor kunskapsbas för både industriella och vetenskapliga tillämpningar. De tillämpningar som dokumenteras i avhandlingen tar upp flödeskarakterisering för samhällsutmaningar med ren och hållbar flygning. Följaktligen utförs mätningar av nyckelflödesfenomen som bestämmer jetbullerspecifikationer, hållbara flygbränslekvaliteter, prestanda för framdrivningssystem och framtida höghastighets civilflygplattformar. Ett antal beräkningsmässiga och experimentella bedömningar genomförs för att utvärdera kapaciteten hos mättekniken och de tillhörande bildbehandlingsalgoritmerna. Dessutom sammanställs en databas med rekommenderade metoder för varje flödesscenario. Den know-how som genereras i denna avhandling utvecklas till en kurs om flödesvisualiseringar under titeln ”att göra det osynliga synligt”, som skildrar kraften hos flödesvisualisering för nästa generation av flygforskare. BOS; en lågkostnad, mycket anpassningsbar, skalbar och tillgänglig mätteknik och den utvecklade kunskapsbasen kommer att visualisera den för närvarande osynliga avkolade och hållbara framtiden för flyg.

Optical Diagnostics with Background Oriented Schlieren
A practical perspective on reactive and non-reactive flow scenarios

Chapter 1

Introduction

The field of aerospace engineering is deeply intertwined with the study of complex fluid dynamics, which plays a critical role in the design, performance, and safety of both aircraft and spacecraft. Fluid dynamics, particularly in the context of aerodynamics and propulsion, involves the behavior of air and other gases as they flow over surfaces, through engines, and around structures at varying speeds and conditions. The challenges presented by these flows are numerous and multifaceted, encompassing a range of phenomena such as turbulence, heat transfer, compressiblity and combustion. Hence, the application of fluid dynamics extends beyond non-reactive flow scenarios in the case of propulsion systems, high-speed flight regimes and atmospheric emissions where the interaction between flow physics and chemistry becomes a key factor dominating the design and integration specifications for aerospace platforms.

Figure 1.1: Flow phenomena observed in aerospace platforms: boundary layer development over the fuselage of A320 airliner (Ghate et al., 2022), wing tip vortices of AT-802A agriculture aircraft (Gallagher, 1992), F22 fighter jet executes a transonic flyby (Dejarnett, 2009), Apollo command module re-entry to Earth atmosphere (Rockwell, 1968), GE F110 turbofan jet engine with afterburner operation (Cole, 2004), F1 rocket engine (NASA, 2000).

Comprehensive understanding of flow physics related phenomena has led to the development of multiple numerical and experimental tools to serve as a powerful arsenal for researchers. As the elevated complexity of problems is associated with an immense demand on resolution, more powerful measurement systems and computational resources are required. In this regard, simplifications with appropriate assumptions are needed to achieve the optimum trade-off between fidelity and computational cost without forfeiting accuracy. Hence, the need for comparative studies between experimental and numerical analysis is further emphasized to ensure the accurate representation of flow physics which makes verification and validation a long lasting need. Therefore, the complexity of fluid dynamics in aerospace applications necessitates a comprehensive approach that integrates theoretical analysis, computational modeling, and experimental validation. Mastery of these elements is essential for advancing aerospace technology and achieving superior performance, safety, and efficiency in modern and future flying vehicles.

1.1 Optical measurement techniques

In order to achieve experimental flow field information without altering the flow behaviour, qualitative and quantitative non-intrusive measurement techniques received a huge interest. They enable direct comparisons between numerical and experimental datasets, whereas intrusive techniques involve multiple stages of theoretical, numerical or empirical corrections to be applied for the rebuilding of flow properties (Allen, 1972; Ninnemann and Ng, 1992; Cutler and Johnson, 1997; Magre et al., 2001). On the other hand, non-intrusive flow measurement techniques utilize advanced image acquisition systems, various forms of coherent and incoherent light sources and optical components to measure and visualize fluid flow phenomena, enabling researchers and engineers to capture detailed information about velocity fields, turbulence structures, and scalar distributions in both experimental and real-world environments.

A large variety of flow properties can be obtained by means of optical techniques. Approaches such as Particle Image Velocimetry (PIV)(Adrian and Westerweel, 2011) and Laser Doppler Anemometry (LDA)(Abbiss et al., 1974) can provide global and point wise velocity information by means of seeding the flow and tracing the particles via optical imaging and frequency shift detection respectively. Surface flow visualizations via oil flow (Lu, 2010), sublimation (Goldstein and Cho, 1995), temperature and pressure sensitive paints (Liu et al., 2005), and IR imaging (Carlomagno et al., 1998) provide essential information regarding the interaction of the flow field surrounding objects for identification of critical phenomena such as separation, boundary layer transition, fluid-structure interaction, and ablation. Flow temperature and species composition information can be acquired locally and globally using Coherent Anti-

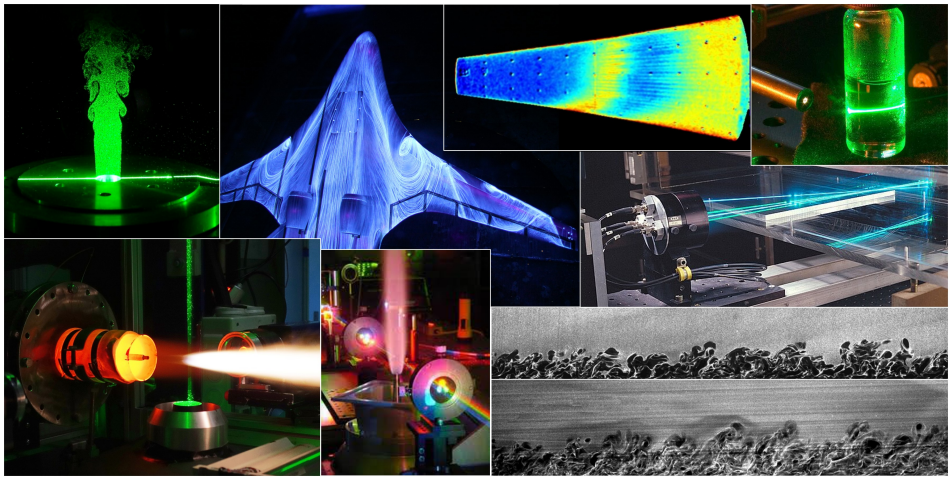

Figure 1.2: Optical measurement techniques: particle image velocimetry on a free jet (Puttinger, 2009) and a microwave plasma heater (RSM, 2023), florescent oil flow visualization of a flying V model (Martin, 2011), Coherent Anti-Stokes Scattering measurements in BOXCARS configuration (Farquharson, 2017), temperature sensitive paint on a flared cone (Sivasubramanian and Fasel, 2016), laser induced fluorescence, laser Doppler anomometry for underwater velocity measurements (NASA, 1992), Rayleigh scattering measurements on hypersonic boundary layer transition (Wang et al., 2019).

Stokes Raman Scattering (CARS) (Begley et al., 1974) and Rayleigh Scattering (Miles et al., 2001) based of inelastic and elastic scattering of light from molecules or small particles. Chemiluminescence (Dec and Espey, 1998) and Laser-Induced Fluorescence (LIF) (Paul and Najm, 1998) can be utilized to obtain heat release, concentration, and density information over a volume or 2D plane which is especially useful in combustion research, environmental monitoring, and mixing studies, where understanding the distribution and interaction of different species is crucial.

1.2 Schlieren Imaging

Schlieren and shadowgraph are powerful optical techniques used extensively in fluid dynamics to visualize and analyze flow phenomena involving variations in fluid density (Settles, 2001). These methods exploit the refractive index changes caused by density gradients in transparent media, enabling the observation of otherwise invisible features like shock waves, thermal plumes, and boundary layers. The non-intrusive nature and high sensitivity of schlieren and shadowgraph imaging make them indispensable tools in both fundamental research and applied engineering. A typical setup consists of a collimated light source, the schlieren object, a knife-edge, and a camera. As light passes through the fluid, it is refracted differently in regions with varying density, causing deviations from its original path. These deviations are captured by

a camera after interacting with a knife-edge which creates the contrast image that highlights areas of density change.

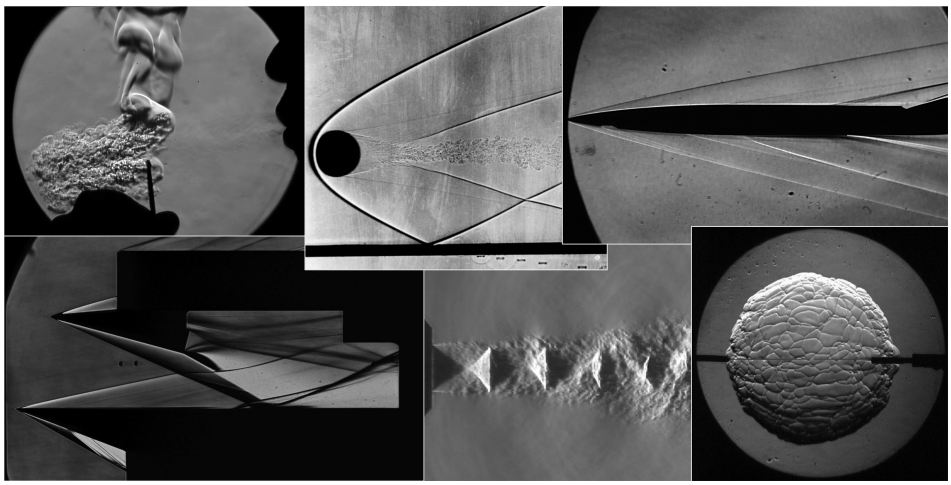

Figure 1.3: Various flow phenomena visualized by schlieren imaging: natural convection over a candle flame (Gorman, 2015), supersonic flow past cylinder (Van Dyke, 1982), hypersonic shock wave boundary layer interaction (Daub et al., 2022), underexpanded supersonic jet flow (Willert et al., 2012), hypersonic cruiser at flight conditions, spherical hydrogen/air flame (Bangalore et al., 2013).

Schlieren methods are extensively used to study shock waves generated by supersonic and hypersonic objects. They allow researchers to observe the formation, propagation, and interaction of shock waves with various surfaces and boundaries. Moreover, they can visualize the development and behavior of boundary layers on aerodynamic surfaces (Laurence et al., 2016), providing insights into drag reduction (Sridhar et al., 2015) and flow control strategies (Lapushkina and Erofeev, 2017). These techniques are used to investigate thermal plumes and convection currents in heat transfer experiments (Tanda and Devia, 1998), offering valuable data on temperature distribution and heat flux (Tanda et al., 2014). Furthermore, in combustion studies, schlieren and shadowgraph imaging help visualize flame fronts (Brequigny et al., 2018), combustion instabilities (Keller et al., 1982), and the mixing of fuel and oxidizer (Gutmark et al., 1991), which are critical for optimizing combustion efficiency and reducing emissions.

Despite their usefulness, schlieren techniques come with certain limitations. First of all, almost all the schlieren setups employed for the characterization of high-speed flows are utilized for qualitative visualizations of the flow features, and although they indicate the presence of key components in the flow, they do not provide any quantitative information regarding their respective intensities. Moreover, although a standard schlieren setup is rather inexpensive, they require proper optical access, and depending on the size considerably large lenses or mirrors. Even though a light-based schlieren setup can be calibrated to quantify the observed density gradients (either by grayscale

or color filters (Hargather and Settles, 2012)), illumination changes and/or setup vibrations (likely to happen in the surrounding environment of high-speed facilities) would yield deviations from the reference calibration data and lead to a misinterpretation of the acquired images.

1.3 Background oriented schlieren

Background oriented schlieren (BOS) is a relatively newer derivative of the light ray based schlieren technique also used to visualize and quantify refractive index changes in transparent media. BOS offers several advantages over traditional schlieren techniques, making it a preferred method for many fluid dynamics and aerodynamics applications. These advantages stem from its simplicity, flexibility, and ability to capture quantitative data with high spatial resolution. BOS requires only a camera, a background pattern, and appropriate lighting, whereas traditional schlieren systems involve complex arrangements of lenses, mirrors, and knife edges. This simplicity reduces the time and expertise needed for setup. The absence of expensive optical components like parabolic mirrors and precision alignment equipment makes BOS a more affordable option for many laboratories and field studies. BOS can be used for a wide range of scales, from small laboratory setups to large atmospheric studies. This versatility allows researchers to apply BOS to a diverse array of experiments without significant modifications to the setup. Due to its minimal optical requirements, BOS can be easily deployed in field conditions.

BOS can capture large areas in a single image, providing a more comprehensive view of the flow field. Traditional schlieren techniques, with their focused light paths, are limited in the size of the observable area. The ability to cover larger areas allows for full-field quantitative measurements, which are crucial for analyzing complex flow phenomena over extensive regions (Hargather, 2013; Raffel, 2014; Trolinger et al., 2015). BOS utilizes digital image processing techniques to calculate background pattern displacements (Meier, 2002), enabling precise quantitative analysis of density gradients and refractive index changes. Advances in digital camera technology and image processing algorithms have significantly improved the spatial resolution of BOS (Atcheson et al., 2008; Cozzi and Göttlich, 2019; Liu et al., 2024), allowing for detailed and accurate measurements. BOS systems are less sensitive to mechanical vibrations and environmental disturbances compared to traditional schlieren setups (Xiong et al., 2020), which rely on precise optical alignments. This robustness enhances the reliability and repeatability of experiments. The quantitative data obtained from BOS can be effectively used to validate and verify Computational Fluid Dynamics (CFD) simulations, providing a powerful tool for combined experimental and computational studies (Sourgen et al., 2004; Ramanah et al., 2007; Wang et al.,

2019). Moreover, since BOS does not require any calibration to be performed, it allows accurate processing of the acquired images even in presence of mild vibrations, provided that a high-quality reference image is present. In consideration of the more recent developments, the need for a reference image can be removed (Gardner et al., 2020; Weisberger and Bathel, 2022) with digital variations on the backgrounds enabling corrections for various sources of bias and random errors (Reichenzer et al., 2021).

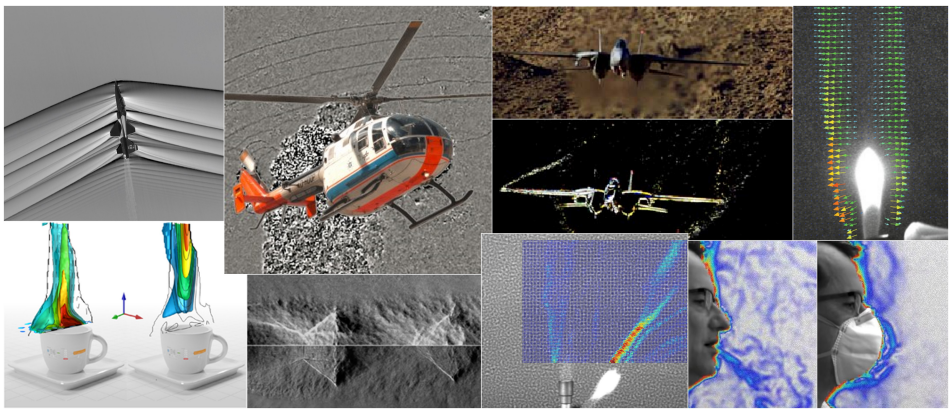

Figure 1.4: Various applications of background oriented schlieren: compressible flow structure around a T-38 fighter jet in supersonic flight (Heineck et al., 2021), blade tip vortices from a helicopter (Bauknecht et al., 2014), wing tip vortices of a F14 tomcat (Raffel et al., 2012), natural convection over a coffee cup (Cai et al., 2021), underexpanded supersonic jet flow (Nicolas et al., 2016), turbulent partially premixed flames (Klemkowsky et al., 2017), plume of a candle flame (Meier and Roesgen, 2013), respiratory measurement for medical mask requirements (LaVision, 2020).

Applications of BOS span a broad spectrum of fluid dynamics research and engineering. BOS is used to visualize shock waves (Sommersel et al., 2008; Fisher et al., 2019; Heineck et al., 2021), boundary layers (Zhu et al., 2022), and flow separation on aerodynamic surfaces (Stadler et al., 2017), aiding in the design and optimization of aircraft and spacecraft. In combustion research, BOS helps visualize flame fronts (Choudhury and Joarder, 2022) and fuel-air mixing (Weilenmann et al., 2018) contributing to the development of more efficient and cleaner combustion systems. BOS is applied to study natural convection (Becher et al., 2020), thermal plumes (Sasono et al., 2023) as well as heating and ventilation flows (Hargather et al., 2011), providing insights into climate conditioning systems. In medical research, BOS can be used to visualize airflow in respiratory studies (Howard et al., 2023) and analyze fluid dynamics phenomena in medical devices (Koponen et al., 2023). BOS is utilized in various industrial processes to monitor and optimize fluid flow in systems such as heat exchangers (Vinnichenko et al., 2014), reactors (Ollegott et al., 2023), and leak detection (Boudreaux et al., 2022; Sun et al., 2023). Recent advancements in high-speed imaging and computational power have further enhanced the capabilities of BOS. High-speed cameras enable capturing transient and dynamic flow events with high

temporal resolution (Ota et al., 2017), while powerful computational tools facilitate real-time image processing and analysis (Wernet, 2019).

1.4 Outlook

This thesis concentrates on the applications and assessment of BOS measurements and associated image processing tools for qualitative and quantitative characterization of density varying flow features in multiple scenarios of non-reactive and reactive flows. The biggest advantage of proving the capabilities of BOS is to showcase a technique which has a major superiority of adaptability and scalability. It does not require complex optical components such as mirrors and knife edges, making the setup simpler and more adaptable to different experimental configurations. This flexibility is particularly beneficial for large-scale or field experiments where traditional setups would be impractical. However, traditionally BOS is associated with major sensitivity and resolution issues which originate from both optical and image processing concerns. Hence, first the theoretical background of BOS and the associated optical restrictions are provided in Chap. 2. Although the problem of inferior sensitivity and resolution can be addressed through the application of different image processing techniques, there is a lack of quantification of their abilities and limitations. Thus, the image processing approaches employed for BOS and corresponding background pattern configurations are detailed. Chap. 3 presents the experimental setups used to evaluate the proposed measurement technique developments and their application to a wide variety of flow fields. A summary of the results acquired from the experimental setups to identify the key aspects of successful BOS measurements in each flow scenario and possible improvements to sensitivity and resolution in absence of complex hardware modifications is reported in Chap. 4. Finally, an overview of the entire research activity and the concluding remarks are established in Chap. 5.

Chapter 2

Background oriented schlieren

Optical visualization techniques for refractive index variations have been extensively used for characterization of non-reactive and reactive flows over many decades. The sensitivity of these methods to refractive index variations (i.e. schlieren, shadowgraphy or interferometry), enable flow property changes such as density, concentration, temperature to be recorded. A relatively newer addition to this family is a technique referred to as the background oriented schlieren which is similar to the human observation of heat haze (mirage)(Fig. 2.1), where local density gradients between the human observer and a distant object distort or even mirror the perceived image. Thus, the name "background-oriented" originates from the use of a pattern in the background of a refractive index variation over which the motion of optical features is traced. The resultant information provides a synthetic schlieren image which is originally obtained as a direct light impingement to a photo detector.

Figure 2.1: Photos of naturally observed heat gaze or mirage (Harrison, 2008; Schaeffer, 2020; Larbalestier, 2022).

2.1 Theoretical background

The BOS technique is based on the relation between the refractive index of a fluid and its density, given by the Lorentz–Lorenz equation, which can be simplified to the Gladstone–Dale equation provided in Eq. 2.1 (Gladstone and Dale, 1863).

$$n = 1 + K\rho \tag{2.1}$$

Here K refers to the Gladstone-Dale constant which has a weak dependency on the wavelength of light utilized to illuminate the background and for air it is K_{air}=0.223×10^{-3} m^3/kg.

$$\varepsilon_{x,y} = \int_S \nabla n ds \tag{2.2}$$

Then the deflection of a single beam contains information about the spatial gradient of the refractive index integrated along the line of sight according to Eq. 2.2 which is an extension of the Snell's law that follows Fermat's principle of light wave propagation (Born et al., 1999).

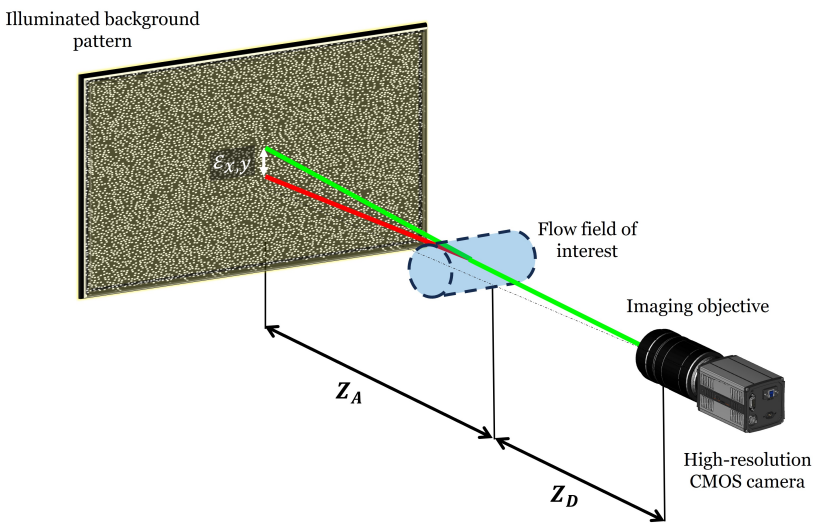

Figure 2.2: Background oriented schlieren (BOS) imaging configuration. The green beam illustrates the original path of the light ray while the red beam is the refracted path.

This deflection is captured by comparing the images recorded with air at rest and exposure through the flow under investigation. The resulting images of both exposures

can then be evaluated by image processing methods. Accordingly, a typical BOS setup is comprised of a camera, a background pattern and a light source that is used to illuminate the background pattern (Fig. 2.2). The background and the camera are placed on opposite sides of the flow field of interest such that the pattern is displaced optically from the perspective of the camera due to the varying refractive index through the flow field.

$$\Delta_s = \frac{M}{M+1}\frac{Z_D}{f_\#} + \frac{d_d}{M}\left(1 - \frac{Z_D}{Z_A + Z_D}\right) \tag{2.3}$$

BOS is associated with a major sensitivity limitation originating from an inherent focusing problem (Raffel, 2015). Considering a generic optical configuration for a BOS setup, increasing the sensitivity demands an amplification of the distance between the object and the background (Z_A), while minimizing the distance between the object and the camera (Z_B). However this is constrained due to two main reasons. First, having the camera close to the object causes divergence of the light rays to dominate the measured displacements related to the refractive index variations within the test section which requires corrections and calibration (Elsinga et al., 2004). Secondly, since the background needs to be in focus to accurately measure the displacements, the object and the associated flow features of interest remain out of focus. Hence, increasing the distance between the background and the flow field amplifies the geometric blur. In combination with the diffraction limited minimum image diameter, it reduces the sensitivity and the physical resolution of the system, severely affecting the accuracy of the measurements (Gojani et al., 2013).

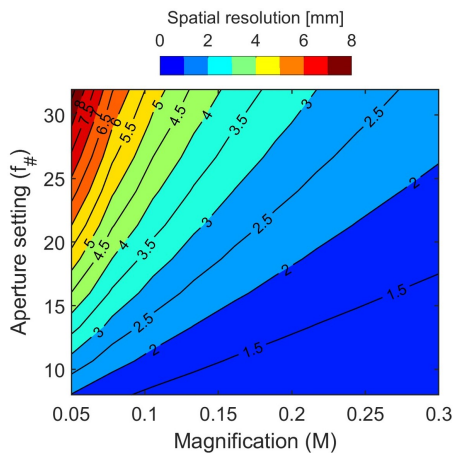

Figure 2.3: Spatial resolution of a background oriented schlieren (BOS) setup for varying magnification and aperture settings computed using Eq.2.3.

An inevitable trade-off exists between the sensitivity and resolution from an optical

stand point. These experimentally verified theoretical predictions are valid regardless of the image processing method of choice since they are associated with the optics instead of the mathematics of image processing algorithms. Accordingly, the spatial resolution (Δ_s) of a BOS setup that can be described via Eqn. 2.3. Here, d_d refers to the diffraction limited minimum image diameter which is the circle of minimum confusion. Utilizing Eqn. 2.3, the resolution limits for the BOS setups with varying optical settings can be computed (Fig. 2.3).

2.2 Background generation

The effectiveness of background oriented schlieren (BOS) relies heavily on the choice of background pattern, as it directly impacts the quality and resolution of the data obtained. Various types of background patterns are used in BOS, each suited for specific applications and experimental conditions. Regardless of the type of pattern used, certain characteristics are essential for the background to be effective in BOS. The pattern must have sufficient contrast to be easily distinguishable in the captured images, ensuring accurate displacement measurement. The pattern should contain a broad range of spatial frequencies to allow for detailed correlation across different scales of displacement. Each small region of the pattern should be unique to prevent ambiguity during the image correlation process. The background must remain stable and unchanged throughout the experiment to avoid introducing errors in displacement measurements.

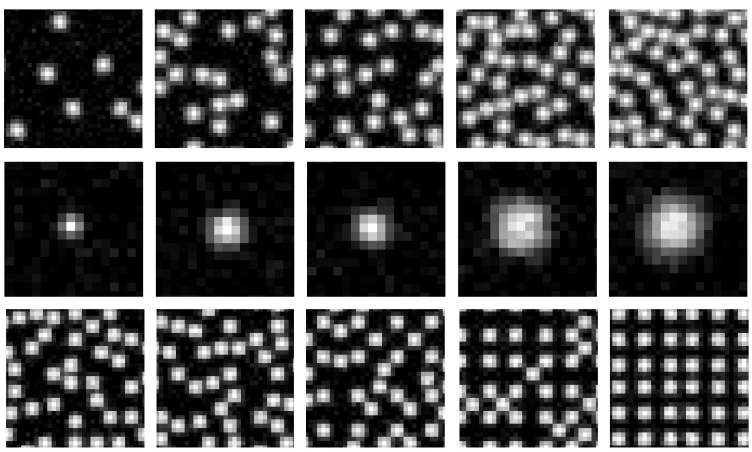

Figure 2.4: Random dot backgrounds generated with varying features of dot concentrations (1st row), dot size (2nd row) and dot distribution randomness ratio (3rd row).

The conventional background patterns in BOS are adjusted to suit the needs of the cross-correlation approach, have a high SNR in correlation maps, which yields random dot patterns based on the optical configuration of the measurement system. Four main image generation parameters can be identified; the dot size (d_P), dot concentration (N_I), interparticle size (Δ_P) and randomness of dot distribution (RR)(Fig. 2.4). Accordingly, an appropriate combinations of these is necessary to maximize contrast, minimize peak-locking and maximize subpixel interpolation accuracy (Adrian and Westerweel, 2011). However, in consideration of the overall uniformity of dot distributions over the entire image plane, the interparticle distance should be maximized for each d_P and N_I combination to prevent empty spots over the background patterns. Hence, the independently controlled number of parameters is reduced to three, eliminating Δ_P.

Alternative to dot patterns, artificial textures, such as noise patterns or computer-generated graphics, can be designed to meet specific experimental requirements. These textures can be optimized for contrast, frequency content, and spatial distribution. In line with the sequential downsampling of images following a coarse-to-fine resolution layout, multi-scale procedural noise patterns can be used as the background image. Thus, the short comings of random noise functions can be avoided which often requires a match between the camera resolution and the background pattern for optimum performance (Yang et al., 2014).

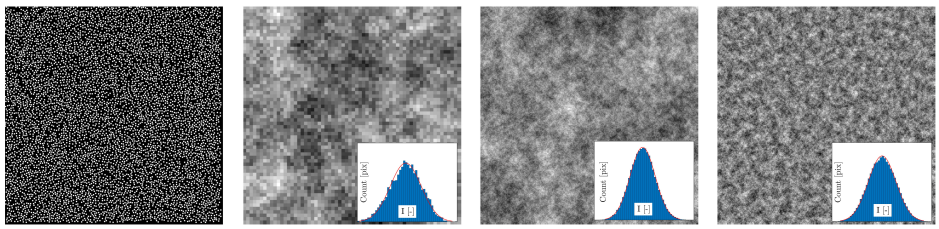

Figure 2.5: Background patterns with random dots (left) and wavelet noise (n_I,n_F)=(2,5)(mid-left), (n_I,n_F)=(2,8) (mid-right) and (n_I,n_F)=(5,8) (right) provided with the corresponding normalized image intensity histograms.

In this regard, the wavelet noise (WN) pattern proposed by Cook and DeRose (2005) is commonly utilized in BOS to construct a background image to capture both large and small scale structures with high accuracy (Atcheson et al., 2008; Bichal and Thurow, 2013; Beermann et al., 2017; Klemkowsky et al., 2017). The content stored within these WN patterns is controlled by means of two parameters, 2^{n_I} (initial resolution) and 2^{n_F} (final resolution). The lower spatial frequency content is modulated by the lower resolution levels where large scale displacements are resolved. This also acts as an anti-aliasing filter when the hierarchical approaches of the OF downsamples the high-resolution image to a lower resolution by preserving orthogonality. Combined

with the high frequency content governed by the final resolution specification, each resolution level of noise represents a bandwidth limited procedural texture that can be tailored to the specific spatial resolution needs of the experimental setup (Fig. 2.5).

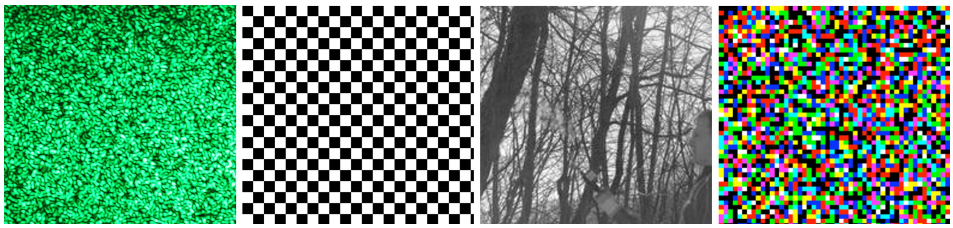

Figure 2.6: Various background patterns utilized in BOS setups: laser speckles (Meier and Roesgen, 2013), checkered pattern (Shimazaki et al., 2022), natural vegetation (Hargather and Settles, 2010) and colored pattern (Ota et al., 2012).

Other background patterns can also be utilized in BOS Fig. 2.6. An alternative is gridded patterns which are composed of regular arrays of intersecting lines, forming a checkerboard-like structure. The uniformity of the grid allows for straightforward displacement measurement. Grid patterns are particularly useful when there is a need for uniform and easily interpretable data (Shimazaki et al., 2022). In some cases, naturally occurring backgrounds, such as foliage, gravel, or textured surfaces, are used as the reference pattern. These backgrounds can provide sufficient contrast and complexity for BOS analysis. Natural backgrounds are particularly advantageous in field studies or outdoor experiments where artificial patterns may be impractical to deploy (Hargather and Settles, 2010). Speckle patterns are similar to random dot patterns but are typically generated using coherent light sources, such as lasers, to create a granular appearance. The speckle pattern's high spatial frequency content makes it highly sensitive to small displacements. Speckle patterns are ideal for high-resolution measurements in small-scale experiments, such as those involving microfluidics or detailed flow structures (Meier and Roesgen, 2013). Moreover, the commonly used monochromatic backgrounds can be replaced by a color coded pattern. The separate treatment of each color channel with various configurations of image processing algorithms allow increased accuracy and spatial resolution (Sourgen et al., 2012).

2.3 Optical imaging

In addition to the background generation parameters, another two important features influencing the imaged intensity patterns are the magnification factor of the optical setup and the utilized aperture setting on the objective. With regard to the latter, whilst the distance Z_D has no influence in terms of varying the imaged intensity distributions over the backgrounds, the change of $f_\#$ modifies the peak and range of

illumination intensities captured surrounding the speckles. Referring to these influences, the geometric blur on the schlieren objects is defined via Eqn. 2.4.

$$d_i = d_A \left[1 - \frac{1}{f} M'(Z_A - f)) \right] \tag{2.4}$$

where the M' refers to the magnification of the schlieren object on the image plane ($M' = Z_i'/Z_A$), f and d_A are the focal length and the aperture diameter respectively. Although, this is not an effective factor on the imaging of the background features, the defocus on the schlieren object and the influence of aperture on the imaged background patterns (which is described through the diffraction limited minimum image diameter d_d using Eqn.2.5) cannot be isolated.

$$d_d = 2.44 f_{\#} (M + 1) \lambda \tag{2.5}$$

in which λ corresponds to the wavelength of the light source which in most BOS applications is in the range of 450< λ <550 nm. Based on the Eqn.??, it is observed that M also influences the diffraction limited diameter of the imaged speckles. However, practical applications of BOS, especially ones where the flow features of interest require a field of view (FOV) significantly larger than the sensor size of the cameras, M has a value in the order of $O(10^{-1})$, hence the contribution of M to d_d is rather insignificant compared to $f_{\#}$ (Fig. 2.7).

$$d_i = \sqrt{(M d_P)^2 + d_d^2} \tag{2.6}$$

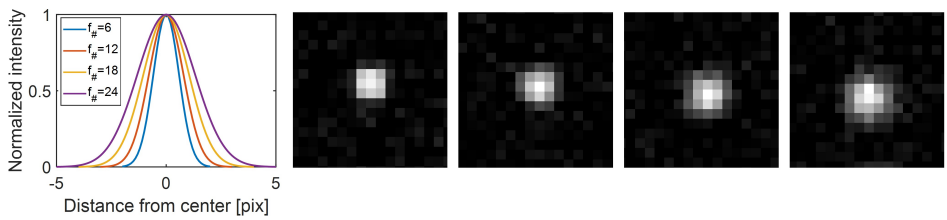

Figure 2.7: The influence of varying aperture on the normalized illumination intensities of diffraction-limited imaging of speckles (1st column). Corresponding images of speckles with $f_{\#}$=6, $f_{\#}$=12, $f_{\#}$=18 and $f_{\#}$=24 (2nd to 5th columns).

2.4 Image processing

The sensitivity and resolution of a BOS system is also governed by the image processing approach utilized to characterize the deviations of the light rays from their original paths. Hence, selecting an appropriate image processing tool that is in agreement with the specific requirements of the physical phenomena of interest and the BOS setup configured plays a critical role in determining the capabilities and limitations of the measurement campaign.

2.4.1 Cross-correlation

The most common method employed for this purpose is the cross-correlation based block matching algorithm (Fig. 2.8, left) developed for particle image velocimetry (Westerweel, 1997). The underlying theory of cross-correlation is computing a measure of similarity of two intensity maps as a function of displacement with respect to the original position of the selected blocks of pixels referred to as interrogation windows (IW) (Loeb et al., 1983). Visually, the correlation concept can be shown using Fig. 2.8 (left). To obtain a quantitative two-dimensional vector field from such images, BOS images must be systematically interrogated. To do so, these recorded images are sampled using IWs, the dimensions of which determine the spatial resolution of the measurement. The IWs can be adjacent to each other, or more commonly, have partial overlap with their neighbors that will allow for increased spatial resolution (Dabiri, 2009).

The corresponding displacement vectors represent an average refractive index variation within the IW (Keane and Adrian, 1992). However, as the minimum size of the IW governed by the necessary signal-to-noise ratios of intensity maps for higher correlation coefficients to be established, resolution of the resulting vector field becomes limited. This limitation not only reduces the resolution, but also yields the gradient information being prone to oversmoothening due to the averaging effects (Hargather and Settles, 2012). Even though multi-pass interrogation schemes exist to enable a larger dynamic range (Scarano and Riethmuller, 2000), these approaches are developed for tracing fluid particle motions within a bulk flow which makes them ineffective against very localized flow features of density variations. Thus, the dependence on neighboring pixel displacements and the documented degradation of accuracy in presence of large displacement gradients (Kähler et al., 2012) further alleviates the accuracy and resolution of BOS measurements when processed with block-matching approaches such as cross-correlation.

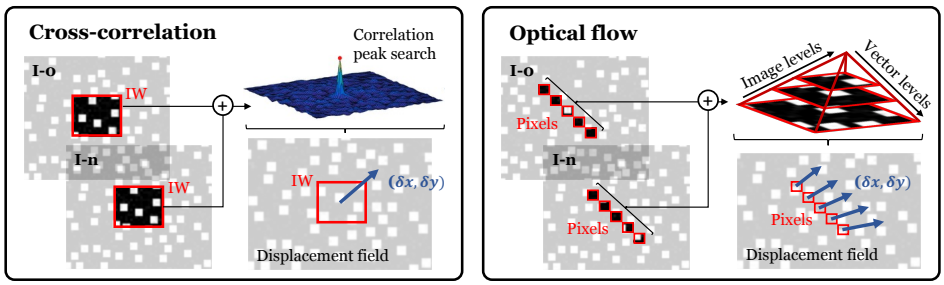

Figure 2.8: Schematic of cross-correlation (left) and optical flow (right) based deflection sensing schemes for background oriented schlieren.

2.4.2 Optical flow

The problem of inferior sensitivity and resolution of BOS using block matching approaches can be addressed through the application of optical flow (OF) image processing technique (Fig. 2.8, right) which defines the motion of objects within the image plane by means of brightness patterns (Davies, 2012). The biggest advantage of using OF for BOS is its capability to capture the displacement of each pixel enabling one vector-per-pixel resolution. This is proven to enable OF to go beyond the resolution and accuracy characteristics of PIV algorithms for reconstructing density field information (Atcheson et al., 2009).

Various approaches to OF analysis can be broadly distinguished to have a common gradient based scheme that is associated with two main assumptions; brightness constancy and spatial smoothness of the intensity distributions (Sun et al., 2008). The combination of these assumptions leads to the governing equation of motion of illumination intensities within the image plane (defined as the optical flow). Hence, a constancy of illumination intensity can be established which suggests the intensity of pixels moving within the image plane is constant and directly related to the motion of illumination gradients within the image plane (Eq.2.7) (Kearney et al., 1987).

$$\begin{aligned} I(x,y,t) &= I(x+\delta x, y+\delta y, t+\delta t) \\ &= I(x,y,t) + I_t + \delta x I_x + \delta y I_y \end{aligned} \tag{2.7}$$

Hence, the displacement $(\delta x, \delta y)$ of normalized illumination intensities (I) can be represented as functions of the temporal $(\partial I/\partial t)$ and spatial pixel intensity gradients $(\partial I/\partial x, \partial I/\partial y)$. For BOS applications, the temporal derivative of illumination intensities correspond to the difference between the disturbed and reference image $(\partial I/\partial t{=}(I_n - I_0)/\Delta t)$ while the nominal time interval is unitary since the difference between I_n and I_0 is independent of time $(\Delta t{=}1)$. Nevertheless, the underdetermined

structure of Eq.2.7 requires a problem closure to obtain a unique solution which leads to the well known aperture problem (Galvin et al., 1998).

2.4.2.1 Horn-Shunck optical flow

In order to address the aperture problem, Horn and Schunck (1981) proposed the use of a quadratic penalty function (ρ_D) for the displacement vectors corresponding to the deviations from the brightness constancy assumption and described an energy functional to be minimized (Eq.2.8). Moreover, Eq.2.8 also included a quadratic penalization (ρ_S) of the displacement vector gradients to increase the robustness of the algorithm against spurious displacement vectors (Barron et al., 1994). The weighting between the contribution of the brightness constancy violations and the vector gradients are controlled by a user defined regularization parameter, λ. However, this global penalization approach enforces the displacement vectors to vary smoothly over the reconstructed domain. Thus, precise selection of its value is crucial for an accurate displacement field estimation which would enable suppression of spurious vectors while preserving physical displacement magnitudes throughout the image plane (Nagel, 1983).

$$E(\delta x, \delta y) = \int_{\Omega} \left[\rho_D(I_{t+\delta t} - I_t) + \lambda \rho_S(\nabla \delta x, \nabla \delta y)\right] d\Omega \tag{2.8}$$

2.4.2.2 Lucas-Kanade optical flow

Alternatively, the algorithm introduced by Lucas and Kanade (1981) assumes that the flow is constant within a small neighborhood (window) around the pixel. This transforms the problem into solving for the best vector field that satisfies the optical flow constraint (Eq. 2.5) for all pixels in this window. For each pixel within the window, the optical flow constraint equation provides one equation. Since there are generally more equations than unknowns, the system is over-determined. The Lucas-Kanade method solves this system using the least squares approach. The set of equations can be written in matrix form and the least squares solution minimizes the error between the predicted and actual temporal gradients, leading to the vector field of interest (Eq. ??). The Lucas–Kanade method reduces the inherent ambiguity of the optical flow equation by incorporating information from multiple neighboring pixels, making it more robust against image noise compared to point-wise techniques (Bruhn et al., 2005). However, as a purely local approach, it is unable to determine flow information within uniform regions of the image.

$$|(I_t + \delta x I_x + \delta y I_y)|_{IW} = 0 \tag{2.9}$$

2.4.2.3 Multi-resolution and multi-scale extensions

The biggest challenge of achieving high resolution displacement fields with optical flow originates from the fact that practical image sequences contain multiple objects in motion independently. This causes occurrence of a global incoherence in terms of the acquired image intensity variations that also contain discontinuities (Deriche et al., 1996). Hence, the derived set of governing equations is only valid for small displacements in absence of any discontinuities. Therefore, additional methods are required to relax the constraints on the brightness constancy based formulation of the optical flow problem that would allow large displacements within the image plane to be reconstructed accurately (Edward H. and James R., 1985).

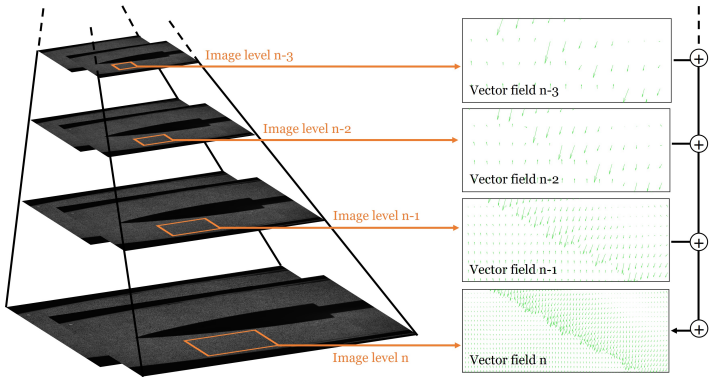

Figure 2.9: Hierarchical algorithm of optical flow with image sequences (left) and the corresponding vector fields (right) for different levels of the pyramid scheme.

Accordingly, hierarchical algorithms are proposed to separate the computation of displacement vectors based on the scales of optical flow contained within the processed images (Anandan, 1989). The acquired images are assumed to contain a wide spatial-frequency spectrum where the high amplitude (low spatial-frequency) intensity variations are represented by the large scale motion within the image plane, while low amplitude (high spatial-frequency) intensity variations provide the detailed structures over a smaller range. Nevertheless, identification of these scales and separating them accordingly requires a proper control strategy since spatial-frequency decomposition based on the sampling rates of the lower-frequency information would lead to a loss of resolution (Burt, 1981). Such a proper decomposition of the image intensities leads to a pyramid scheme that is composed of different spatial-frequency channels (Tanimoto and Pavlidis, 1975)(Fig. 2.9).

2.4.3 Phase correlation

Beyond the standard optical flow and cross-correlation methods, there are alternative image processing approaches utilized based on specific measurement environments and flow scenarios. Benefiting from the noise isolation capabilities, phase modulation and phase capturing based image processing algorithms are utilized in BOS (Ramaiah et al., 2023). In combination with gridded patterns (which offer high-contrast, repetitive structures making it particularly sensitive to small distortions), a fast checkerboard demodulation (FCD) algorithm can be employed leveraging the periodic structure of this pattern to efficiently decode the displacement information by extracting phase and amplitude data from the distorted image (Shimazaki et al., 2022). This process allows for rapid and accurate calculation of the displacement fields without the need for complex or time-consuming cross-correlation methods (Wildeman, 2018). Another approach that utilizes Fourier domain analysis is the Fourier Transform Profilometry (FTP). It involves projecting a known, periodic pattern—such as fringes or grids—onto the background and capturing the distorted image caused by refractive index changes in the flow. The Fourier transform is then applied to these images to convert the spatial information into the frequency domain, where the phase shifts corresponding to the flow-induced distortions can be isolated and analyzed (Vinnichenko et al., 2023). Phase demodulation approaches can also be extended to multi-scale and multi-resolution schemes. In this regard, Rajshekhar and Ambrosini (2018) introduced a diffractive optical element based BOS. This approach relies on accurately estimating the phase encoded within the fringe pattern through a windowed Fourier transform, followed by a multi-scale analysis of the extracted phase using a continuous wavelet transform. Since the phase directly corresponds to refractive index fluctuations caused by temperature gradients, the multi-scale analysis offers valuable insights into the underlying heat flow dynamics.

2.5 Work flow of background oriented schlieren

The first stage of building a BOS setup is determining the region of interest in the flow field. This has two main implications for the configuration of the setup. First implication is identifying the placement of setup components over which the measurements are intended. Although a BOS setup requires through optical pathway, not every facility is equipped with two way optical access. Moreover, due to the differences between different facilities, different imaging and illumination conditions might exist. It is common that not every facility allows the placement of powerful light sources such as lasers or big LED arrays due to physical constraints of space or logistics. Accordingly, the choice of lighting configuration, background type and background material needs

to be made to meet the requirements imposed by the facility (Fig. 2.10, 1st stage). The second implication is determining the imaging conditions. Depending on the spatial resolution and sensitivity requirements based on the flow features of interest, a correct combination of imaging objective, background size, and the distances Z_D and Z_A needs to be selected (Fig. 2.10, 2nd stage). Finally, the trade-off between depth of field and illumination intensity is optimized by selecting an aperture setting for the imaging lens. While a large depth of field is always preferred to minimize the blur on the schlieren object, a large $f_\#$ would cause the light intensity captured by the camera to be significantly reduced and the diffraction effects on the background to be amplified, thus weakening the contrast among the background features.

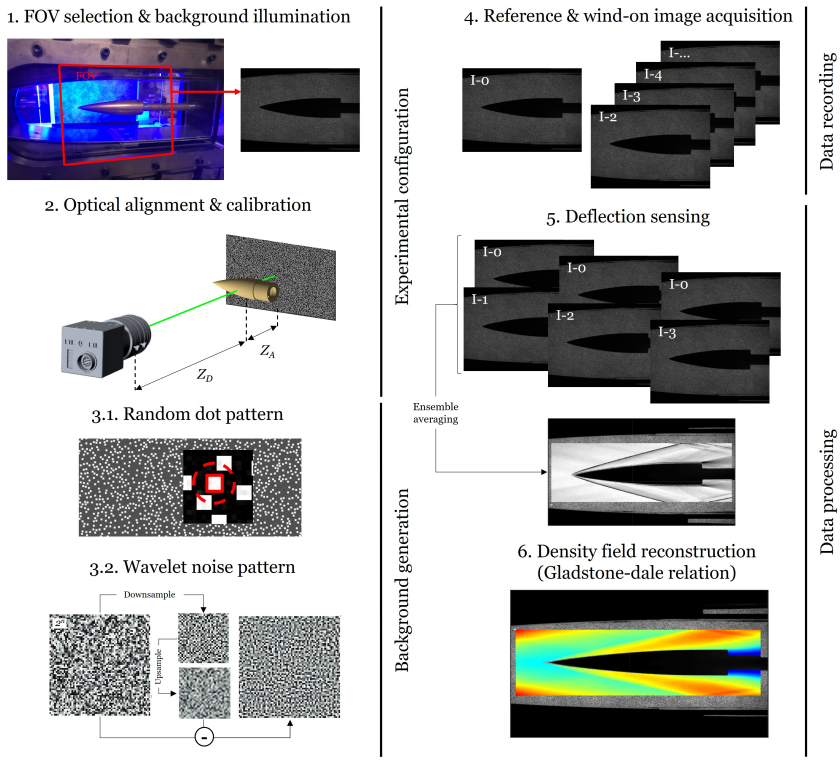

Figure 2.10: Workflow for the background oriented schlieren (BOS) measurement technique.

After the optical setup is configured, calibration images are acquired to verify the estimates of the magnification factor (M). In accordance to the measured M, the necessary parameters for the background generation are determined (Fig. 2.10, 3rd stage). Then reference images are acquired prior to the facility operation (Fig. 2.10, 4th stage). Following the reference images, wind on images can be acquired by activating the facility and generating flow conditions with varying refractive index (Fig. 2.10, 4th stage). Once the images are acquired, displacement fields are computed by

means of any of the aforementioned image processing algorithms (Fig. 2.10,5th stage). It is shown in multiple studies that for accurate reconstruction of displacement fields, each wind-on image should be processed individually with respect to the reference image without performing any statistical processing over the raw images. This enables preservation of imaging conditions and avoid deterioration of optical resolution specifications. Statistical sampling (i.e., ensemble averaging) can be performed over the displacement fields. Depending on the objectives of the experiments, the displacement field can be related to the density field by means of the Gladstone dale relation (Fig. 2.10, 6th stage). Nonetheless, it should be kept in mind that since BOS is a line of sight technique, in absence of tomographic imaging, assumptions regarding the in-depth variation of density gradients are required for the planar density distribution to be reconstructed.

Chapter 3

Experimental applications

The high versatility of background oriented schlieren (BOS) allows a wide spectrum flow scenarios (both reactive and non-reactive) to be investigated without the need of major modifications to the measurement technique hardware. However, each application demands slight variations in the optical configuration and image processing sequences to achieve the highest accuracy and precision of flow property determination. These requirements are driven by the flow phenomena of each specific flow regime and the corresponding configurations of the testing facilities. The wide spectrum of applications provided within this chapter establishes a knowledge base detailing the specifics of measurement technique setups employed for each flow field with the challenge of maintaining low complexity of setup components while explaining the reasoning behind the need of each application for BOS.

3.1 Thermodynamics of swirling subsonic heated jets

Due to the scarcity of quantitative assessments on the use of optical flow for BOS, a proper characterization of background pattern specifications does not exist. Rather, the available literature concentrates on the performance of various optical flow algorithms over the set of background images optimized for cross-correlation (Li et al., 2023) or the variation in the generation algorithm of patterns (Vinnichenko et al., 2023). Although it is still the case that speckle or random dot based backgrounds are the most popular choice among the BOS users (Hayasaka et al., 2016; Nicolas et al., 2017; Beermann et al., 2017; Grauer et al., 2018; Unterberger and Mohri, 2022), the background generation rules relying on the cross-correlation algorithm lack compatibility with the mathematical background of optical flow estimation. Thus, even

though optical flow is able to establish sensitivity and resolution limits far beyond what cross-correlation was capable of, without the optimization of background patterns, the measurement technique lacks a serious step of evolution. Accordingly, this study aims to respond to this need of creating a framework for background pattern optimization for maximizing the image processing capabilities of optical flow for BOS.

An experimental assessment by means of a heated air jet is conducted to demonstrate the theoretical and applicability considerations associated with the use of random dot backgrounds with various configurations. The heated air jet generated by a Steinel HL 1610 S heat gun. It has two operation modes, ejecting heated air at temperatures of 575 K and 783 K with speeds of 4.7 m/s and 8.2 m/s respectively from a nozzle with diameter 0.033 m. The corresponding nozzle diameter based Reynolds numbers of the operation modes are Re_D=3200 and Re_D=3400. For the present experimental assessment, only the first (low speed and low temperature) mode of the heat gun is utilized to enable the spatial and temporal resolution limits of the measurement system to fall within the range of instantaneous flow scales as much as possible.

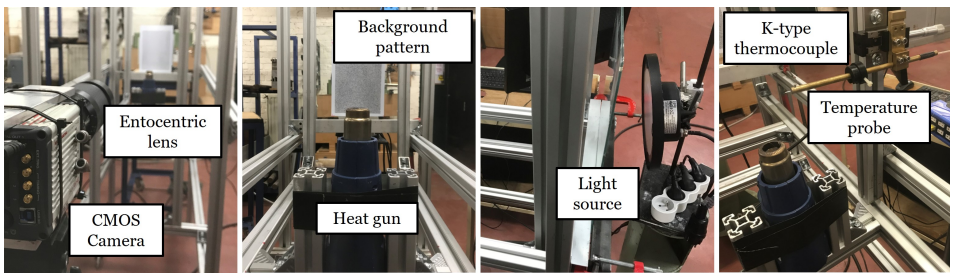

Figure 3.1: Background oriented schlieren (BOS) experimental setup with the heat gun.

Configuration of the BOS setup is composed of a Hamamatsu ORCA-Flash4.0 V3 Digital CMOS camera, a f = 100 mm Nikkor lens, a 10000 lm 80 Watt cool white LED as the light source and backgrounds laser printed on 240 g/m^2 paper (Fig. 3.1). The backgrounds are generated via uniformly downsampling the total range of parameters to obtain 37 combinations of varying dot size (d_P), dot concentration (N_I) and distribution randomness (RR). The distance between the light source, and the background is adjusted to optimize the trade-off between light intensity and uniformity. The distances between the camera, the background and the heat gun are configured in consideration of three different factors. On top of the trade-off between increased sensitivity and defocusing of the schlieren object, the resolution of the flow features in the spatial domain are aimed to be limited to a spatial resolution level which can be matched by the maximum shutter speed of the camera with a continuous light source. Accordingly, 1000 images for each background pattern at an acquisition frequency of f_{aq}=100Hz are recorded with an exposure time of t=5 milliseconds to limit the temporal averaging of flow features and to allow sufficient illumination signal to

be captured utilizing an aperture of $f_{\#}$=16. Finally, local temperature measurements are performed over the jet axis at 6 different longitudinal positions (1≤L/D≤6) from the exit of the heat gun via a K-type thermocouple (Fig. 3.1, right).

3.2 Aerothermodynamics of transonic low-pressure turbine cascades

Compressible phenomena play a crucial role in turbomachinery flows, significantly affecting boundary layer behavior and loss mechanisms within the turbine cascades (Gier and Hübner, 2005; Martinstetter et al., 2010). Despite the importance of density varying flow features, the application of background oriented schlieren (BOS) to high-speed flows in turbomachinery remains underutilized with only a few examples reported by Alhaj and Seume (2010) and Gong et al. (2018). The SPLEEN (Secondary and Leakage Flow Effects in High-Speed Low Pressure Turbines) test case focuses on transonic low-pressure turbines, which are characterized by low Reynolds numbers, to address the shortage of experimental data in this area. To complement the experimental work by Simonassi et al. (2022) and Lopes et al. (2022), the current study aims to perform BOS measurements to characterize compressible turbine flows and provide guidelines for applying this technique to the specific flow conditions under investigation. The images were processed using cross-correlation and optical-flow methodologies, and the results from these algorithms were compared with CFD data presented by Rosafio et al. (2023).

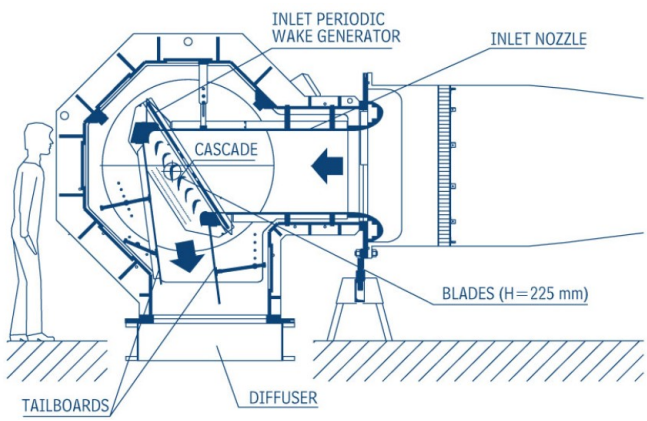

Figure 3.2: Schematic of the VKI-S1 continuous high speed cascade wind tunnel.

The experiments were carried out in the closed-loop high-speed, low-Reynolds number wind tunnel S-1/C of von Karman Institute (Fig. 3.2 and Fig. 3.3, A). This facility allows the independent variation of the Reynolds and Mach numbers, hence the en-

gine representative conditions can be effectively reproduced. The facility is driven by a 615 kW axial compressor, controlling the mass flux and therefore the Mach number, while the Reynolds number is fine-tuned by a vacuum pump which enables reaching pressure levels below 5000 Pa. Before admitting the air into the test section, a series of screens and honeycombs are used to ensure homogeneous axial flow conditions. A passive turbulent grid placed 400 mm upstream the cascade central blade can be used to increase the free stream turbulence intensity up to 2.4%.

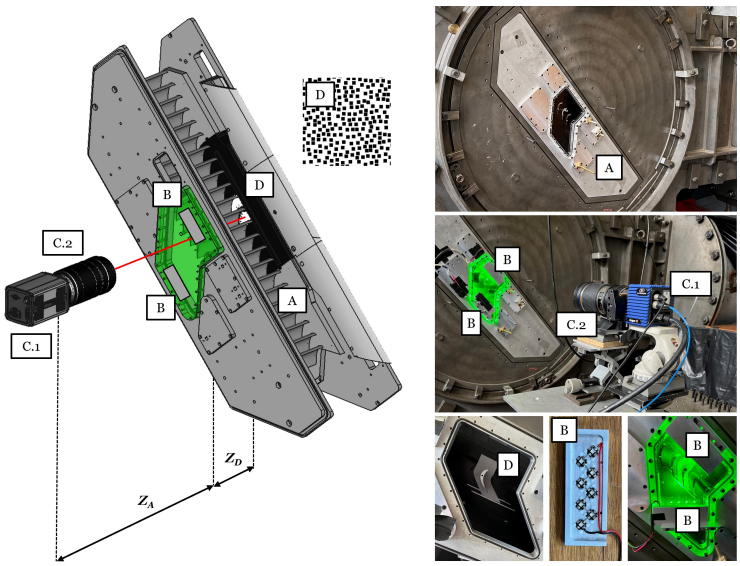

Figure 3.3: Background oriented schlieren (BOS) experimental setup configured in the VKI-S1 wind tunnel.

The tested turbine cascade is representative of a blade hub-endwall section of future generation of small-mid range aircraft engines. Hence, these specific blades were designed for transonic outlet Mach numbers, low acceleration and high deflection flow exiting the turbine stage. Details about the specific blade geometries are described by Simonassi et al. (2022). The BOS measurements were implemented with three optical configurations that use different digital CMOS detectors (Hamamatsu ORCA-FLASH 4.0 V3 and Imager SX 4M cameras for low-frequency measurements, and a Dantec Dynamics SpeedSense 2012 for time-resolved measurements)(Fig. 3.3, C.1). All three optical setups use a Tamron SP 180 mm lens (Fig. 3.3, C.2). A computer-generated speckle pattern is designed based on the guidelines provided by Cakir et al. (2024). A background pattern with a particle concentration of 0.027 ppp is laser printed on 220 g/m^2 paper at a resolution of 1200 dpi (Fig. 3.3, D). The size of the background dots was optimized for each combination of camera and FOV. The test section features a single optical access, as visible in Fig. 3.3, therefore the background location was constrained to be on the cascade end-wall. The backgrounds were front-

illuminated by two racks of eight Cree XP-E2 Q5 Green LEDs mounted on the outer surface of the optical window, as shown in Fig. 3.3 (B).

3.3 Aeroacoustics of supersonic dual-stream co-axial jets

Dual-stream co-axial supersonic jets contribute significantly to the acoustic signature of future aircraft concepts intended for use in supersonic civil aviation. There are three primary noise-generating mechanisms present in supersonic jets: broadband shock-associated noise, jet screech, and turbulent mixing noise (Tam, 1995). Although these mechanism are well established for single-stream supersonic jets, investigations on dual-stream cases with co-axial convergent-divergent nozzles is limited. As a consequence, the objective is to generate a database that features a dual-stream supersonic convergent-divergent nozzle operating at several expansion conditions. Similarly, BOS is previously emplyed for qualitative and quantitative characterization (Wernet et al., 2021), control (Kumar et al., 2011) and three-dimensional reconstruction (Nicolas et al., 2017) of supersonic jets, but never before for measurements of dual-stream jet configurations. Accordingly, BOS is utilized to identify the shock-cell structures both single- and dual-stream configurations that are the basis for the shock-associated noise generation.

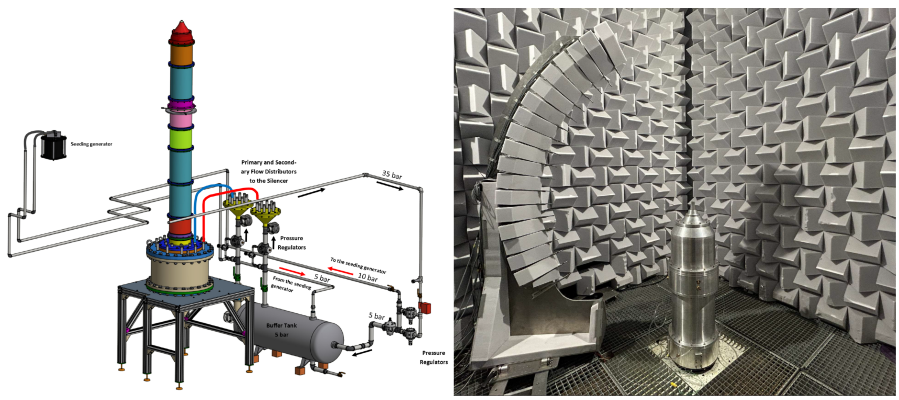

Figure 3.4: Air supply of VKI-JAFAAR facility (left). Anechoic room and microphone far-field antenna (right).

The experiments are performed in the JAFAAR facility (Jet Aeroacoustic Facility for Aeronautical and Aerospace Research) of the von Karman Institute (Fig. 3.4). The facility is operated using a 40 bar pressure network (Fig. 3.4, left) employing two identical pressure regulators and ensuring a sufficient mass flow. Downstream the twin regulators, an electrical regulated valve is used in combination with a control loop to maintain constant flow conditions at the jet outlet. A single buffer tank of 500 L is then used downstream of the valve to dampen pressure oscillations from the pipeline.

In order to control the jet streams of the coaxial nozzle separately, the independent pressure lines are drawn from the buffer tank. Further information regarding the dual stream piping design is available in Guariglia et al. (2018). The coaxial jets discharge in an anechoic room with the dimensions of 4 x 3 x 4 m^3 and with a cut-off frequency of about 200 Hz. Both pipes are equipped with static pressure probes and thermocouples to control the flow conditions through the isentropic flow relations.

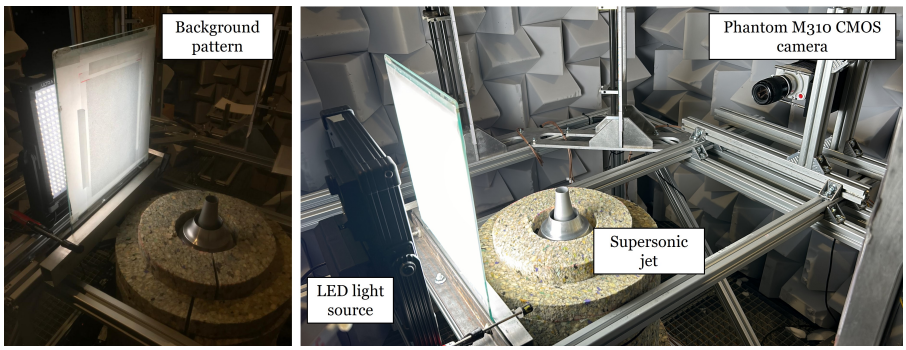

Figure 3.5: Background oriented schlieren (BOS) experimental setup configured in the VKI-JAFAAR facility.

Configuration of the BOS setup is composed of a Phantom Miro M-310 Digital CMOS camera (1280×800 pixels, 12-bit, 20 μm pixel size), a f = 150 mm focal length Nikkor lens and a 10000 lm 80 Watt cool white LED as the light source (Fig. 3.5). The backgrounds composed of speckle patterns generated under the guidelines established by Cakir et al. (2024) are printed on translucent paper. A diffuser sheet is placed between the background and the light source to achieve a high uniformity of illumination intensity over the field of view. The distances between the camera, the background, and the supersonic jet are configured in consideration of three different factors. On top of the trade-off between increased sensitivity and defocusing of the schlieren object, the resolution of the flow features in the spatial domain is aimed to be limited to a spatial resolution level that can be matched by the maximum shutter speed of the camera while a continuous light source is employed. Accordingly, the aperture and the exposure time are set to $f_{\#}$=16 and 20μs respectively. The BOS data is acquired at a rate of f_{aq}=200 Hz for 20 seconds which amounts to 4000 images for each operating condition.

3.4 Aerodynamics of supersonic flows

As the BOS measurements are increasingly employed for the development and validation of computational fluid dynamics models (Ramanah et al., 2007; Kirmse et al., 2011), the cross-correlation based BOS becomes vulnerable to fall short of the cor-

responding resolution and accuracy requirements, whereas OF is showcased as a viable solution. Despite its utilization in various occasions (Atcheson et al., 2008; ?; Grauer et al., 2018; Heineck et al., 2021), a lack of quantitative characterization of its capabilities and application details exists, especially in high-speed flows. Thus, its utilization requires proper quantification of the resolution, sensitivity and accuracy of OF based BOS, as well as the optimization of the experimental and image processing configurations. This study aims to quantify the accuracy characteristics of optical flow compared to cross-correlation employing various background patterns. Accordingly, the experimental applicability of the deflection sensing and background generation methods under investigation is demonstrated by conducting BOS measurements of Mach 3.5 supersonic flows over a von Karman Ogive and a 10^o wedge.

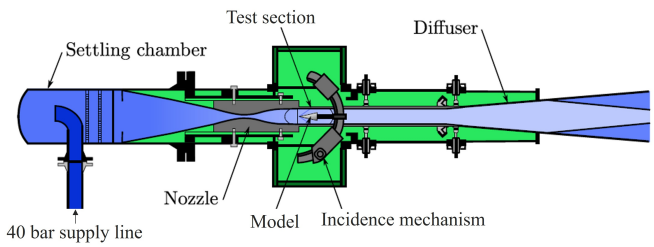

Figure 3.6: Schematic of the VKI-S4 supersonic wind tunnel.

The experimental setup employed in this section is implemented on the VKI-S4 supersonic wind tunnel of the von Karman Institute (VKI) (Fig. 3.6). The VKI-S4 rig is a blow-down wind tunnel equipped with a 2D contoured nozzle providing Mach 3.5 supersonic flow into a test section of 8×10 cm^2. The reservoir pressure can be adjusted within a range of 3 to 18 bars to achieve a typical unit Reynolds number of 5×10^7/m. Configuration of the BOS setup is composed of a Hamamatsu ORCA-Flash 4.0 V3 Digital CMOS camera, a Nikkor entocentric lens of focal length f = 200 mm and four Chazon 100W 10x10 blue (465 nm) LED arrays as the light source (Fig. 3.7). The LEDs, supplied with a DC power source, are utilized to illuminate the backgrounds from behind to enhance the recorded contrast and eliminate reflection effects. The backgrounds are laser printed on 240 g/m^2 paper sheets. A random dot background pattern with particle density of N_I=0.027 ppp is created with the dots generated as white squares over a black background. Moreover, four wavelet noise backgrounds are generated based on 3 different noise patterns with constant initial resolution level (n_I=2), while the final resolution level is varied between $10\leq n_F\leq12$. The supersonic tests are conducted with two different models of a von Karman ogive and a 10^o wedge (end-to-end). The exposure time of the camera is set to 100 ms. Accordingly, 40 wind-on images are recorded for each model and background combination with an acquisition frequency of f_{aq}=10Hz. An aperture of $f_{\#}$=22 is used to minimize the defocusing effects of blur and diffraction in the vicinity of the model surface.

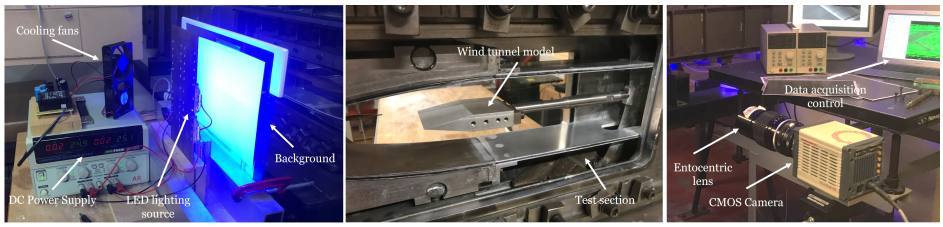

Figure 3.7: Background oriented schlieren (BOS) experimental setup configured in the VKI-S4 wind tunnel.

3.5 Hypersonic shockwave boundary layer interactions

Shockwave boundary layer interactions have been a canonical case for combined numerical and experimental investigations, which drives the interaction of high-speed arial vehicles with the compressible flow field, dictating their performance specifications and design constraints (Delery, 1985). Accordingly, various experimental tools have been used to characterize the flow behavior in SBLI scenarios, mainly focusing on the non-intrusive techniques to infer the specifications of flow features optically. In this regard, BOS provides a unique opportunity to quantitatively characterize density varying flows by means of an inexpensive and simple setup (Raffel, 2015). Although the availability of new advancements in hardware and software extended the resolution limits of BOS imagery significantly (Ota et al., 2017; Weisberger and Bathel, 2022; Cakir, Lavagnoli, Saracoglu and Fureby, 2022; Molnar et al., 2023), the possibility of using BOS in a shockwave boundary layer interaction (SBLI) scenario is yet to be explored. Hence, this study targets a detailed analysis of the flow features obtained over a stainless steel cone (7.5°) flare (17.5°) model with a blunt (1.5 mm of radius) exposed to Mach 5 hypersonic freestream using BOS setups of different configurations to highlight the specifications and the resultant flow visualization characteristics.

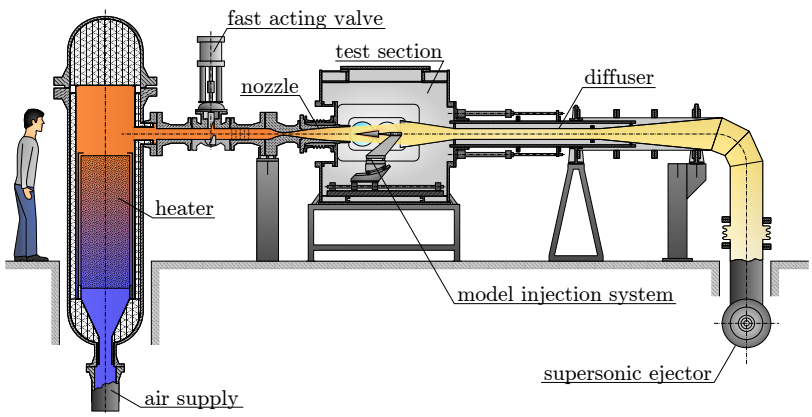

Figure 3.8: Schematic representation of VKI-H3 hypersonic wind tunnel facility.

The VKI-H3 wind tunnel (Fig. 3.8) is a low enthalpy, blow-down facility designed to generate hypersonic flows at large Reynolds numbers (Simeonides, 1990). For the present investigations, its operational capabilities are extended with the addition of a newly designed and integrated axisymmetric contoured nozzle, producing a uniform Mach 5 free jet with an inviscid diameter of 120 mm (Cakir, Grossir, Paris and Saracoglu, 2022) which allows the free-stream unit Reynolds number to be varied from 5×10^6 to 35×10^6 /m with the current Mach 5 nozzle (Gyenge et al., 2024). The BOS measurements are performed with 2 different optical configurations. As illustrated in Fig. 3.9 (A), a conventional BOS setup is constructed with a diverging light ray arrangement in which the light collection optics directly face the background pattern through an entocentric lens. On the other hand, in case of a telecentric configuration, the imaging arrangement only focuses the parallel light beams coming from the target on the sensor where an aperture is placed at the focal point, canceling non-parallel light rays (Fig. 3.9, B). This optical arrangement can either be achieved via mirrors (Ota et al., 2015) or by means of a telecentric lens (Cozzi et al., 2017). In the current case, the telecentric setup has one focusing mirror (f_1), a flat mirror, an aperture and the imaging objective (f_2). In this setup, the imaging objective and the focusing mirror are placed with a separation of f_1+f_2 to collimate the parallel light beams coming from the background pattern and the aperture is placed at the focal point of both mirror and objective.

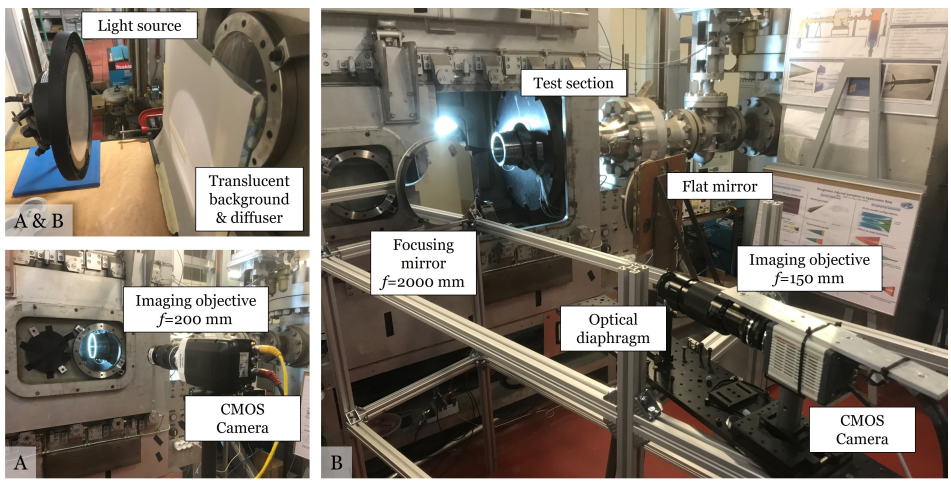

Figure 3.9: Entocentric (A) and telecentric (B) background oriented schlieren (BOS) experimental setups configured in the VKI-H3 wind tunnel.

Two different cameras, Hamamatsu ORCA-Flash 4.0 V3 (2048×2048 pixels, 16-bit, 6.6μm pixel size) and Phantom Miro M-310 Digital CMOS camera (1280×800 pixels, 12-bit, 20μm pixel size), are successively employed for the acquisition of the BOS images. A Nikkor entocentric lens of variable focal length is mounted to both of the

cameras. While the objective is set to f=200mm for the diverging BOS configuration, f = 135mm is used for the telecentric setup. When image acquisition is performed using Hamamatsu ORCA-Flash 4.0 V3 digital camera, the exposure time is set to 1ms which allows an acquisition frequency of f_{acq}=100Hz. On the other hand, the larger sensor size of the Phantom Miro M-310 Digital CMOS camera enables shorter exposure times at 10μs with image acquisition at a frequency of f_{acq}=1kHz. For the diverging BOS setup, the aperture is set to the minimum available on the imaging objective $f_{\#}$=22, while for the telecentric configuration the depth of field control is manipulated via the additional aperture. For each field of view, backgrounds composed of speckle patterns are generated under the guidelines established by Cakir et al. (2024) and printed on translucent paper. A diffuser sheet between the background and the light source is placed to achieve a high uniformity of illumination intensity over the field of view while the backgrounds are illuminated from the rear via a 10000 lm 80 Watt cool white LED (Fig. 3.9). In addition to the BOS measurements, oil flow visualization technique is also employed to visualize the flow features attached to the model surface as the shear forces exerted on the model surface shape the spatial distribution of oil/titanium powder mixture. For improved contrast, the model is painted in black and the oil mixture is illuminated with four Chazon 100W 10x10 blue (465 nm) LED arrays (Fig. 3.10). The oil flow visualization images are acquired with the Phantom Miro M-310 Digital CMOS camera over a period of 20 seconds to record the full oil pattern evolution.

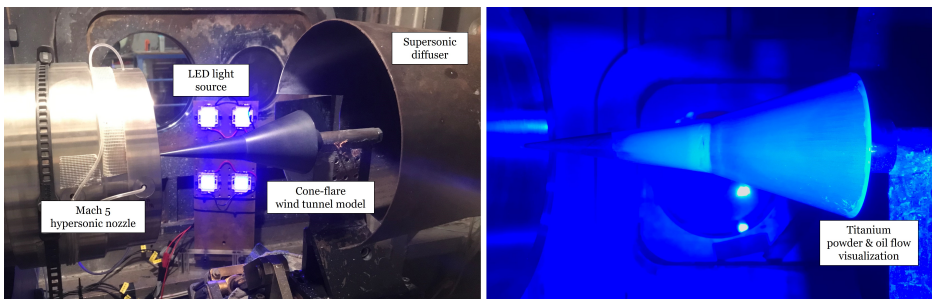

Figure 3.10: Test section of the VKI-H3 wind tunnel and the oil flow visualization setop.

3.6 Laminar burning velocity measurements on Bunsen burners

The advancement and implementation of novel sustainable aviation fuels necessitate a comprehensive understanding of their chemical attributes and combustion characteristics. A central fuel characteristic is the laminar burning velocity (LBV), representing the speed of laminar flame propagation in a combustible gas mixture, and is influ-

enced by pressure, temperature and composition (Konnov et al., 2018). This fundamental flame property encompasses the combined effects of heat release, diffusivity, and reactivity within the mixture. Although background oriented schlieren (BOS) is demonstrated to be both reliable and accurate for density field characterization in reactive flows (Bauwens et al., 2017; Grauer et al., 2018; Choudhury and Joarder, 2022; Wahls and Ekkad, 2022; Baek et al., 2022), to the authors' best knowledge BOS has never been used for characterization of LBV. Hence, this study aims to demonstrate and assess the use of BOS as a means to perform flame front reconstruction and, in turn, evaluate LBV on a series of premixed flames.

3.6.1 High-pressure Bunsen burner

Fig. 3.11 displays a schematic of the burner utilized in the study. The high-pressure rig, made of stainless steel, has a cylindrical design. It can operate at a maximum pressure of 36 bar and withstand ambient temperatures up to 220°C. The chamber's internal volume is 25 liters, with an inner height of 500 mm and an inner diameter of 254.5 mm. To facilitate comprehensive optical diagnostics, the chamber is equipped with four view-ports positioned at 0°, 90°, 180°, and 270°. Pressure within the chamber is maintained at a constant level by electronically controlling the gas flow with back-pressure regulators, ensuring a steady operation at desired conditions. Further details of the high pressure rig are provided by Joo et al. (2015).

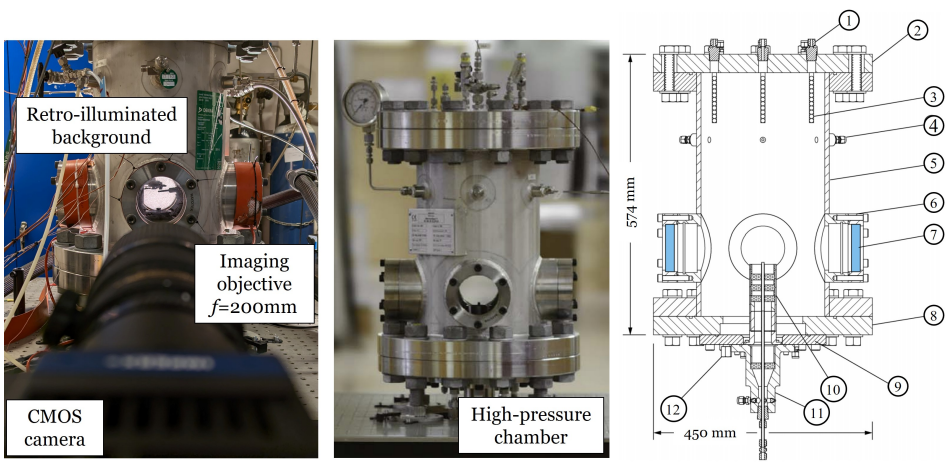

Figure 3.11: Background oriented schlieren (BOS) setup configured in the high-pressure Bunsen burner and general schematics of the high pressure combustion apparatus. 1—Access ports. 2—Top cap flange. 3—Cooling coils in series. 4—Access ports. 5—Chamber tube. 6—Window frames. 7—Anti-reflection coated sapphire windows. 8—Bottom cap flange. 9—Mounting plate. 10—Interchangeable burner module. 11—Chamber burner module. 12—Access ports. Adapted from Joo et al. (2015).

Configuration of the BOS setup comprised a IMPERX PoE-C6410 camera (6480×4860

pixels, 12-bit, 3.45μm pixel size) and a f=200mm constant focal length Nikkor lens which enabled the visualization of a 150x150mm field of view (Fig. 3.11, left). The minimum aperture setting ($f_{\#}$=32) is selected to maximize depth of field as the background is placed 600mm from the burner axis and the camera is placed at 1.2m from the burner axis on the opposite side. The high light intensity available to the imaging sensor enabled short exposure imaging where the exposure time is set to 1μs. In order to enhance statistical convergence in the temporal domain, a low acquisition frequency of f=10Hz is utilized and in total 100 images are acquired for each operating condition. The background is composed of a computer generated speckle pattern and printed on thick paper, and retro illuminated with a flood lamp.

3.6.2 Atmospheric Bunsen burner

The main component of the experimental setup is a water-cooled stainless steel Bunsen burner comprised of an extended premixing tube, length 600 mm, and a convergent nozzle (Fig. 3.12) with an exit diameter of 15 mm. The air and gaseous fuel supply is controlled using two Bronkhorst mass flow controllers. The configuration of the BOS setup is composed of a Basler ace acA1920-40gm Digital CMOS camera (1920×1200 pix resolution with 5.86 μm pixel size), a Nikkor entocentric lens of focal length f = 28 mm, and a flood lamp as the light source (Fig. 3.12). The aperture of the objective was set to $f_{\#}$=16 to maximize the depth of field. A computer-generated speckle pattern is created based on the guidelines provided by Cakir et al. (2024) and laser printed on 240 g/m^2 paper.

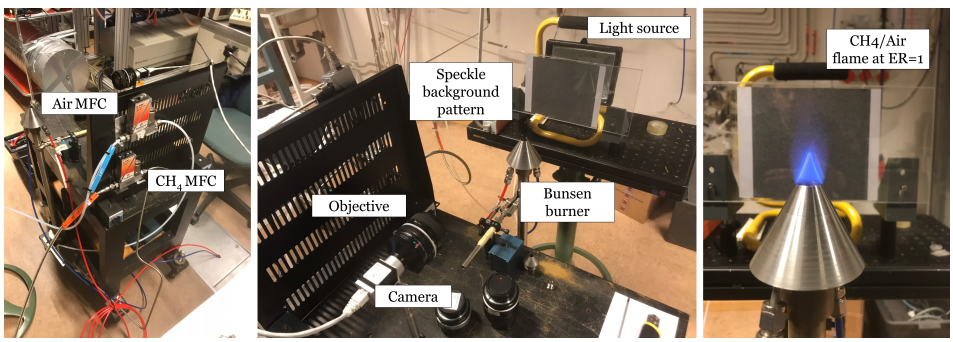

Figure 3.12: Background oriented schlieren (BOS) setup configured around the atmospheric Bunsen burner.

An alternative method that can compete with the adaptability and ease of application of BOS is direct chemiluminescence imaging. During the chemical reactions that take place in proximity of the flame front, radicals are formed in an excited state. Hence, the decay of the radicals from this excited state causes spontaneous emission of light at specific wavelengths depending on the chemical composition. The highest

concentration of excited radicals exists within the flame front where the reactions take place, thus the high emission intensity captured by the camera allows the flame front to be detected. The same optical acquisition setup that was utilized for BOS was also used to acquire chemiluminescence images of the flames. A dark non-reflective surface was then placed between the background mount and the investigated flame to prevent reflections and reduce background luminosity. However, since the intensity of the flame chemiluminescence was significantly lower than that of the BOS light source, the aperture was adjusted to $f_{\#}$=2.5, and the flame was put in the optical focus.

3.7 Swirl-stabilized turbulent flames in gas turbine combustors

To maximize efficiency and ensure optimal performance in a gas turbine combustor, it is crucial to reduce fuel consumption and minimize pollutant emissions in line with current environmental regulations. Accordingly, lean premixed combustion reduces flame temperatures and prevents the formation of high-temperature hotspots, thereby mitigating NOX emissions (Correa, 1998; Bauer, 2004; Lefebvre and Ballal, 2009). The CeCOST burner, modeled based on the EV/AEV burner (Sattelmayer et al., 1992), features intricate turbulence-flame interactions similar to those seen in industrial settings (Hodzic et al., 2018) which often use swirl-stabilized flames because they provide high heat and power output in a compact design while maintaining stable combustion across various operating conditions (Lilley, 1977; Weber and Dugué, 1992). Although the flame dynamics and combustion characteristics of the CeCOST burner are well studied (Subash et al., 2020; Liu et al., 2021; Pignatelli et al., 2022, 2024), there has never been an attempt to visualize temperature induced density gradients. In this regards, BOS provides a unique opportunity of utilizing the already installed imaging system (for PIV and chemiluminesce imaging) without interfering with the optical configuration owing to the obliterated need for configuring a collimated light system in comparison to the conventional schlieren approaches.

The CeCOST burner (Pignatelli et al., 2022; Feuk et al., 2022) is integrated in the atmospheric combustion rig of Combustion Physics Division of Lund University. Schematics and photos of the burner assembly are provided in Fig. 3.13. Bulk air flow is provided into the burner via a compressor based blower system while the fuel injection is performed through injection holes on a spiral tube installed inside the settling chamber (Pignatelli et al., 2022). Premixed conditions are achieved by means of a quarter-cone (Fig. 3.13, left-red circle) swirler which induces a counter-clockwise swirl followed by a premixing tube (diameter 50 mm, height 100 mm) mounted between

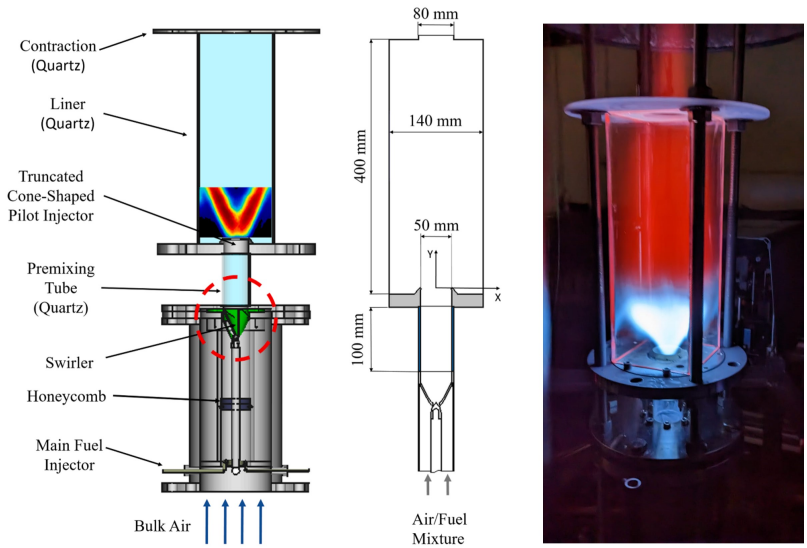

Figure 3.13: General schematics and photo of the CeCOST atmospheric combustion rig adapted from Pignatelli et al. (2024).

the swirler and the combustion chamber. At the exit of the burner, a quartz quadratic cross-section (140×140 mm^2) 400mm long combustion chamber is located which allows full optical access for non-intrusive diagnostics. The combustion chamber exit is constrained by means of a quartz plate with a central circular outlet of 80 mm diameter which exhausts the combustion products towards the ventilation system.

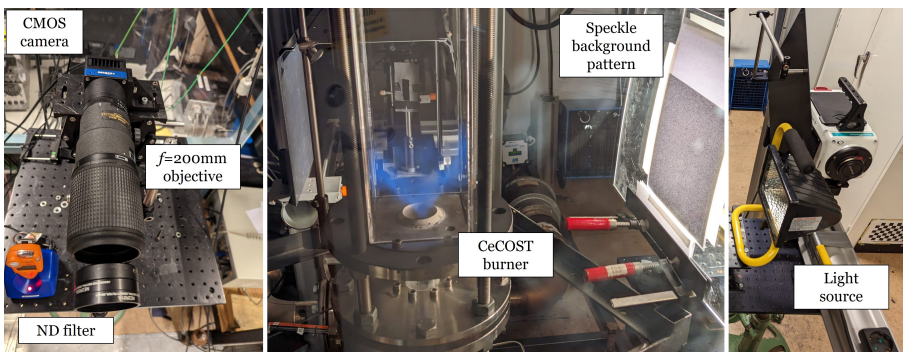

Figure 3.14: Background oriented schlieren (BOS) setup configured in the CeCOST atmospheric combustion rig.

In the BOS setup, a IMPERX PoE-C6410 camera (6480×4860 pixels, 12-bit, 3.45μm pixel size) is used. Due to the binning (2x2 pix^2) performed on the imaging sensor, a large integrated light intensity was obtained even at the lowest exposure setting.

Hence, a natural density (ND) filter of level 0.6 is utilized to suppress the excessive light intensity on the camera sensor. For the imaging, a f=200mm constant focal length Nikkor lens is employed which images a field of view size 150x200mm. The minimum aperture setting with $f_{\#}$=32 is selected to maximize depth of field as the background is placed 600mm from the burner axis and the camera is placed at 2m from the burner axis on the opposite side. The high light intensity available to the imaging sensor enabled short exposure imaging where the exposure time is set to 1μs. In order to enhance statistical convergence in the temporal domain, a low acquisition frequency of f=10Hz is utilized and in total 100 images are acquired for each operating condition. The background is composed of a computer generated speckle pattern and printed on thick paper, which is retro illuminated with a flood lamp (Fig. 3.14, right).

Chapter 4

Summary of results

This chapter summarizes the flow characterizations derived from the experimental setups discussed in Chap. 3. The results are presented in two parts: qualitative visualizations of flow field features, and quantitative characterizations of density fields or extraction flow properties, captured through refractive index variations. The qualitative analysis focuses on the flow visualization capabilities of the background oriented schlieren (BOS) technique, while the quantitative analysis highlights BOS's advantage over conventional schlieren methods—namely, the ability to reconstruct quantitative flow information without calibration. Each section details the process of extracting quantitative flow properties using displacement fields, reconstructed through an optical flow-based image processing approach.

4.1 Thermodynamics of swirling subsonic heated jets

To evaluate the resolution and sensitivity of optical flow-based BOS under different configurations of random dot background patterns, a parametric study was conducted using a heated jet of air. This scenario presents a challenging case due to its highly turbulent flow field, with scales that exceed the spatial and temporal resolution limits of the optical setup. Prior to the experiments, synthetic analyses were carried out on shock tube and density-driven turbulence flow fields, which identified varying optimal configurations for maximizing local resolution and sensitivity. Consequently, background generation parameters were selected to align with the anticipated flow field characteristics in the experiments. The increased complexity of the displacement vector distribution in the heated jet case further highlighted the tunability of the background patterns. Specifically, it was found that larger speckles with a high

concentration enhance local resolution in highly turbulent flow fields, while greater sensitivity to the randomness of the speckle distribution was observed.

Fig. 4.1 (middle) shows an instantaneous snapshot of the processed BOS images of the heated jet. A strong swirling behavior is induced by the fan that accelerates the flow out of the nozzle. This allows the heat gun to discharge air with large scale turbulent structures. The shear layers are observed between the jet and the still air over which Kelvin-Helmholtz (KH) instabilities are induced. The length scales of these instabilities are rather small in proximity of the jet exit. Further downstream, the eddies generated via the KH instabilities grow in size, spreading the jet spatially at a relatively constant rate which is confirmed via the time averaged displacement map (Fig. 4.1, right). This also yields an increase in the rate of heat transfer as the eddies existing over the shear layers not only transport momentum but also thermal energy between the fast jet and the surrounding still air. These findings are in line with the literature on heated jets (Simonich et al., 2001; Viswanathan, 2004; Andersson et al., 2005; Zhu et al., 2018).

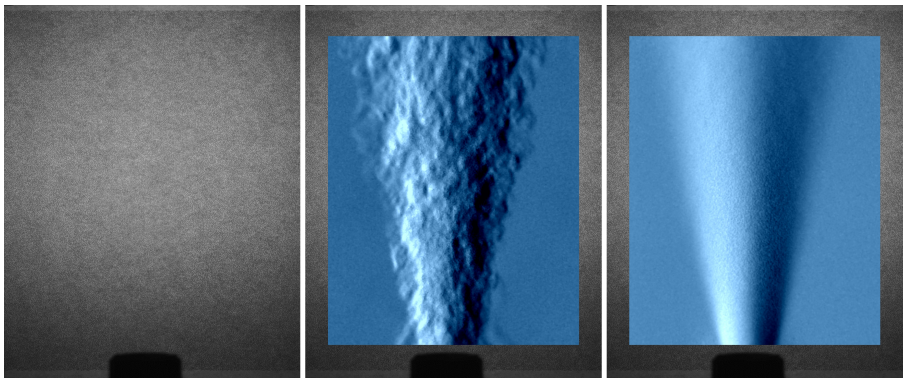

Figure 4.1: A raw image from the background oriented schlieren (BOS) setup (left), instantaneous snapshot of the displacement field reconstructed via optical flow (middle), and time-averaged displacement field (right).

BOS also allows the temperature field to be computed by relating the displacements to density gradients which in turn yields a temperature field using the ideal gas relation. Since, the averaged profile of the jet is axisymmetric, the inverse Abel transform can be employed to compute planar temperature gradients which can be directly related to the changes in refractive index as described by Xiong et al. (2020). Accordingly, the temperature profiles employing background patterns with fully random distribution of speckles (RR=100%) are reconstructed to perform investigations of the response of optical flow to varying speckle size (d_P) and concentration (N_I) (Fig. 4.2). Starting with the smallest speckle size (d_P=1 pix) to assess the effect of speckle concentration on temperature reconstruction accuracy and precision, a clear underprediction of the temperature towards the center of the jet axis is observed. The low concentration of

speckles yielding a less populated pattern results in a low level of signal to noise ratio since the only illumination features optical flow can utilize belong to the interference pattern of the light source with the thick paper. As the speckle concentration is increased, a gradual improvement in reconstruction accuracy is captured for the temperature field in proximity of the jet exit (L/D=1) whilst achieving considerably good accuracy for L/D=3 and L/D=5 directly above N_I>0.012. Overall, highest accuracy and precision for d_p=1 pix is obtained at N_I= 0.070 ppp whilst there exist local extremes exist in the error distribution, yielding a large overall accuracy deficit especially for N_I<0.060 ppp (Fig. 4.2).

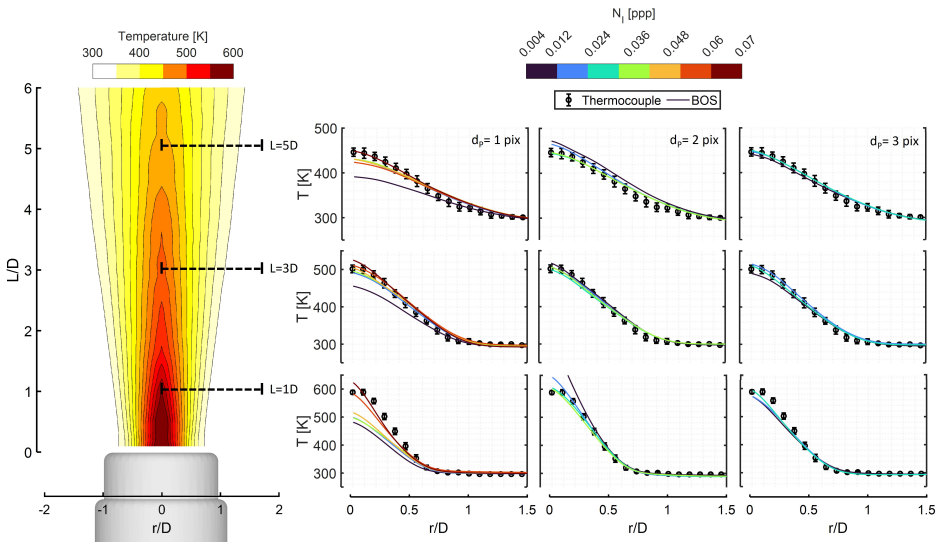

Figure 4.2: Time averaged temperature fields reconstructed by means of optical flow based background oriented schlieren (BOS) using fully random (RR=100%) background patterns of varying speckle sizes (d_P) and speckle concentrations (N_I). A sample time averaged global temperature field is provided with the temperature information extracted over three locations for comparison with the thermocouple measurements.

Furthermore, investigating the influence of speckle size on the performance of optical flow based BOS, an accuracy jump between the patterns with d_P=1 pix and d_P>1 pix is attained. Using speckles with size d_P=2 pix and d_P=3 pix, much larger illumination regions are obtained providing high SNR of illumination gradient maps for the displacements induced over the backgrounds. Thus, the resultant temperature gradients are reconstructed with greater accuracy. The best reconstruction capability is attributed to the highest concentration of speckles (N_I=0.036) while no significant difference between the results of N_I=0.024 ppp and N_I=0.036 ppp is observed qualitatively. Nevertheless, when the error distribution over the entire low field is extracted, both the mean and median error values are observed to be lower with N_I=0.036 ppp for d_p=2 pix, indicating not only better temperature reconstruction accuracy but also higher precision (Fig. 4.2). Increasing the speckle size further to d_p=3 pix, the accu-

racy deficit between different levels of speckle concentrations gets even smaller. Going beyond the speckle size of d_P>3 pix, the accuracy of reconstruction is observed to be decreasing. As a result, the highest accuracy for RR=100% is obtained with d_P=3 pix at the given concentration levels as optical flow requires more densely populated patterns with smaller speckles to avoid large illumination features, which is analogical to peak locking for block matching (Scharnowski and Kähler, 2020).

4.2 Aerothermodynamics of transonic low-pressure turbine cascades

The straightforward setup of BOS enabled density gradient measurements within a single optical access turbine cascade which required a highly sensitive configuration to capture all relevant flow characteristics effectively. The flow field was analyzed from both time-averaged and time-resolved perspectives using two displacement detection algorithms: cross-correlation and optical flow. Compared to the cross-correlation results, the optical flow method provided smoother displacement trends and more reliable values across all critical regions of the FOV. BOS successfully detected shock-wave patterns, boundary layer thickness, shock-wave boundary layer interactions, trailing edge flows, and shock unsteadiness. The results were consistent with previous studies on shock-wave boundary layer interactions in LPT cascades under similar Mach and Reynolds number conditions.

BOS images visualizing the compressible flow features within the transonic blade passage for varying Mach and Reynolds numbers are provided in Fig. 4.3. The typical flow structures of a shock wave within a turbomachinery row were clearly detected. Just upstream the shock wave, the flow in the passage accelerates due to the passage geometry. When the sonic condition is reached, the passage chokes. Owing to the further contraction of the passage (boundary layer growth on suction and pressure sides), the flow suddenly compresses through a normal shock (Graham and Kost, 1979). Moreover, in fully convergent turbine cascades, shocks and expansion waves inside the cascade emanate from the blade trailing edge, and impinge on the adjacent blade suction side (Gostelow et al., 2009). From the BOS images in Fig. 4.3, it can be deduced that the shock intensity is correlated to the Reynolds number. Accordingly, the weakest shock intensity is captured for the lower boundary of the test matrix in terms of Reynolds number (Re_2=70×10^3). Then, as the Reynolds number is increased to Re_2=120×10^3, the passage shock gets stronger with a 57% increase in the captured displacement. This is promoted by the changing thickness of the boundary layers as the Reynolds number varies, which dictates the effective contraction ratio within the channel between the two turbine blades.

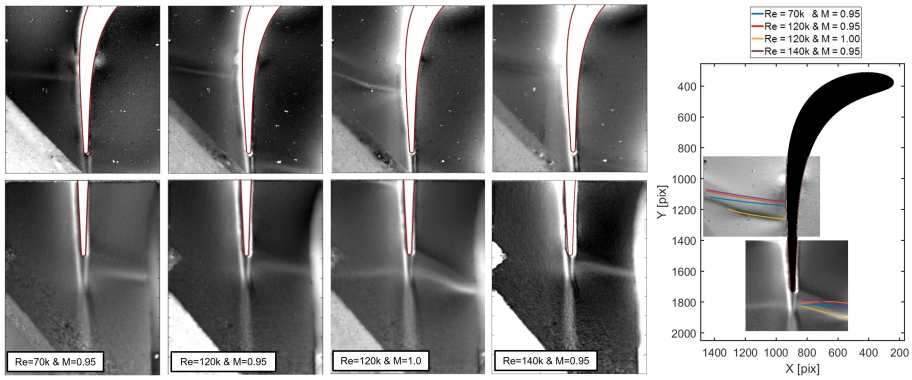

Figure 4.3: Visualization of shock impingement on the blade suction side and wake region for Re_2=70$\times$10^3 M_2=0.95 (1st column), Re_2=120$\times$10^3 M_2=0.95 (2rd column), Re_2=140$\times$10^3 M_2=0.95 (3rd column), Re_2=120$\times$10^3 M_2=1.00 (4th column) and reconstructed shock waves (5th column).

Furthermore, while the Reynolds number had a modest impact on the location of shock wave impingement, it significantly influenced the shock intensity. The orientation and behavior of the compressible flow features were observed to be insensitive to the turbulence level controlled by an upstream wake generator. In contrast, the Mach number affected both the shock impingement position and shock intensity. Additionally, the shock wave-induced boundary layer separation observed on the suction side of the turbine was compared with a previous experimental study by Lopes et al. (2022). The BOS results aligned with this study, indicating a boundary layer separation at $x/c \approx$0.68 for M_2=0.95 (where c refers to the chord length of the turbine blade). The FOV capturing the rear part of the turbine blade (at the bottom of Fig. 4.3) revealed the trailing edge flow topology. At M_2=0.95, the trailing edge shock was observed to emanate only from the pressure side, whereas for M_2=1, trailing edge shock waves were generated downstream of both the suction and pressure sides of the turbine blade. The shock waves for the various Reynolds and Mach numbers tested are plotted in Fig. 4.3(5th column). As a general trend, the shock wave originates closer to the trailing edge as the Reynolds number increases due to changes in the state of the boundary layer (Rossiter et al., 2022).

To detect the spatial orientation of the dominant modes of shock wave oscillations, proper orthogonal decomposition (POD) analysis was conducted on a focused region containing the shock wave. This analysis was performed for the highest Mach number case (M_2=1), with results presented in Fig. 4.4. The POD analysis targeted the fluctuating displacement across the shock wave. Mode 1, the most energetic mode, represents the average displacement of the shock wave. Mode 2 reveals closely spaced displacement peaks, indicating the unsteady and complex structure of the density field surrounding the shock wave. Mode 3's spatial function mirrors that of Mode

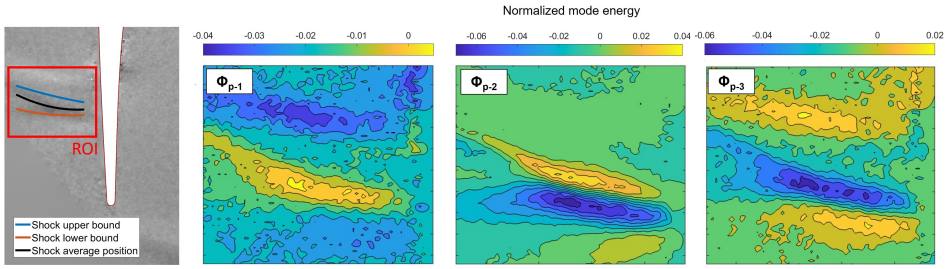

Figure 4.4: Proper Orthogonal Decomposition (POD) analysis on shock wave dynamics.

1 but with an opposite sign, accounting for phase-oriented relocation of the shock wave. This analysis was validated by reconstructing the displacement field. When only Modes 1 and 2 are considered, the shock wave's center remains stationary while its width and intensity fluctuate over time. However, Mode 3 causes the shock wave to shift in the streamwise direction. Further investigation is required to identify the sources of the shock wave instability.

4.3 Aeroacoustics of supersonic dual-stream co-axial jets

BOS optical measurements were used to characterize the complex interactions within the shock-cell structure when the dual supersonic streams of a coaxial jet interact under varying nozzle pressure ratios. The BOS data provided visualization of the density gradients both within and around the jets, facilitating the spatio-temporal decomposition of flow structures related to different noise generation mechanisms. The study confirms the presence of three primary noise mechanisms in supersonic jets operating under non-design conditions: Broadband Shock-Associated Noise (BBSAN), jet screech, and Turbulent Mixing Noise (TMN). For the dual-stream case, two BBSAN humps were observed, likely resulting from the interaction between the inner and outer shear layers with shock-cell structures. Jet screech, characterized by fundamental tones and their harmonics, was prominent in non-adapted cases. Mixing noise dominated the low-frequency spectrum, exhibiting a directional characteristic downstream. Overexpansion or underexpansion conditions, along with variations in secondary stream velocity, significantly impacted shock-associated noise and tonal components.

4.3.1 Flow characteristics of supersonic dual-stream co-axial jets

The analysis of the BOS measurements for different exit Mach numbers of the primary nozzle, with no flow through the secondary nozzle (Fig. 4.5), confirms a well-documented evolution in the jet structure (Norman et al., 1982; Raman, 1998). As the primary jet stream reaches supersonic speeds, the jet is overexpanded below the design Mach number (1.1$\leq M_P \leq$1.4). Hence, a conical shock wave attached to the lip of the nozzle exists which compresses the lower exit pressure to the ambient conditions. The shear layers acting as a contact discontinuity separate the jet stream from the surrounding air over which the pressure is constant while density varies (Fig. 4.5). A very distinctive feature of overexpanded supersonic jets can also be observed from the BOS results which is the increasing spacing of shock cells with increasing nozzle pressure ratio (increasing M_P). Since the nozzle is designed to have perfect expansion to ambient conditions at design condition, no shock structure is observed and the only density-varying feature is the shear layer that surrounds the primary jet stream for M_P=1.5. Finally, as the primary jet stream reaches M_P=1.6, the jet is underexpanded above the design Mach number with an expansion fan attached to the nozzle exit that is followed by a shock train.

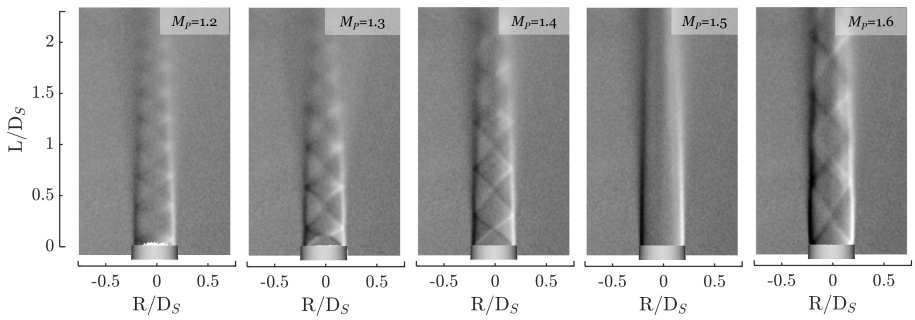

Figure 4.5: Visualization of radial density gradients reconstructed with background oriented schlieren (BOS) for varying primary jet Mach number (1.2$\leq M_P \leq$1.6).

Moving on to the dual-stream flow behavior illustrated in Fig. 4.6, as the secondary stream is accelerated to 1.2$\leq M_S$, the regular shock-shock interaction (RI) observed at the primary jet centerline transitions to Mach interaction (MI) which is captured as a quasi-normal shock segment (Hornung, 1986). The intensity of the MI is observed to increase between M_S=1.2 and M_S=1.3 in which the shock wave generated at the primary nozzle lip inside the secondary jet stream reflects from the outer shear layer and penetrates into the primary jet stream. Accordingly, the opening angle of the initial shock wave is observed to be detrimental in terms of its influence on the primary jet behavior. For M_S<1.4, the opening angle is small, hence the reflected shock impinges too closely to the RI of the first conical shock wave inside the pri-

mary jet stream leading to the MI. As the M_S increased, the sizes of the shock cells are increased which also increases the angle between the shocks and the radial axis.

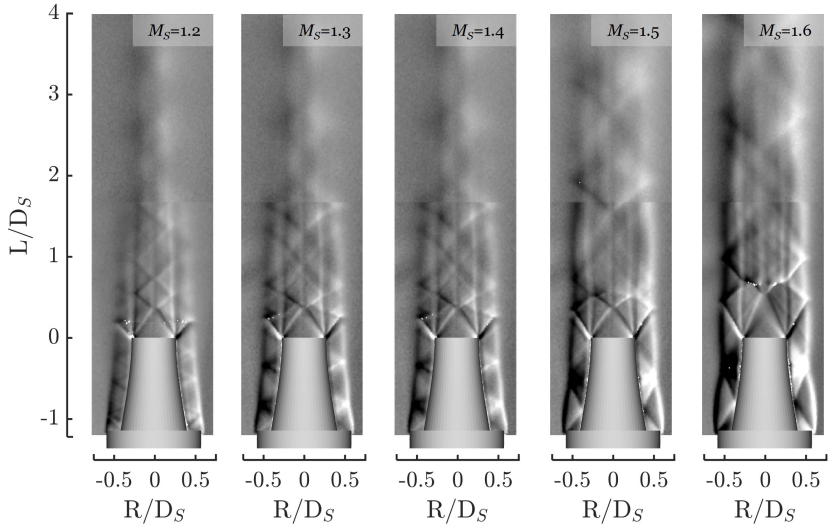

Figure 4.6: Visualization of radial density gradients reconstructed with background oriented schlieren (BOS) for the constant primary jet Mach number (M_P=1.5) and varying secondary jet Mach number (1.2$\leq M_S \leq$1.6).

Increasing the Mach number beyond the design condition leads to an underexpanded jet, hence the expansion fan appears attached to the lip of the secondary nozzle. As the shear layers of the secondary nozzle follow a concave curvature, the flow experiences a compression which leads to the generation of the barrel shock that is followed by a shock train due to the reflection of the shocks between the outer shear layer and the primary nozzle surface. Finally, the combined shock cell structure observed for the design condition is stretched significantly at each Mach number increment over M_S=1.4. This leads to the presence of MIs not only for shock-shock interactions between the secondary and primary streams, but also within the core flow of the primary stream itself. Thus weakening the intensity of the compressible flow features downstream of the first interaction zone.

4.3.2 Noise characteristics of supersonic dual-stream co-axial jets

Following the seminal work of Tam (1995), three different types of noise-generating mechanisms are present in supersonic jets operating under non-design conditions: broadband shock-associated noise (BBSAN) (André et al., 2013), jet screech (Raman, 1999), and turbulent mixing noise (TMN) (Jordan and Colonius, 2013). The latter is produced by coherent turbulent structures traveling downstream the jet, the so-called

wavepackets (Maia et al., 2019; Cavalieri et al., 2019), and is present in subsonic and supersonic regimes. Jet screech and BBSAN are due to the interaction between the spatio-temporal wavepackets and the quasi-steady shock-cell structures. BBSAN is a non-discrete noise mechanism that dominates the sideline directions and the high frequencies (Wong et al., 2021). On the other hand, jet screech is a tonal sound mechanism, caused by a self-reinforcing feedback loop (Edgington-Mitchell et al., 2021).

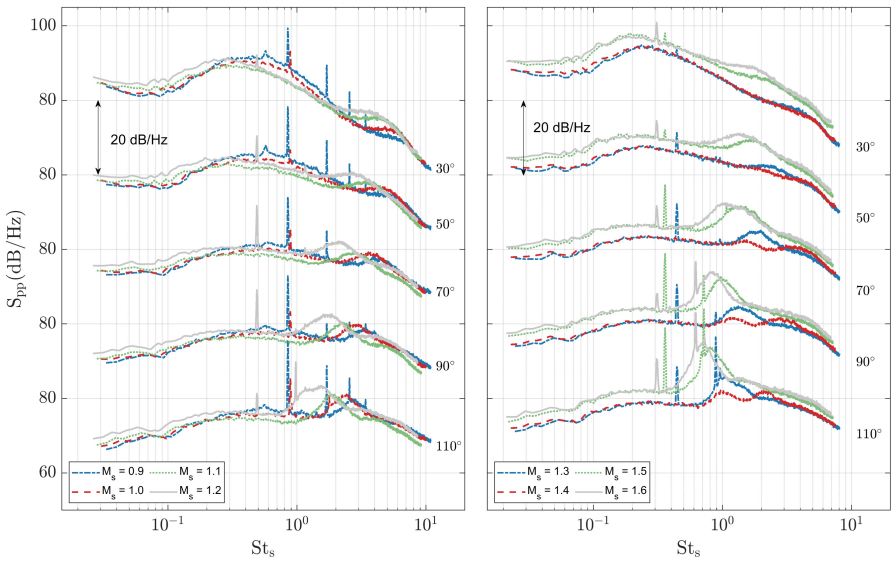

Figure 4.7: Far-field noise spectra at different polar angles for the dual-jet case with $0.9 \leq M_S \leq 1.2$ (left) and $1.3 \leq M_S \leq 1.6$ (right) at constant primary nozzle pressure ratio (M_P=1.5).

Fig. 4.7 demonstrates the sound spectra reconstructed from far field microphone measurements for the cases with varying secondary nozzle isentropic Mach number $0.9 \leq M_S \leq 1.2$ while primary nozzle is kept at M_P=1.5. Focusing on the acoustic signature of the dual supersonic stream cases (Fig. 4.7, right), it is noted that for all four conditions within this range, the maximum contribution of TMN occurs around St_s=0.25. For all cases except the baseline at M_S=1.4, both the fundamental tone and its first harmonic are identified, increasing in intensity as the observer moves towards upstream directions and shifts towards lower St_s values with increasing M_S. A reduction in the contribution of BBSAN is observed in the baseline case at M_S=1.4, which exhibits two distinct humps of similar intensity (clear from 70° and beyond) and no tonal contribution. Even in the other cases, the high-frequency BBSAN hump is present, which is presumably related to the interaction between the outer shear layer and the shock-cell structures, reaches a maximum at 110° and M_S=1.6, where it is

12 dB higher than the maximum TMN contribution.

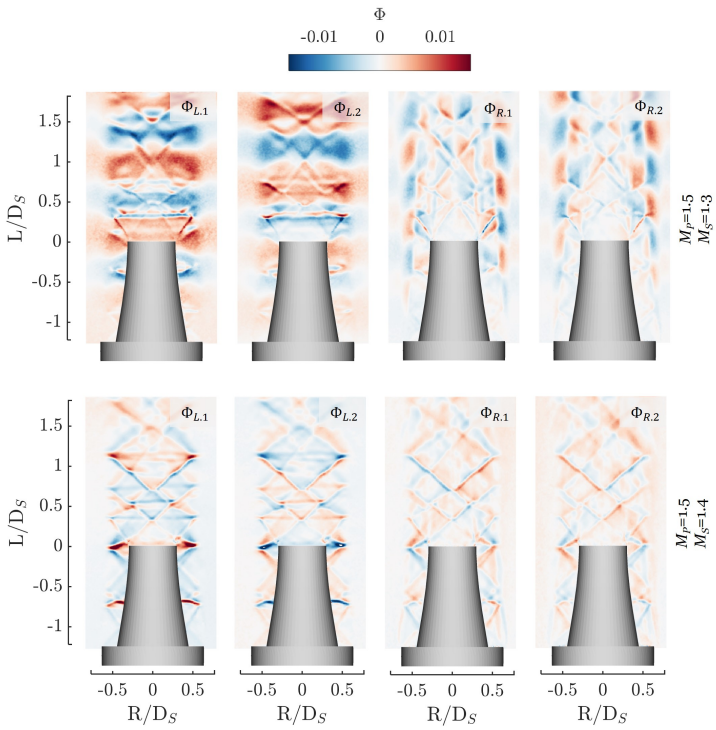

Figure 4.8: Visualization of 1st and 2nd POD modes of radial and axial density gradients reconstructed with background oriented schlieren (BOS) for M_S=1.3 (1st row) and M_S=1.4 (2nd row) at M_P=1.5.

In order to understand the contribution of compressible flow features to the noise generation mechanisms, the dominating spatial flow field features are decomposed via performing a proper orthogonal decomposition (POD) analysis. Fig. 4.8 shows leading modes of density gradients along the jet axis and the radial direction for two different cases. At constant primary nozzle pressure ratio (M_P=1.5), for M_S=1.3 a strong interaction is observed between the vortices in the shear layers of the secondary nozzle and the shock structure (Fig. 4.8, 1st row). The K-H instabilities at the exit of the secondary nozzle are amplified as they propagate downstream and the local eddy size increases. As these larger eddies reach the exit of the primary nozzle, they interact with the shock-cells generated between the two supersonic streams, increasing the intensity of the turbulent structures. This leads to a strong interaction between the shockcells and the viscous instability within the shear layers leading to the noise generation mechanism, referred to as screech. The noise spectra extracted from microphone measurements also highlights the existence of screech tones (Fig. 4.7, right). On the other hand, in case of M_S=1.4 there is no strong periodic unsteadiness captured that relates to the the vortices in the shear layers. Instead, the dominant unsteadiness is

purely associated with the localized oscillations of the shock structures. Thus, any constructive interference between the shear layer instabilities and the shockcells is demolished, preventing the generation of screech tones (Fig. 4.7, right).

4.4 Aerodynamics of supersonic flows

In order to assess the respective capabilities of background oriented schlieren (BOS) and various computational approaches for capturing flow structures to relevant high-speed aviation platforms, a joint experimental and numerical analysis of a full scale wind tunnel scenario with a 10° wedge exposed to Mach 3.5 supersonic conditions is performed. The experimental data is acquired by means of a background oriented schlieren (BOS) setup where the optical flow (OF) based reconstructions are compared against the ones obtained via cross-correlation (XCOR). Superior characteristics of resolution and sensitivity is observed with OF which allows higher accuracy reconstructions of density variations. Moreover, numerical simulations are performed with different modeling strategies which yielded a dataset with variations in flow field structures that are key to accurate description of the flow physics. In this regard, the impact simulation domain definition, the treatment of temporal domain and turbulent structures are investigated against the experimental results while highlighting the specific features of the BOS measurement technique in use for validation studies.

4.4.1 Assessment and application of optical flow in background oriented schlieren for compressible flows

Initial assessment of the experimental results is performed by analyzing the reconstructed flow structures of the supersonic flow over the two models. Fig. 4.9 (left) denotes a strong conical shockwave attached to the nose of the ogive. Although this shock is generated with a conical form at the tip, its angle reduces towards the downstream of the model. On the other hand, the leading edge shock of the wedge is observed to be straight due to the planar structure of the model (Fig. 4.9, right). Yet its thickness increases further away from the model due to the end wall effects of a relatively low aspect ratio test section (Wang et al., 2015). Downstream of the oblique shock, the supersonic flow proceeds towards the expansion shoulder of the wedge where it re-aligns with the incoming stream and generates a strong expansion fan.

The increased resolution brought by OF enables a sharper identification of the shock location at the tip both with RD (Fig. 4.9, 2nd row-left) and WN (Fig. 4.9, 3rd row-left) backgrounds compared to XCOR (Fig. 4.9, 1st row-left). The differences between the utilized reconstruction approaches become more severe when finer details in the weak

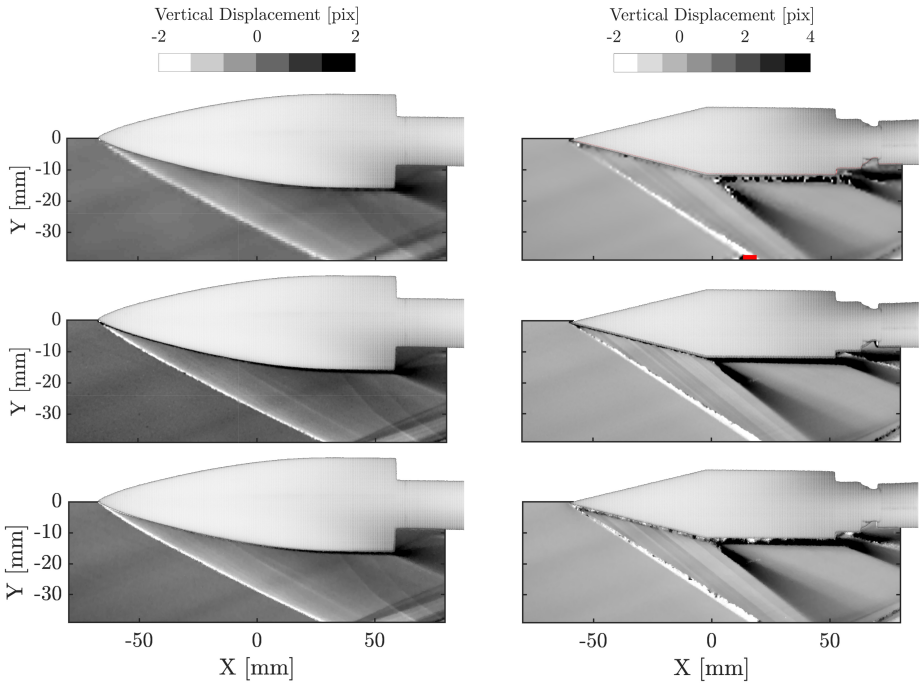

Figure 4.9: Time averaged vertical displacements for supersonic flow past von Karman ogive (left column) and 10^{o} wedge (right column) reconstructed with cross-correlation (1st row), optical flow with random dot (2nd row) and wavelet noise (3rd row) backgrounds.

expansion region over the ogive surface is investigated (Fig. 4.9, 2nd & 3rd rows-left). Moreover, the clarity of the flow features in the base region of the ogive (separated shear layer, the lip shock and the reattachment shock) further highlights the increased resolution characteristics of OF against XCOR (Fig. 4.9, 1st row). In addition to the resolution limit, the bandwidth limited characteristic of XCOR restricts the dynamic range of the ray displacements. Hence, in close proximity of the expansion shoulder, the displacement magnitudes reach beyond ∼8 pixels which is above the resolvable limit of 16×16 pix^2 IWs with 50% overlap. Thus, in combination with the spatial smoothing effect, the displacements are severely underestimated (Fig. 4.9, 1st row). Nonetheless, in regions further away from the model where the density gradients are more outspread with lower amplitudes, the displacement vectors are reconstructed with similar accuracy using both XCOR and OF based approaches (Fig. 4.9, right).

The density profiles over three lines (Y=-17mm, -21mm and -25mm) are extracted to perform quantitative comparisons with the theoretical values of density variations across the shock wave and the expansion fan (Fig. 4.10). Even though the OF based approaches are able to capture a higher increase of density, the results are observed deviate up to 70% of the theoretical values for the oblique shockwave. This is mainly

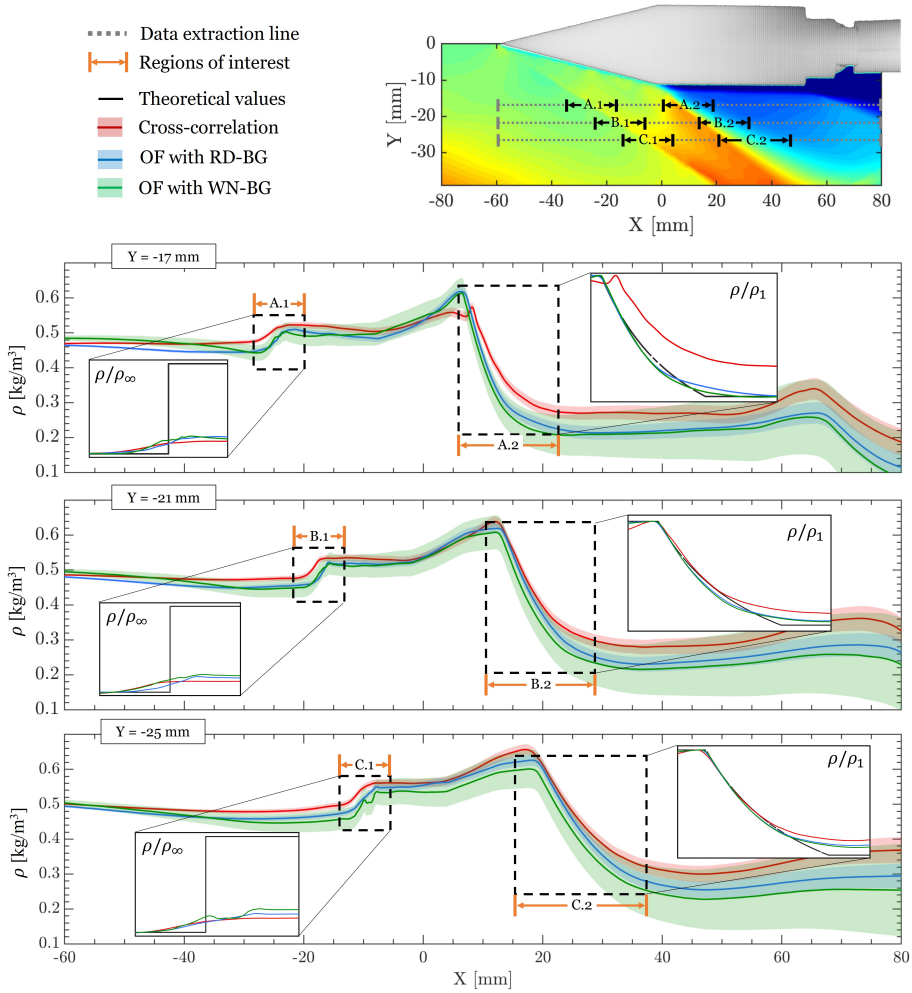

Figure 4.10: Time averaged density variations over the flow fields of 10^o wedge at Y=-17mm (top), Y=-21mm (middle) and Y=-25mm (middle).

governed by the fact that the density variation across the shockwave is not resolvable due to the optical limitations of the setup. Regarding the expansion fan, a good agreement of the density variations using OF in comparison to the theoretical values is obtained closer to the model, while measurements with XCOR are significantly off from the theory (Fig. 4.10, top-A.2). This is a clear quantification of the inaccuracies introduced by the combined effect of the bandwidth filtering and lower resolution of the XCOR method in comparison to the multi-scale reconstruction algorithm of OF based deflection sensing. Yet, reducing the effective resolution of the schlieren object in order to have the background in focus causes density gradients to be dissipated

even for OF. Additionally, the smoothness constraints associated with OF prevents displacements to be discontinuous which is a severe limitation for capturing the edges of the theoretical expansion fan. Moreover, further away from the model the differences between the XCOR and OF reconstructions are reduced owing to the mitigated localization of the expansion fan and the corresponding reduction in the amplitude of the density gradients.

4.4.2 Investigations of shock wave boundary layer interactions at high Reynolds numbers

The flow feature composition of a SBLI scenario is well explored via various experimental and numerical approaches (Gaitonde, 2015). Yet there is a lack of comparative studies especially within a practically interesting Re range and dimensional specification. Hence, the case of a 10° wedge exposed to Mach 3.5 supersonic flow in a full scale wind tunnel operating at a high Re ($Re_{1/m}$=46.8×10^6 1/m and $Re_{\theta_{M_\infty}} \sim 10^4$) provides a unique scenario in which the influence of various upstream features on the formation of the SBLI can be investigated (Fig. 4.11). Accordingly, a comparative study is comprised of experimental data acquired by means of BOS and numerical simulations performed using two different turbulence treatment methods; Reynolds Averaged Navier Stokes (RANS) and Large Eddy Simulations (LES). Regarding the RANS setup, due to its superior accuracy in similar computational studies involving interactions of shock waves with boundary layers (Boychev et al., 2021), the $k-\omega$ SST turbulence model is employed (Menter, 1994). In the case of LES, the influence of the fluctuations stored in the subgrid scales is computed by solving a transport equation for the subgrid-scale turbulent kinetic energy proposed by Kim and Menon (1995) as the localized dynamic k_{sgs} equation model (LDKM).

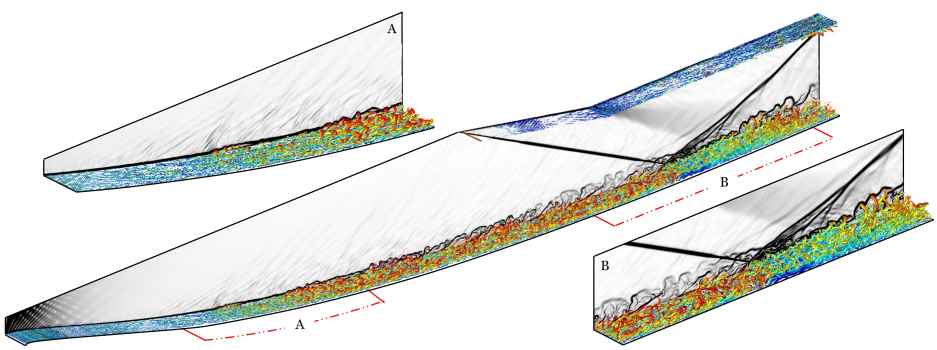

Figure 4.11: Instantaneous flow structures over the wind tunnel walls demonstrated via isosurfaces of $0.01(\lambda_2)_{max}$ (colored by the Mach number distribution) and distribution of density gradient magnitude.

Analyzing the flow structures of the incidence shockwave turbulent boundary layer interaction captured by the experimental data, the shockwave generated at the leading edge of the wedge (Fig. 4.12, C1) impinges on the boundary layers developing over the walls of the nozzle contour (Fig. 4.12, BL2). Upon the impingement, a reflected shockwave (Fig. 4.12, C3) is generated whose foot (Fig. 4.12, C2) is resolved to be upstream of the incident shockwave impingement location. This indicates the presence of a separation region induced by the strong adverse pressure gradients (Fig. 4.12, C1). The separated shear layers act as an effective compression surface to move the foot of the reflected shock upstream. Downstream of the reflected shockwave, an expansion fan (Fig. 4.12, E2) is generated, notifying that the size of the separation bubble is sufficiently large to create a crest over which the flow following the separated shear layer experiences a strong deflection towards the wind tunnel wall. As the flow passing through the expansion fan gets deflected towards the surface, the separated shear layer reattaches to the nozzle wall. The flow following the shear layer gets compressed gradually through a series of weak compression waves which coalesce to form the reattachment shock (Fig. 4.12, C4).

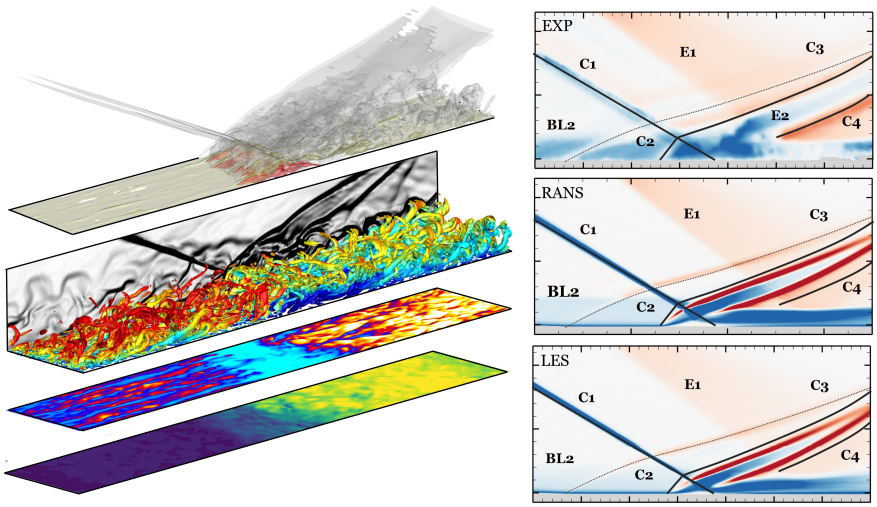

Figure 4.12: Instantaneous flow structures within the SBLI region demonstrated via isosurfaces of pressure gradient magnitude (gray), sonic surface (gold) and flow reversal region (red)(left-1st row), isosurfaces of $0.01(\lambda_2)_{max}$ (colored by the Mach number distribution) and distribution of density gradient magnitude (left-2rd row), surface skin friction (left-3rd row), pressure coefficient distributions (left-4th row). Steady-state (RANS) and time averaged (BOS and LES) vertical density gradient distributions within the SBLI region (right).

The differences between the results obtained with RANS and LES, and the experimental data are concluded to be mainly driven by the treatment of the temporal domain and the turbulence closure method. In the case of LES, the resolution of turbulent fluctuations provided a superior accuracy of capturing the physics involved within the formation of boundary layers which in turn affected the flow features develop-

ing over the wedge as well as dictating the formation of the flow structures within the region of SBLI. In this regard, better agreement with the experimental data in terms of capturing the effective viscous surface is denoted with LES. On the other hand, the absence of transition modelling in the case of RANS led to the premature imposition of fully turbulent boundary layers. This not only impeded with accurate capturing of the density jump accuracy over the oblique shock, but also caused an overprediction of the flow retardation close to the wall within the boundary layers while the latter contributed to the overestimation of the shear layer separation within SBLI. Moreover, the comparisons of 2D and 3D mesh configurations demonstrated the differences between wall-resolved and wall-modelled approaches on capturing the flow features accurately. Although the wall resolved approach enabled RANS to have more cells within close proximity of the wall, the overestimation of the separation region induced by time averaging and underestimation of incoming boundary layer momentum could not be avoided. Contrarily, the wall modelled LES required wall functions to compute the flow properties in the wall adjacent cells. Nonetheless, a greater agreement of the LES results with the relevant physical phenomena that the experimental data represents was noted as well as considerably good agreement with the higher fidelity simulation results provided in the literature.

4.5 Hypersonic shockwave boundary layer interactions

In order to assess different optical configurations for BOS setups and demonstrate the performance of BOS in comparison to conventional schlieren in a challenging scenario, BOS measurements of transitional shock-wave/boundary-layer interactions in hypersonic flow are performed using entocentric (ento-BOS) and telecentric (tele-BOS) optical configurations. Although tele-BOS is proposed to resolve the drawback of defocusing by increasing the depth of field of the optical setup significantly (Ota et al., 2015; Cozzi et al., 2017), its applications involve a trade-off between the attainable depth of field and spatial resolution. This contradicts with the need to use cameras capable of recording at high acquisition frequencies for high-speed testing environments due to their low spatial resolution specifications. Moreover, the telecentric imaging configuration for BOS requires large focusing mirrors with a suitable focal length. This can be inferred as an argument opposing the superior scalability and adaptability of BOS. Thus, justifying the use of a telecentric setup requires proper assessment of the accuracy and precision deficit between ento-BOS and tele-BOS, which is performed via comparing the resolution and sensitivity of the flow visualizations obtained via BOS against conventional schlieren images, numerical simulation, data and oil surface visualizations.

Fig. 4.13 provides results from laminar numerical simulations, conventional schlieren

images with two different FOVs (global-left and focus-right), as well as surface oil flow visualizations, which illustrate the physical phenomena taking place as the Mach 5 freestream interacts with the cone-flare model. Due to the slightly blunt leading edge of the model, a bow shock detached from the nose of the cone is present (Fig. 4.13, C1). The hypersonic flow following the surface of the cone interacts with the compression corner yielding a conical shockwave (Fig. 4.13, C2), separating the boundary layer over the cone, which leads to a recirculation zone surrounding the cone-flare joint (Fig. 4.13, R). As the adverse pressure gradients propagate upstream within the subosnic portion of the boundary layer, the flow reversal region grows towards upstream and moves the shock foot upstream (Fig. 4.13, S). The recirculation region accordingly separates the incoming boundary layer forming a shear layer which reattaches to the surface of the flare generating a reattachment shock (Fig. 4.13, C3). The concave curvature of the effective compression surface with the adverse pressure gradients yields the generation of Görtler vortices (Fig. 4.13, G), and transitions the boundary layer to turbulent state as the instabilities within the shear layer are significantly amplified (Knight and Mortazavi, 2018).

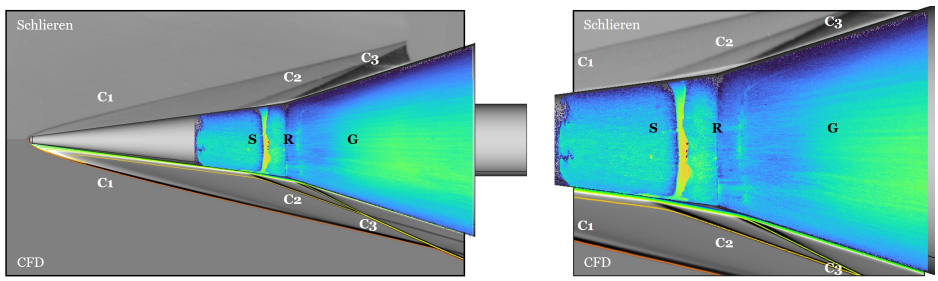

Figure 4.13: Time averaged horizontal knife-edge schlieren images, surface skin friction lines extracted by surface oil flow visualization and steady state vertical density gradients computed via numerical simulations.

Starting with the ento-BOS configuration, the overall flow topology is captured with very good agreement in comparison to the knife-edge schlieren images which were already shown to match the CFD and oil flow visualization results. Regarding the bow shock and separation shock, the knife-edge schlieren data is observed to have a slightly higher signal to noise ratio compared to the BOS data (Fig. 4.14, top). This is due to the fact in BOS the schlieren features are defocused in order to focus on the background pattern and the small aperture settings induce a diffraction induced loss of resolution in order to maximize depth of field. Moreover, there is a certain neighborhood dependency induced by the choice of regularization constant which is necessary to prevent spurious vectors. Finally, the shockwave is a source of strong shadowgrapy effects. In the case of conventional schlieren, these are superimposed over the schlieren effects, enhancing the signal intensity treated as positive density gradient changes across the shock. However, in the case of BOS images, shadowg-

raphy effects induce an image blur without any apparent motion of the background pattern. Thus, the resolution and sensitivity of displacement detection over the shock-wave reduces. Nonetheless, one major disadvantage of schlieren over BOS is the large mirrors mounted with a long separation distance to enhance sensitivity. Therefore, it becomes vulnerable to vibrations causing the focal point of the schlieren light beam to vary with respect to the knife-edge location, varying the sensitivity of the schlieren setup during image acquisition. These vibrations are almost completely eliminated with the BOS setup since an optical path of in total 2 m (from BG to camera) is sufficient to capture flow features with similar resolution and sensitivity in comparison to ∼10 meters for the optical path length of the knife-edge schlieren setup.

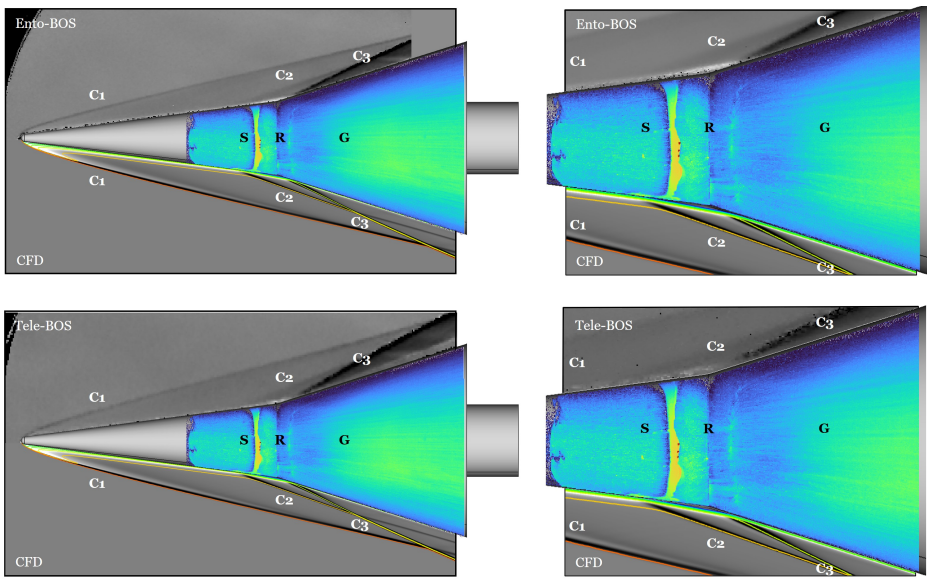

Figure 4.14: Time averaged vertical density gradients reconstructed by entocentric (top) and telecentric (bottom) background oriented schlieren (BOS) setups, surface skin friction lines extracted by surface oil flow visualization and steady state vertical density gradients computed via numerical simulations.

The comparison between entocentric and telecentric optical configurations reveals that the key factor relating the differences between the results of two optical configurations is the choice of imaging lenses and it's impact on the depth of field. In the telecentric setup, using a large focal length objective drastically reduces the depth of field, amplifying defocusing of the schlieren object. Conversely, using a small focal length objective increases the depth of field but expands the field of view, resulting in a smaller portion of the imaging sensor being covered by the flow field, leading to a noticeable reduction in resolution (Fig. 4.14, bottom). Additionally, the reduced sensor coverage diminishes illumination intensity, which is already limited by the additional diaphragm to eliminate non-parallel light rays from the background. Regarding the

flow structures captured in the displacement fields, the bow shock intensities remain comparable between ento-BOS and tele-BOS, and the resolution of the reattachment region does not significantly degrade when transitioning to tele-BOS. A key advantage of tele-BOS is the reduction of perspective effects, which improves the resolution of the transitioning boundary layer downstream of the reattachment zone. However, tele-BOS captures the flow reversal region with lower intensity, a consequence of both the lower spatial resolution of the imaging configuration and the reduced depth of field. The latter is particularly critical when focusing on the cone-flare intersection, where a reduced depth of field introduces significant geometric blurring and diffraction effects, degrading the imaging quality of background features near the model (Fig. 4.14, bottom-right). These regions are where the flow field features of interest, such as the separation region, are located, resulting in diminished reconstruction quality of density variations induced by flow features near the model. Thus, although tele-BOS increases the optical setup's complexity, ento-BOS, with an appropriate choice of conventional imaging lenses and setup parameters, achieves more accurate results with a more flexible configuration composed of fewer components, provided the same image acquisition tools are used for both setups.

4.6 Laminar burning velocity measurements on Bunsen burners

Ease of application and the possibility for versatile adaptability to different experimental settings promoted BOS as an alternative non-intrusive optical measurement technique for the extraction of laminar burning velocity (LBV) information. This is further supported by the direct relationship between temperature gradients and refractive index variation under known pressure conditions, which allows BOS to preserve superior accuracy regardless of any change in luminosity (e.g. hydrogen flames or flameless combustion processes operated under dilute conditions) or other experimental settings. It is shown that the availability of vectorial displacement field provides unique opportunities for maximizing reconstruction accuracy and precision which is a clear superiority of BOS over standard schlieren approaches. Overall, BOS provides a significant agreement with available data in the literature and the chemiluminescence imaging results which can match the low complexity specifications. Even though Bunsen burners are associated with certain limitations, the burner setup does not restrict the capabilities of BOS for LBV measurements, which can also be used in spherical flames, flat flames, etc.

4.6.1 High-pressure Bunsen burner

The experiments are performed with n-heptane and bio jet fuels. Prior to mixing with air, both liquid fuels are evaporated and transferred to the mixing chamber via heated stainless steel pipes. Although the pipes are covered with thermal isolation material and heated throughout the fuel supply system, significant deviation of the fuel/air mixture temperature from the desired settings is observed upon injection into the combustion chamber. Accordingly, although the measurements are performed for both fuels over a ϕ range of $0.8 \leq \phi \leq 1.5$, the suboptimal thermal configuration of the fuel supply system caused significant stability issues for flames at low ϕ values. As this issue was too pronounced for the bio-jet fuel measurements, only results of n-heptane are reported here.

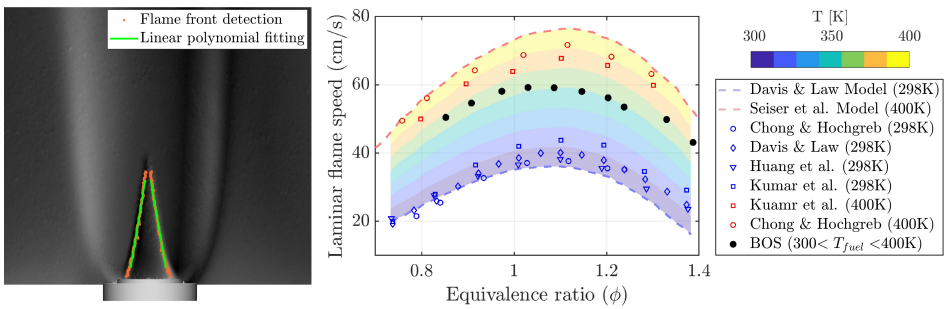

Figure 4.15: Time averaged density gradient magnitude and flame front detection on the Bunsen burner (left). Laminar burning velocity of n-heptane/air mixtures at 1 atm extracted by means of background oriented schlieren (BOS) in comparison to modeling and experimental data from literature (Davis and Law, 1998; Huang et al., 2004; Kumar et al., 2007; Chong and Hochgreb, 2011).

Once the images are processed with optical flow, horizontal and vertical displacements induced by the temperature gradients over the flame are reconstructed. This allows post analysis to be performed either directly on the vectorial components of the displacements or various derivatives such as vector magnitude and second order gradients. After analyzing the images and the data set constructed, horizontal density/temperature gradients (radial with respect to the burner axis) are utilized to capture the flame front position and orientation. The flame front is reconstructed by scanning both sides of the burner radially at different longitudinal coordinates along the flame height during which the flame front location is identified as the location of maximum radial temperature gradient. Then the extracted coordinates are classified based their longitudinal location with respect to the burner exit and the flame tip. In accordance with Hu et al. (2018), the central (60%) portion of the flame is selected for the LBV calculation. This prevents flame stretching effects at the tip and heat loss to the burner affecting flame speed calculations as they yield deviations from the theoretical conical shape.

Fig. 4.15 shows the LBV variation with ϕ captured via BOS plotted against available experimental and modeling data from literature, given at different injection temperatures of n-heptane/air mixtures. The overall trend of the LBV variation with ϕ is consistent with the reference datasets since the computed LBV values reside between 380K and 350K. This is an expected result due to the aforementioned issues regarding the fuel supply system. At low ϕ values a proximity to the LBV data that corresponds to a higher mixture temperature is observed while the opposite is valid for the high ϕ settings. This can be explained due to the increasing mass flow rate of liquid fuel which reduces the residence time of the fuel as it passes through the portion of fuel supply system that is actively heated. Although the uncertainties involved with these measurements hindered the possibility of showcasing the full potential of BOS as an alternative approach for calculating LBV, they acted as a preliminary assessment for the approach and allowed further tailoring of the post processing algorithms for improved precision of flame front reconstruction, which is explained in detail in the following section.

4.6.2 Atmospheric Bunsen burner

The experiments using the atmospheric Bunsen burner setup were performed with CH_4/air mixtures with equivalence ratio (ϕ) varied over a range of $0.8 \leq \phi \leq 1.4$. During burner operation, some instabilities in the flame position and orientation were observed. In order to capture unsteady effects and prevent flame front broadening due to averaging in time, the acquired images are processed instantaneously. This enables the extraction of probability distributions of the instantaneously computed LBV for the acquisition of temporal statistics.

The time-averaged flame structures are reconstructed via chemiluminescence (Fig. 4.16, 2^{nd} column) and BOS (Fig. 4.16, 3^{rd} to 6^{th} columns). The bright luminosity from the radicals indicates the flame front position and orientation in the chemiluminescence images. Whereas the high displacement magnitude caused by the localized high-amplitude temperature gradients visualize the reaction zone in the case of BOS. As seen in Fig. 4.16 (1^{st} column), the raw photos of the flame already provide a clear indication of the shape and position. The approaches employed for the reconstruction of the flame front using BOS rely on features represented by different intensity fields. The horizontal displacements are induced by the refractive index gradients parallel to the burner exit plane. Hence, they enable an accurate description of the central portion of the flame since the conical apex angle (α) of the flame is smaller than 45^o. The flame front can then be captured as the outer edge in Fig. 4.16 (3^{rd} column). On the other hand, using vertical displacements, a complete flame surface can be captured since the flame tip and skirts induce refractive index changes in the vertical direction

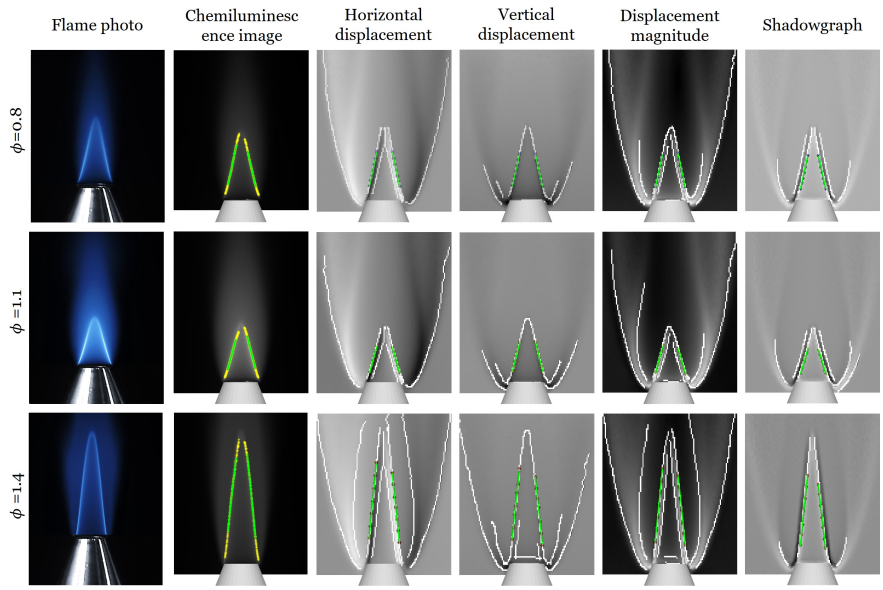

Figure 4.16: Raw photos of the flame (1st column), flame front detection with chemiluminescence imaging (2rd column) and background oriented schlieren (3rd to 6th columns) for different equivalence ratios (ϕ).

due to their curvature. Moreover, using the displacement magnitude, a higher contrast intensity field is obtained, which is beneficial for the flame front detection as it relies on sharp gradients of pixel intensity values. The ability to extract a shadowgraph image from the displacement field by computing the Laplacian is again unique to BOS. The Laplacian represents the regions of high rate of change of displacement amplitudes, and it provides a clear definition for the boundaries of the flame front and the secondary heating zone.

A comparison of laminar burning velocities extracted using BOS against direct chemiluminescence imaging, 1D numerical simulations and experimental data from literature is provided in Fig. 4.17. Overall, a considerably good agreement is present with the 1D simulations. Hence, these results confirm a high accuracy of LBV measurements using Bunsen burners, provided that the region of regularization over the flame front is selected appropriately (Hu et al., 2018). However, there are differences among the employed image processing approaches which need to be addressed. In the case of lean and rich mixtures, for which LBV values are lowest, the apex angle of the conical flame reduces. This enables an increased precision for flame front reconstructions using the horizontal displacement field. Contrarily, for equivalence ratios at which the LBV is maximized ($\phi \sim 1$), the increasing cone angle refers to a smaller flame with the flame font approaching the horizontal axis. This reduction in horizontal displacements lowers the precision of extracted LBV values through the images of

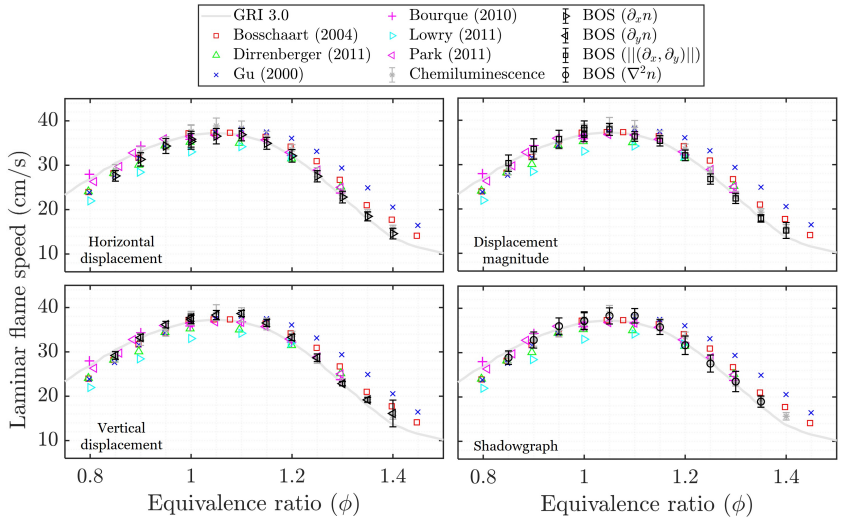

Figure 4.17: Laminar burning velocity of CH_4/air mixtures at 298K and 1 atm extracted by means of background oriented schlieren (BOS) in comparison to direct chemiluminescence imaging, 1D numerical simulations and experimental data from literature (Bosschaart and de Goey, 2004; Dirrenberger et al., 2014; Gu et al., 2000; Bourque et al., 2009; Park et al., 2011; Lowry et al., 2011).

$\partial_x n$. The opposite is valid for the flame front reconstructions performed using the vertical displacement field. For $\phi \sim 1.1$, the flame tip approaches towards the burner rim, increasing the cone apex angle. Hence, the weighting on the refractive index gradients oriented in the vertical direction increases, providing suitable conditions to reconstruct the flame front and compute the LBV more precisely.

Flame front reconstructions and LBV computations performed using the displacement magnitude field reveal symptoms from the results obtained with the individual vector components. As such, the low precision of LBV computations for conditions with reduced cone angle is inherited from horizontal displacements. For $1.1 \leq \phi \leq 1.35$, the reconstructions with the displacement magnitude are considerably precise and accurate. Similarly, the reduced precision for the richest mixture (ϕ=1.4) originates from the contribution of $\partial_y n$. Nevertheless, the overall best match with the results of the GRI 3.0 mechanism is obtained using the displacement magnitude field. Finally, using the shadowgraph field, despite the good agreement, an additional numerical discretization error exists, which contributes to the slightly amplified uncertainty range. Yet, the high contrast edge information provided to the flame front reconstruction procedure enables relatively constant precision for all the evaluated ϕ values.

4.7 Swirl-stabilized turbulent flames in gas turbine combustors

The experiments on the CeCOST model stationary gas turbine combustor are performed with premixed methane (CH_4) and air using both confined and unconfined configurations. Throughout the measurements, the full operating condition range of the CeCOST burner with Reynolds number ranging between $10\times10^3 \leq Re_D \leq 20\times10^3$ is scanned at different equivalence ratios. The flame behavior of the CeCOST burner can be classified in three different regimes as lean blow-off, stabilized flame and flashback. While the lean blow-off limit is almost constant for the entire range of Reynolds numbers considered, the flashback limit is around ϕ=0.6 at lower Reynolds numbers and increases rapidly around Re=20×10^3 indicating that the flame can be stabilized in a wider regime for even larger Re. Accordingly, the BOS images are acquired at two different Reynolds numbers (Re_D=10×10^3 and Re_D=20×10^3) and at three different equivalence ratios (ϕ=0.7, ϕ=0.72 and ϕ=0.8). The images are processed with the optical flow image processing algorithm and the reconstructed displacements are represented in terms of instantaneous and time-averaged displacement magnitude within a region of interest 10cm downstream from the premixing tube exit. The displacement magnitudes indicate the shape, intensity and orientation of the premixed flame, reaction zone and integrated heat release. Moreover, they are directly correlated to the intensity temperature gradients, which due to constant atmospheric pressure environment.

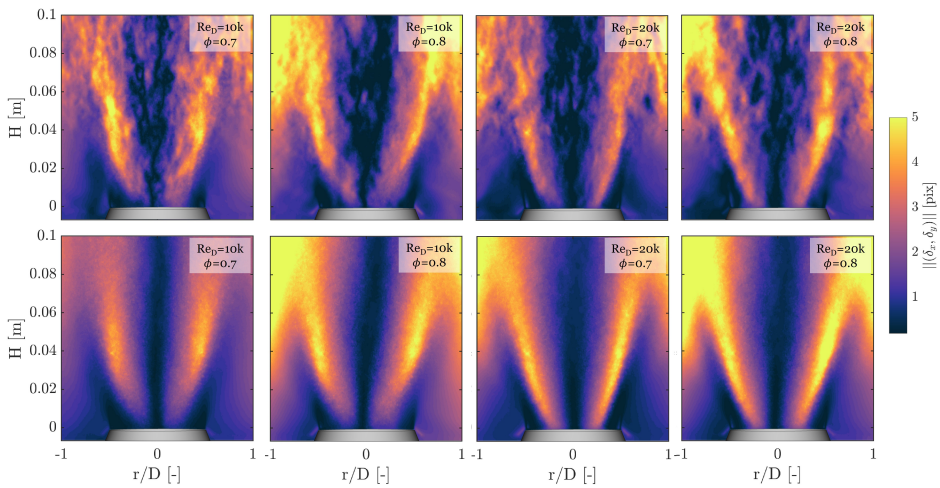

Figure 4.18: Instantaneous (top) and time-averaged (bottom) displacement magnitudes reconstructed via background oriented schlieren (BOS) for varying operating conditions.

Fig. 4.18 shows that the flame is stabilized in the combustion chamber for both Re_D=10×10^3 and Re_D=20×10^3 at ϕ=0.7 and ϕ=0.8. The density magnitude contours reveal the conical shape of the flame with the high intensity of heat release concentrating over the outer shear layers of the swirling air-fuel mixture. The swirling mixture leads to a vortex breakdown provided that the swirl intensity is sufficiently high which stabilizes the flame within a central recirculation zone (CRZ) (Billant et al., 1998; Stone and Menon, 2001). Subash et al. (2020) performed particle image velocimetry measurements in previous experimental investigations to determine swirl number to be S=0.6 for both cases, using the ratio between tangential momentum and axial momentum normalized by the mixing tube radius (Hodzic et al., 2018). Hence, the high tangential momentum, indicated by the magnitude of the swirl number, generates centrifugal forces causing a strong radial pressure gradient and the occurrence of the CRZ. Moreover, as the fuel/air mixture exiting the mixing tube expands into the combustion chamber, an outer recirculation zone (ORZ) is created between the swirl cone and the flange of the combustion chamber. However, due to the unconfined conditions used during the acquisition of BOS images, the ORZ is much smaller compared to the confined configuration. This is mainly due to the large mass flow entertainment of air from the surrounding environment enforced by the shear layers of the swirling jet.

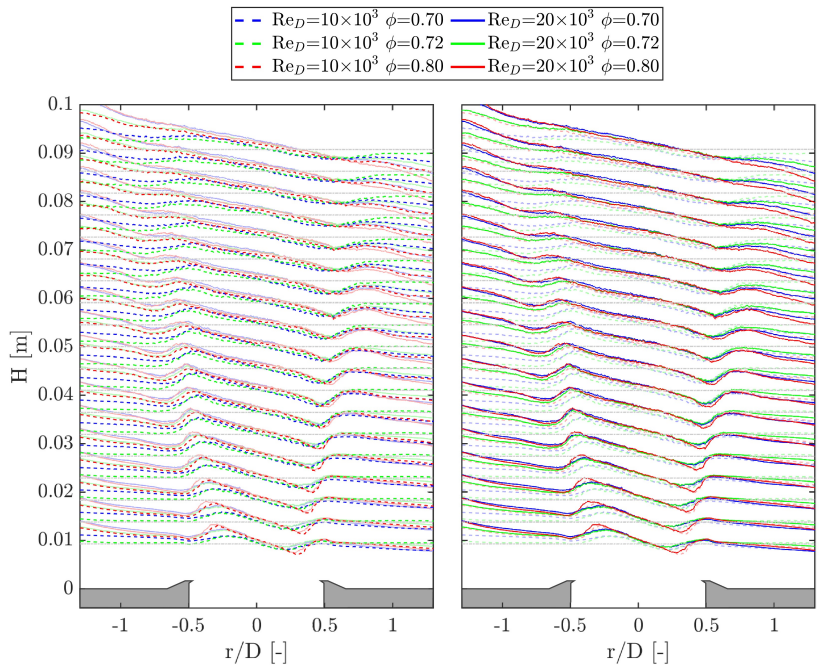

Figure 4.19: Time-averaged horizontal temperature gradients reconstructed via background oriented schlieren (BOS) for varying operating conditions.

For both Re_D, the displacement magnitude is relatively low at ϕ=0.7 due to lower heat release per unit mass of air flow. Nonetheless, for higher Re_D the amplitude of displacements increases at constant ϕ value as the thermal power increases with higher mass flow rates of fuel (Fig. 4.19). Low signal intensity was found in the center due to the central recirculation zone (CRZ) and in the corners due to an outer recirculation zone (ORZ). The visualized flame shape via BOS does not vary significantly for different Re_D values due to the nearly identical swirl numbers. Accordingly, the high amplitude of average displacement values (which can also be inferred as locations of high probability for the reaction zones) indicate that the flame stabilization is over the shear layers of the CRZ. However, the heat release (large displacement magnitude) zone can hardly be observed in the outer shear layer for the unconfined scenario investigated using BOS despite the low flow speed. This can be due to the rapid cooling of the reactant stream due to wall heat losses and heat losses to the entrained room temperature air as well as reduced residence time, influenced by the entrainment of surrounding air. Furthermore, the propagation of the reaction zones closer to the ORZ is mitigated due to the quenching of the flame in proximity of the burner flange which supports the generation of a V-shaped heat release zone. This observation is supported by the high-fidelity numerical investigations performed using the CeCOST burner configuration, where it was shown by that the V-shaped flame was captured only when heat loss to the combustor walls were considered to be non-negligible (Chong et al., 2009).

Chapter 5

Conclusions

The schlieren imaging technique is one of the oldest and most versatile non-intrusive measurement methods. However, it is associated with certain drawbacks due to the need for calibration, vulnerability to vibrations, the need for proper optical access, large lenses, and mirrors. This not only yields a higher expense in terms of the setup components, but also severely restricts the flexibility of the applications. In this regard, background oriented schlieren (BOS) provides a cost-effective alternative for quantitatively characterizing density-varying flows by means of an inexpensive and straightforward setup. Leveraging its ease of application, demonstrating BOS's superior adaptability and scalability across a wide range of applications offers a significant advantage to the field of experimental fluid dynamics. Therefore, this thesis is concentrated on the application and evaluation of BOS, along with associated image processing tools, for qualitative and quantitative characterization of density-varying flow features in various reactive and non-reactive flow scenarios.

Measurement technique developments

Traditionally, BOS is known to have degraded resolution and sensitivity characteristics, which outweighed its benefits when compared to parallel light schlieren systems. Accordingly, optical flow (OF) has demonstrated to provide a means to recover high-fidelity density field variations at the deflection detection stage of BOS without altering the level of complexity of the experimental setups. In order to gain full comprehension of OF's capabilities over the conventional cross-correlation (XCOR) approach, a comparative study was conducted including both synthetic and experimental measurements of supersonic flows over various models. The OF-based recon-

structions revealed superior characteristics of resolution and sensitivity in comparison to XCOR, allowing higher accuracy reconstructions of displacement vectors. The hierarchical schemes enabled OF to resolve the full spatial-frequency spectrum of the displacements contained within the image plane, where the bandwidth-limited nature of XCOR suffered not only from smoothing due to spatial averaging, but also from a limited dynamic range.

Despite the proven success of optical flow, the most popular background patterns employed in BOS setups were designed to suit the needs of the XCOR approach, whereas OF is associated with a substantially different mathematical background. Therefore, in order to characterize the resolution and sensitivity response of OF-based BOS to the background generation configurations, a parametric study was performed composed of theoretical, numerical and experimental assessments. Based on the results obtained for the compressible flow fields, the optimal choice for maximizing local resolution was established as a high density of small speckles. However, turbulent flow fields posed a more challenging case in terms of flow structures with scales ranging well beyond the spatial and temporal resolution limits of the optical setup. Hence, in contrast to the compressible flow scenarios, the highest accuracy of reconstructions was obtained with larger speckles while still maximizing concentration. The effect of randomness ratio is also observed to be more critical in the case of turbulent flow fields, where the resolution capabilities were maximized with the highest level of pattern randomness.

Experimental applications

Having discovered the application considerations of BOS, and performance specifications of OF, the focus was shifted toward exploring the capabilities in challenging flow visualization applications. In this regard, thermodynamics of a swirling heated subsonic jet of air was investigated, where the instantaneous temperature gradients were used to visualize the jet and to reconstruct the time averaged temperature field across the jet. Compressible flow features in a transonic low pressure turbine were captured to characterize the impact of operating conditions on passage shocks and trailing edge flow structures. The unique capability of BOS to perform optical measurements using a single optical access enabled the reconstruction of steady-state density gradients within the cascade flow, characterizing the airfoil wake formation, boundary layers, and shock waves, as well as time-resolved analysis on the shock wave boundary interactions. Moreover, the modular configuration of a BOS setup was also used to visualize the flow topology of dual-stream co-axial supersonic jets. Aimed at reducing the acoustic signature of supersonic aviation platforms, the experimental campaign discovered the underlying physics of noise generation mechanism in the case of inter-

actions between the shock-cells and shear layers when a supersonic annular co-flow is added to a supersonic jet. Furthermore, BOS is used to provide non-intrusive reconstruction of density varying flow features around objects at supersonic speeds and in a region of incidence shock wave boundary layer interactions at higher Reynolds numbers. While the flow visualization results are employed to extract quantitative properties through advanced image post-processing techniques, density fields are computed to provide information on the flow evolution within the wind tunnel test section and around the models. Additionally, the results obtained in scales relevant to applications and boundary conditions are used as a reference, and compared against numerical simulations of varying fidelity.

Expanding the application envelope to reactive flows, BOS is demonstrated as an alternative approach for flame visualization in Bunsen burners and for laminar burning velocity measurements of methane/air mixtures. Thus, BOS extends the capabilities of schlieren imaging and its ability to visualize flame structures of low luminescence, e.g. burning hydrogen or diluted mixtures under flameless conditions, making it applicable for studies of combustion concepts aimed at reducing CO_2 emissions. Furthermore, BOS is utilized for characterizing temperature and heat release in a model gas turbine combustor. Turbulent flow-flame interactions in the CeCOST burner were visualized across various operating conditions for swirl-stabilized turbulent flames of premixed methane/air. The effect of changing Reynolds number and equivalence ratio on the flame stabilization and orientation are highlighted, comparing the intensity of temperature gradients captured via BOS. These findings contribute to advancements in energy transition efforts for power generation and air transport, as the insights gained from BOS on lean premixed combustion play a key role in reducing pollutant emissions and enhancing combustion efficiency.

Knowledge transfer

The new discoveries made in thesis must be shared, preserved, and applied across disciplines and generations to sustain innovation and address complex global challenges. Without this continuous exchange, the engineering community would be trapped in a cycle of rediscovery, unable to surpass the current state of knowledge. Inspired by da Vinci's words *"Study the science of art. Study the art of science... Realize that everything connects to everything else."*, a course on flow visualization is developed to equip the next generation of researchers and engineers with the skills to truly "see" what they observe. The knowledge generated in this thesis has been integrated into the course, alongside established techniques, with the guiding principle of *"making the invisible visible."* Though complex, the students of the von Karman Institute's Research Master program were trained both theoretically and practically to master various flow

visualization methods, combined with advanced data processing approaches. Having completed the third edition of the Lab, the success of the course is demonstrated by the exponential increase in the number of students enrolled and the subsequent successes achieved by each of these students in their projects, demonstrating their excellence in experimental research.

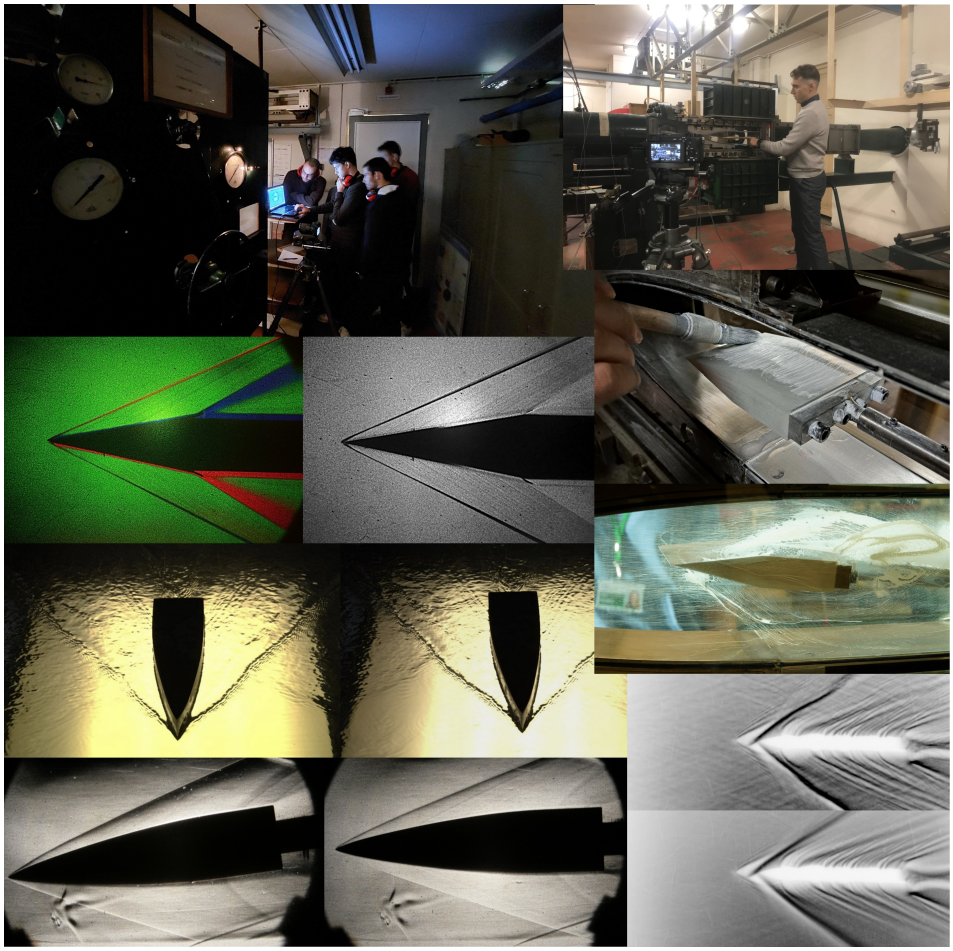

Figure 5.1: Photos and flow visualizations from the first two editions of the flow visualization course at von Karman Institute's Research Master program.

References

Abbiss, J., Chubb, T. and Pike, E. (1974), 'Laser doppler anemometry', *Optics & Laser Technology* **6**(6), 249–261.

Adrian, R. and Westerweel, J. (2011), *Particle Image Velocimetry*, Cambridge Aerospace Series, Cambridge University Press.

Alhaj, O. and Seume, J. R. (2010), Optical investigation of profile losses in a linear turbine cascade, Vol. 7: Turbomachinery, Parts A, B, and C of *Turbo Expo: Power for Land, Sea, and Air*, pp. 1503–1513.

Allen, J. M. (1972), 'Impact probe displacement in a supersonic turbulent boundary layer', *AIAA Journal* **10**(4), 555–557.

Anandan, P. (1989), 'A computational framework and an algorithm for the measurement of visual motion', *International Journal of Computer Vision* **2**(3), 283–310.

Andersson, N., Eriksson, L.-E. and Davidson, L. (2005), 'Large-eddy simulation of subsonic turbulent jets and their radiated sound', *AIAA Journal* **43**(9), 1899–1912.

André, B., Castelain, T. and Bailly, C. (2013), 'Broadband shock-associated noise in screeching and non-screeching underexpanded supersonic jets', *AIAA Journal* **51**(3), 665–673.

Atcheson, B., Heidrich, W. and Ihrke, I. (2009), 'An evaluation of optical flow algorithms for background oriented schlieren imaging', *Experiments in Fluids* **46**(3), 467–476.

Atcheson, B., Ihrke, I., Heidrich, W., Tevs, A., Bradley, D., Magnor, M. and Seidel, H.-P. (2008), 'Time-resolved 3d capture of non-stationary gas flows', *ACM Trans. Graph.* **27**(5).

Baek, S., Lee, S., Shin, M., Lee, J. and Lee, K. (2022), 'Analysis of combustion and exhaust characteristics according to changes in the propane content of LPG', *Energy* **239**, 122297.

Bangalore, P. V., Entremont, J., Meyer, S., Bane, S. and Grubelich, M. (2013), High-pressure combustion and deflagration-to-detonation transition in ethylene/nitrous oxide mixtures, *in* '8th U.S. National Combustion Meeting 2014, 9-22 May 2013, Park City, UT'.

Barron, J. L., Fleet, D. J. and Beauchemin, S. S. (1994), 'Performance of optical flow techniques', *International Journal of Computer Vision* **12**(1), 43–77.

Bauer, H.-J. (2004), 'New low emission strategies and combustor designs for civil aeroengine applications', *Progress in Computational Fluid Dynamics* **4**(3/4/5), 130 – 142.

Bauknecht, A., Ewers, B., Wolf, C., Leopold, F., Yin, J. and Raffel, M. (2014), 'Three-dimensional reconstruction of helicopter blade–tip vortices using a multi-camera BOS system', *Experiments in Fluids* **56**(1), 1866.

Bauwens, C., Bergthorson, J. and Dorofeev, S. (2017), 'Experimental investigation of spherical-flame acceleration in lean hydrogen-air mixtures', *International Journal of Hydrogen Energy* **42**(11), 7691–7697. Special issue on the 6th International Conference on Hydrogen Safety (ICHS 2015), 19-21 October 2015, Yokohama, Japan.

Becher, L., Voelker, C., Rodehorst, V. and Kuhne, M. (2020), 'Background-oriented schlieren technique for two-dimensional visualization of convective indoor air flows', *Optics and Lasers in Engineering* **134**, 106282.

Beermann, R., Quentin, L., Pösch, A., Reithmeier, E. and Kästner, M. (2017), 'Background oriented schlieren measurement of the refractive index field of air induced by a hot, cylindrical measurement object', *Appl. Opt.* **56**(14), 4168–4179.

Begley, R., Harvey, A. and Byer, R. L. (1974), 'Coherent anti-stokes raman spectroscopy', *Applied Physics Letters* **25**(7), 387–390.

Bichal, A. and Thurow, B. S. (2013), 'On the application of background oriented schlieren for wavefront sensing', *Measurement Science and Technology* **25**(1), 015001.

Billant, P., Chomaz, J.-M. and Huerre, P. (1998), 'Experimental study of vortex breakdown in swirling jets', *Journal of Fluid Mechanics* **376**, 183–219.

Born, M., Wolf, E., Bhatia, A. B., Clemmow, P. C., Gabor, D., Stokes, A. R., Taylor, A. M., Wayman, P. A. and Wilcock, W. L. (1999), *Basic properties of the electromagnetic field*, Cambridge University Press, p. 1–74.

Bosschaart, K. and de Goey, L. (2004), 'The laminar burning velocity of flames propagating in mixtures of hydrocarbons and air measured with the heat flux method', *Combustion and Flame* **136**(3), 261–269.

Boudreaux, P., Venkatakrishnan, S., Iffa, E. and Hun, D. (2022), 'Application of reference-free natural background–oriented schlieren photography for visualizing leakage sites in building walls', *Building and Environment* **223**, 109529.

Bourque, G., Healy, D., Curran, H., Zinner, C., Kalitan, D., de Vries, J., Aul, C. and Petersen, E. (2009), 'Ignition and flame speed kinetics of two natural gas blends with high levels of heavier hydrocarbons', *Journal of Engineering for Gas Turbines and Power* **132**(2), 021504.

Boychev, K., Barakos, G. N., Steijl, R. and Shaw, S. (2021), 'Parametric study of multiple shock-wave/turbulent-boundary-layer interactions with a Reynolds stress model', *Shock Waves* **31**(3), 255–270.

Brequigny, P., Endouard, C., Mounaïm-Rousselle, C. and Foucher, F. (2018), 'An experimental study on turbulent premixed expanding flames using simultaneously schlieren and tomography techniques', *Experimental Thermal and Fluid Science* **95**, 11–17.

Bruhn, A., Weickert, J. and Schnörr, C. (2005), 'Lucas/Kanade meets Horn/Schunck: combining local and global optic flow methods', *International Journal of Computer Vision* **61**(3), 211–231.

Burt, P. J. (1981), 'Fast filter transform for image processing', *Computer Graphics and Image Processing* **16**(1), 20–51.

Cai, S., Wang, Z., Fuest, F., Jeon, Y. J., Gray, C. and Karniadakis, G. E. (2021), 'Flow over an espresso cup: inferring 3-D velocity and pressure fields from tomographic background oriented schlieren via physics-informed neural networks', *Journal of Fluid Mechanics* **915**, A102.

Cakir, B. O., Grossir, G., Paris, S. and Saracoglu, B. H. (2022), On the design of a mach 5 axisymmetric contoured nozzle for the VKI H3 hypersonic tunnel, *in* 'HiSST: 2nd International Conference on High-Speed Vehicle Science & Technology, 11-16 September 2022, Bruges, Belgium'.

Cakir, B. O., Lavagnoli, S., Saracoglu, B. H. and Fureby, C. (2022), 'Assessment and application of optical flow in background-oriented schlieren for compressible flows', *Experiments in Fluids* **64**(1), 11.

Cakir, B. O., Lavagnoli, S., Saracoglu, B. H. and Fureby, C. (2024), 'Sensitivity and resolution response of optical flow-based background-oriented schlieren to speckle patterns', *Measurement Science and Technology* **35**(7), 075201.

Carlomagno, G., Cardone, G., Meola, C. and Astarita, T. (1998), 'Infrared thermography as a tool for thermal surface flow visualization', *Journal of Visualization* **1**, 37–50.

Cavalieri, A. V. G., Jordan, P. and Lesshafft, L. (2019), 'Wave-Packet Models for Jet Dynamics and Sound Radiation', *Applied Mechanics Reviews* **71**(2), 020802.

Chong, C. T. and Hochgreb, S. (2011), 'Measurements of laminar flame speeds of liquid fuels: Jet-a1, diesel, palm methyl esters and blends using particle imaging velocimetry (PIV)', *Proceedings of the Combustion Institute* **33**(1), 979–986.

Chong, L., Dutta, R. and Rahman, M. F. (2009), Design and thermal considerations of an interior permanent magnet machine with concentrated windings, *in* '2009 International Conference on Electrical Machines and Systems, 15-18 November 2009, Tokyo, Japan'.

Choudhury, S. P. and Joarder, R. (2022), 'High-speed photography and background oriented schlieren techniques for characterizing tulip flame', *Combustion and Flame* **245**, 112304.

Cole, J. (2004), 'F110 jet engine is tested inside the engine test cell operated by the 20th component maintenance squadron at shaw air force base, s.c.'. Accessed: 2024-08-27.

Cook, R. L. and DeRose, T. (2005), 'Wavelet noise', *ACM Trans. Graph.* **24**(3), 803–811.

Correa, S. M. (1998), 'Power generation and aeropropulsion gas turbines: From combustion science to combustion technology', *Symposium (International) on Combustion* **27**(2), 1793–1807.

Cozzi, F. and Göttlich, E. (2019), 'Enhanced background oriented schlieren (ebos)', *Journal of Physics: Conference Series* **1249**(1), 012017.

Cozzi, F., Göttlich, E., Angelucci, L., Dossena, V. and Guardone, A. (2017), 'Development of a background-oriented schlieren technique with telecentric lenses for supersonic flow', *Journal of Physics: Conference Series* **778**(1), 012006.

Cutler, A. D. and Johnson, C. H. (1997), 'Analysis of intermittency and probe data in a supersonic flow with injection', *Experiments in Fluids* **23**(1), 38–47.

Dabiri, D. (2009), 'Digital particle image thermometry/velocimetry: a review', *Experiments in Fluids* **46**(2), 191–241.

Daub, D., Willems, S. and Gülhan, A. (2022), 'Experiments on aerothermoelastic fluid–structure interaction in hypersonic flow', *Journal of Sound and Vibration* **531**, 116714.

Davies, E. (2012), Chapter 19 - motion, *in* 'Computer and Machine Vision (Fourth Edition)', fourth edn, Academic Press, Boston, pp. 505–522.

Davis, S. and Law, C. (1998), 'Laminar flame speeds and oxidation kinetics of iso-octane-air and n-heptane-air flames', *Symposium (International) on Combustion* **27**(1), 521–527.

Dec, J. E. and Espey, C. (1998), 'Chemiluminescence imaging of autoignition in a di diesel engine', *SAE transactions* pp. 2230–2254.

Dejarnett, R. (2009), 'An air force F-22 raptor executes a supersonic flyby over the flight deck of the aircraft carrier uss john c. stennis (CVN 74)'. Accessed: 2024-08-27.

Delery, J. M. (1985), 'Shock wave/turbulent boundary layer interaction and its control', *Progress in Aerospace Sciences* **22**(4), 209–280.

Deriche, R., Kornprobst, P. and Aubert, G. (1996), Optical-flow estimation while preserving its discontinuities: A variational approach, *in* 'Recent Developments in Computer Vision', Springer Berlin Heidelberg, Berlin, Heidelberg, pp. 69–80.

Dirrenberger, P., Glaude, P., Bounaceur, R., Le Gall, H., da Cruz, A. P., Konnov, A. and Battin-Leclerc, F. (2014), 'Laminar burning velocity of gasolines with addition of ethanol', *Fuel* **115**, 162–169.

Edgington-Mitchell, D., Wang, T., Nogueira, P., Schmidt, O., Jaunet, V., Duke, D., Jordan, P. and Towne, A. (2021), 'Waves in screeching jets', *Journal of Fluid Mechanics* **913**, A7.

Edward H., A. and James R., B. (1985), 'Spatiotemporal energy models for the perception of motion.', *Journal of the Optical Society of America. A, Optics and image science* **2 2**, 284–99.

Elsinga, G. E., van Oudheusden, B. W., Scarano, F. and Watt, D. W. (2004), 'Assessment and application of quantitative schlieren methods: Calibrated color schlieren and background oriented schlieren', *Experiments in Fluids* **36**(2), 309–325.

Farquharson, L. (2017), 'Coherent anti-stokes raman spectroscopy used to measure temperature in an H2/O2 flame'. Accessed: 2024-08-27.

Feuk, H., Pignatelli, F., Subash, A., Bi, R., Szász, R.-Z., Bai, X.-S., Lörstad, D. and Richter, M. (2022), 'Impact of methane and hydrogen-enriched methane pilot injection on the surface temperature of a scaled-down burner nozzle measured using phosphor thermometry', *International Journal of Turbomachinery, Propulsion and Power* 7(4).

Fisher, T. B., Quinn, M. K. and Smith, K. L. (2019), 'An experimental sensitivity comparison of the schlieren and background-oriented schlieren techniques applied to hypersonic flow', *Measurement Science and Technology* **30**(6), 065202.

Gaitonde, D. V. (2015), 'Progress in shock wave/boundary layer interactions', *Progress in Aerospace Sciences* **72**, 80–99.

Gallagher, Gerald L, H. L. B. K. L. A. P. P. W. (1992), 'Fixed wing performance', *Contract* **421**(90-C), 0022.

Galvin, B., McCane, B., Novins, K., Mason, D. and Mills, S. (1998), Recovering motion fields: An evaluation of eight optical flow algorithms, *in* 'Proceedings of the British Machine Vision Conference', BMVA Press, pp. 20.1–20.10.

Gardner, A. D., Raffel, M., Schwarz, C., Braukmann, J. N. and Wolf, C. C. (2020), 'Reference-free digital shadowgraphy using a moving BOS background', *Experiments in Fluids* **61**(2), 44.

Ghate, A. S., Stich, G.-D., Kenway, G. K., Housman, J. A. and Kiris, C. C. (2022), A wall-modeled les perspective for the high lift common research model using lava, *in* 'AIAA AVIATION 2022 Forum, 27 June - 1 July 2022 Chicago, IL'.

Gier, J. and Hübner, N. (2005), Design and analysis of a high stage loading five-stage lp turbine rig employing improved transition modeling, Vol. Volume 6: Turbo Expo 2005, Parts A and B of *Turbo Expo: Power for Land, Sea, and Air*, pp. 759–769.

Gladstone, J. H. and Dale, T. P. (1863), 'Xiv. researches on the refraction, dispersion, and sensitiveness of liquids', *Philosophical Transactions of the Royal Society of London* **153**, 317–343.

Gojani, A. B., Kamishi, B. and Obayashi, S. (2013), 'Measurement sensitivity and resolution for background oriented schlieren during image recording', *Journal of Visualization* **16**(3), 201–207.

Goldstein, R. and Cho, H. (1995), 'A review of mass transfer measurements using naphthalene sublimation', *Experimental Thermal and Fluid Science* **10**(4), 416–434.

Gong, H., Xu, J., Yu, K., Liu, S. and Liu, X. (2018), Preliminary measurements of transonic gasturbine linear cascade using background oriented schlieren technique, *in* 'Proceedings of 18th International Symposium on Flow Visualization (ISFV18), 26-29 June 2018, Zurich, Switzerland'.

Gorman, J. (2015), 'The hidden complexities of the simple match'. Accessed: 2024-08-13.

Gostelow, J., Mahallati, A., Andrews, S. and Carscallen, W. (2009), Measurement and computation of flowfield in transonic turbine nozzle blading with blunt trailing edges, Vol. 7: Turbomachinery, Parts A and B of *Turbo Expo: Power for Land, Sea, and Air*, pp. 979–991.

Graham, C. and Kost, F. (1979), Shock boundary layer interaction on high turning transonic turbine cascades, Vol. Volume 1A: Gas Turbines of *Turbo Expo: Power for Land, Sea, and Air*, p. V01AT01A037.

Grauer, S. J., Unterberger, A., Rittler, A., Daun, K. J., Kempf, A. M. and Mohri, K. (2018), 'Instantaneous 3D flame imaging by background-oriented schlieren tomography', *Combustion and Flame* **196**, 284–299.

Gu, X., Haq, M., Lawes, M. and Woolley, R. (2000), 'Laminar burning velocity and markstein lengths of methane–air mixtures', *Combustion and Flame* **121**(1), 41–58.

Guariglia, D., Rubio Carpio, A. and Schram, C. (2018), 'Design of a facility for studying shock-cell noise on single and coaxial jets', *Aerospace* **5**(1).

Gutmark, E., Parr, T. P., Hanson-Parr, D. M. and Schadow, K. C. (1991), 'Simultaneous oh and schlieren visualization of premixed flames at the lean blow-out limit', *Experiments in Fluids* **12**(1), 10–16.

Gyenge, A., Cakir, B. O., Grossir, G., Saracoglu, B. H. and Chazot, O. (2024), Flow characterization of the mach 5 hypersonic nozzle of vki-h3 wind tunnel, *in* 'AIAA SCITECH 2024 Forum, 8-12 January 2024, Orlando, FL'.

Hargather, M. J. (2013), 'Background-oriented schlieren diagnostics for large-scale explosive testing', *Shock Waves* **23**(5), 529–536.

Hargather, M. J., Lawson, M. J., Settles, G. S. and Weinstein, L. M. (2011), 'Seedless velocimetry measurements by schlieren image velocimetry', *AIAA Journal* **49**(3), 611–620.

Hargather, M. J. and Settles, G. S. (2010), 'Natural-background-oriented schlieren imaging', *Experiments in Fluids* **48**(1), 59–68.

Hargather, M. J. and Settles, G. S. (2012), 'A comparison of three quantitative schlieren techniques', *Optics and Lasers in Engineering* **50**(1), 8–17.

Harrison, P. M. (2008), 'Raptor heat haze'. Accessed: 2024-08-13.

Hayasaka, K., Tagawa, Y., Liu, T. and Kameda, M. (2016), 'Optical-flow-based background-oriented schlieren technique for measuring a laser-induced underwater shock wave', *Experiments in Fluids* **57**(12), 179.

Heineck, J. T., Banks, D. W., Smith, N. T., Schairer, E. T., Bean, P. S. and Robillos, T. (2021), 'Background-oriented schlieren imaging of supersonic aircraft in flight', *AIAA Journal* **59**(1), 11–21.

Hodzic, E., Yu, S., Subash, A. A., Liu, X., Liu, X., Szasz, R.-Z., Bai, X.-S., Li, Z. and Alden, M. (2018), Numerical and experimental investigation of the cecost swirl burner, Vol. Volume 4A: Combustion, Fuels, and Emissions of *Turbo Expo: Power for Land, Sea, and Air*, p. V04AT04A056.

Horn, B. K. and Schunck, B. G. (1981), 'Determining optical flow', *Artificial Intelligence* **17**(1), 185–203.

Hornung, H. (1986), 'Regular and mach reflection of shock waves', *Annual Review of Fluid Mechanics* **18**(Volume 18, 1986), 33–58.

Howard, N. S., Alrefaie, A., Mejia, N. A., Ugbeye, T. and Schmidt, B. E. (2023), 'Characterizing Aerosol Generating Procedures With Background Oriented Schlieren', *Journal of Biomechanical Engineering* **145**(7), 074502.

Hu, S., Gao, J., Gong, C., Zhou, Y., Bai, X., Li, Z. and Alden, M. (2018), 'Assessment of uncertainties of laminar flame speed of premixed flames as determined using a bunsen burner at varying pressures', *Applied Energy* **227**, 149–158.

Huang, Y., Sung, C. and Eng, J. (2004), 'Laminar flame speeds of primary reference fuels and reformer gas mixtures', *Combustion and Flame* **139**(3), 239–251.

Joo, P. H., Gao, J., Li, Z. and Aldén, M. (2015), 'Experimental apparatus with full optical access for combustion experiments with laminar flames from a single circular nozzle at elevated pressures', *Review of Scientific Instruments* **86**(3), 035115.

Jordan, P. and Colonius, T. (2013), 'Wave packets and turbulent jet noise', *Annual Review of Fluid Mechanics* **45**, 173–195.

Kähler, C. J., Scharnowski, S. and Cierpka, C. (2012), 'On the resolution limit of digital particle image velocimetry', *Experiments in Fluids* **52**(6), 1629–1639.

Keane, R. D. and Adrian, R. J. (1992), 'Theory of cross-correlation analysis of piv images', *Applied Scientific Research* **49**(3), 191–215.

Kearney, J. K., Thompson, W. B. and Boley, D. L. (1987), 'Optical flow estimation: An error analysis of gradient-based methods with local optimization', *IEEE Transactions on Pattern Analysis and Machine Intelligence* **PAMI-9**(2), 229–244.

Keller, J. O., Vaneveld, L., Korschelt, D., Hubbard, G. L., Ghoniem, A. F., Daily, J. W. and Oppenheim, A. K. (1982), 'Mechanism of instabilities in turbulent combustion leading to flashback', *AIAA Journal* **20**(2), 254–262.

Kim, W.-W. and Menon, S. (1995), 'A new dynamic one-equation subgrid-scale model for large eddy simulations', *33rd Aerospace Sciences Meeting and Exhibit, 9-12 January 1995, Reno, NV* .

Kirmse, T., Agocs, J., Schröder, A., Martinez Schramm, J., Karl, S. and Hannemann, K. (2011), 'Application of particle image velocimetry and the background-oriented schlieren technique in the high-enthalpy shock tunnel göttingen', *Shock Waves* **21**(3), 233–241.

Klemkowsky, J. N., Fahringer, T. W., Clifford, C. J., Bathel, B. F. and Thurow, B. S. (2017), 'Plenoptic background oriented schlieren imaging', *Measurement Science and Technology* **28**(9), 095404.

Knight, D. and Mortazavi, M. (2018), 'Hypersonic shock wave transitional boundary layer interactions - a review', *Acta Astronautica* **151**, 296–317.

Konnov, A. A., Mohammad, A., Kishore, V. R., Kim, N. I., Prathap, C. and Kumar, S. (2018), 'A comprehensive review of measurements and data analysis of laminar burning velocities for various fuel+air mixtures', *Progress in Energy and Combustion Science* **68**, 197–267.

Koponen, E., Leskinen, J., Tarvainen, T. and Pulkkinen, A. (2023), 'Background-oriented schlieren sensitivity in terms of geometrical parameters of measurement setup', *The Journal of the Acoustical Society of America* **154**(6), 3726–3736.

Kumar, K., Freeh, J. E., Sung, C. J. and Huang, Y. (2007), 'Laminar flame speeds of preheated iso-octane/o2/n2 and n-heptane/o2/n2 mixtures', *Journal of Propulsion and Power* **23**(2), 428–436.

Kumar, R., Ali, M. Y., Alvi, F. S. and Venkatakrishnan, L. (2011), 'Generation and control of oblique shocks using microjets', *AIAA Journal* **49**(12), 2751–2759.

Lapushkina, T. and Erofeev, A. (2017), 'Supersonic flow control via plasma, electric and magnetic impacts', *Aerospace Science and Technology* **69**, 313–320.

Larbalestier, L. (2022), 'Bizarre floating tanker ship is rare 'superior mirage''. Accessed: 2024-08-27.

Laurence, S. J., Wagner, A. and Hannemann, K. (2016), 'Experimental study of second-mode instability growth and breakdown in a hypersonic boundary layer using high-speed schlieren visualization', *Journal of Fluid Mechanics* **797**, 471–503.

LaVision (2020), 'Covid-19: LaVision imaging technique shows how masks restrict the spread of exhaled air'. Accessed: 2024-08-27.

Lefebvre, A. H. and Ballal, D. R. (2009), *Gas turbine combustion*, 3 edn, CRC Press, Boca Raton, FL.

Li, H., Ma, Z. and Zhu, H. (2023), 'Background oriented schlieren image displacement estimation method based on global optical flow', *Flow Measurement and Instrumentation* **93**, 102420.

Lilley, D. G. (1977), 'Swirl flows in combustion: A review', *AIAA Journal* **15**(8), 1063–1078.

Liu, T., Sullivan, J. P., Asai, K., Klein, C., Egami, Y. et al. (2005), *Pressure and temperature sensitive paints*, Vol. 1, Springer.

Liu, X., Bertsch, M., Subash, A. A., Yu, S., Szasz, R.-Z., Li, Z., Petersson, P., Bai, X.-S., Aldén, M. and Lörstad, D. (2021), 'Investigation of turbulent premixed methane/air and hydrogen-enriched methane/air flames in a laboratory-scale gas turbine model combustor', *International Journal of Hydrogen Energy* **46**(24), 13377–13388.

Liu, Y., Xing, F., Su, L., Tan, H. and Wang, D. (2024), 'A mini-review of recent developments in plenoptic background-oriented schlieren technology for flow dynamics measurement', *Aerospace* **11**(4).

Loeb, G. E., White, M. W. and Merzenich, M. M. (1983), 'Spatial cross-correlation', *Biological Cybernetics* **47**(3), 149–163.

Lopes, G., Simonassi, L., Torre, A., Patinios, M. and Lavagnoli, S. (2022), An experimental test case for transonic low-pressure turbines-part 2: Cascade aerodynamics at on-and off-design reynolds and mach numbers, *in* 'Turbo Expo: Power for Land, Sea, and Air', Vol. 86106, American Society of Mechanical Engineers, p. V10BT30A027.

Lowry, W., de Vries, J., Krejci, M., Petersen, E., Serinyel, Z., Metcalfe, W., Curran, H. and Bourque, G. (2011), 'Laminar Flame Speed Measurements and Modeling of Pure Alkanes and Alkane Blends at Elevated Pressures', *Journal of Engineering for Gas Turbines and Power* **133**(9), 091501.

Lu, F. K. (2010), 'Surface oil flow visualization', *The European Physical Journal Special Topics* **182**(1), 51–63.

Lucas, B. D. and Kanade, T. (1981), An iterative image registration technique with an application to stereo vision, *in* 'Proceedings of the 7th International Joint Conference on Artificial Intelligence - Volume 2', IJCAI'81, Morgan Kaufmann Publishers Inc., San Francisco, CA, USA, p. 674–679.

Magre, P., Collin, G., Pin, O., Badie, J., Olalde, G. and Clément, M. (2001), 'Temperature measurements by CARS and intrusive probe in an air–hydrogen supersonic combustion', *International Journal of Heat and Mass Transfer* **44**(21), 4095–4105.

Maia, I. A., Jordan, P., Cavalieri, A. V. G. and Jaunet, V. (2019), 'Two-point wavepacket modelling of jet noise', *Proceedings of the Royal Society A: Mathematical, Physical and Engineering Sciences* **475**(2227), 20190199.

Martin, P. (2011), 'Fluorescent oil surface visualization on a 5.8 percent scale model of a futuristic hybrid wing body during tests in the 14 by-22-foot subsonic wind tunnel of NASA langley.'. Accessed: 2024-08-27.

Martinstetter, M., Niehuis, R. and Franke, M. (2010), Passive boundary layer control on a highly loaded low pressure turbine cascade, Vol. Volume 7: Turbomachinery, Parts A, B, and C of *Turbo Expo: Power for Land, Sea, and Air*, pp. 1315–1326.

Meier, A. H. and Roesgen, T. (2013), 'Improved background oriented schlieren imaging using laser speckle illumination', *Experiments in Fluids* **54**(6), 1549.

Meier, G. (2002), 'Computerized background-oriented schlieren', *Experiments in Fluids* **33**(1), 181–187.

Menter, F. R. (1994), 'Two-equation eddy-viscosity turbulence models for engineering applications', *AIAA Journal* **32**(8), 1598–1605.

Miles, R. B., Lempert, W. R. and Forkey, J. N. (2001), 'Laser rayleigh scattering', *Measurement Science and Technology* **12**(5), R33.

Molnar, J. P., Venkatakrishnan, L., Schmidt, B. E., Sipkens, T. A. and Grauer, S. J. (2023), 'Estimating density, velocity, and pressure fields in supersonic flows using physics-informed BOS', *Experiments in Fluids* **64**(1), 14.

Nagel, H. H. (1983), Constraints for the estimation of displacement vector fields from image sequences, *in* 'Proceedings of the Eighth International Joint Conference on Artificial Intelligence - Volume 2', IJCAI'83, p. 945–951.

NASA (1992), '2D-laser doppler velocimeter at a flow channel'. Accessed: 2024-08-13.

NASA (2000), 'RS-68 rocket engine at NASA's stennis space center.'. Accessed: 2024-08-27.

Nicolas, F., Donjat, D., Léon, O., Le Besnerais, G., Champagnat, F. and Micheli, F. (2017), '3D reconstruction of a compressible flow by synchronized multi-camera bos', *Experiments in Fluids* **58**(5), 46.

Nicolas, F., Micheli, F., Donjat, D., Plyer, A., Champagnat, F. and Le Besnerais, G. (2016), 3D reconstruction of compressible flow by synchronized multi camera BOS, *in* '18th International Symposium on applications of laser techniques to fluid mechanics, 4-7 July 2016, Lisbon, Portugal', Lisbon, Portugal.

Ninnemann, T. A. and Ng, W. F. (1992), 'A concentration probe for the study of mixing in supersonic shear flows', *Experiments in Fluids* **13**(2), 98–104.

Norman, M., Winkler, K.-H., Smarr, L. and Smith, M. (1982), 'Structure and dynamics of supersonic jets', *Astronomy and Astrophysics, vol. 113, no. 2, Sept. 1982, p. 285-302.* **113**, 285–302.

Ollegott, K., Wirth, P., Oberste-Beulmann, C., Sakthi, G. S. M., Magazova, A., Hermanns, P., Peters, N., Schücke, L., Bracht, V., Agar, D. W., Awakowicz, P. and Muhler, M. (2023), 'Investigation of flow characteristics in a twin-surface dielectric barrier discharge reactor by schlieren imaging', *Journal of Physics D: Applied Physics* **56**(26), 265201.

Ota, M., Kurihara, K., Arimoto, H., Shida, K. and Inage, T. (2017), Background Oriented Schlieren (BOS) measurement in supersonic flow with 4K high-speed camera, *in* T. G. Etoh and H. Shiraga, eds, 'Selected Papers from the 31st International Congress on High-Speed Imaging and Photonics', Vol. 10328, International Society for Optics and Photonics, SPIE, p. 103281E.

Ota, M., LEOPOLD, F., AGUSINSKI, F. and Maeno, K. (2012), 'A comparison of measurement results for supersonic flow field by colored-grid background oriented schlieren (CGBOS) and colored background oriented schlieren (CBOS) technique', *The Proceedings of the Fluids engineering conference* **2012**, 199–200.

Ota, M., Leopold, F., Noda, R. and Maeno, K. (2015), 'Improvement in spatial resolution of background-oriented schlieren technique by introducing a telecentric optical system and its application to supersonic flow', *Experiments in Fluids* **56**(3), 48.

Park, O., Veloo, P. S., Liu, N. and Egolfopoulos, F. N. (2011), 'Combustion characteristics of alternative gaseous fuels', *Proceedings of the Combustion Institute* **33**(1), 887–894.

Paul, P. H. and Najm, H. N. (1998), Planar laser-induced fluorescence imaging of flame heat release rate, *in* 'Symposium (international) on combustion', Vol. 27, Elsevier, pp. 43–50.

Pignatelli, F., Kim, H., Subash, A., Liu, X., Szasz, R., Bai, X., Brackmann, C., Aldén, M. and Lörstad, D. (2022), 'Pilot impact on turbulent premixed methane/air and hydrogen-enriched methane/air flames in a laboratory-scale gas turbine model combustor', *International Journal of Hydrogen Energy* **47**(60), 25404–25417.

Pignatelli, F., Sanned, D., Derafshzan, S., Szasz, R., Bai, X., Richter, M., Ehn, A., Lörstad, D., Petersson, P. and Subash, A. (2024), 'Impact of pilot flame and hydrogen enrichment on turbulent methane/hydrogen/air swirling premixed flames in a model gas turbine combustor', *Experimental Thermal and Fluid Science* **152**, 111124.

Puttinger, S. (2009), 'Free jet illuminated by laser'. Accessed: 2024-08-27.

Raffel, M. (2014), 'Background-oriented schlieren imaging for full-scale and in-flight testing', *Journal of the American Helicopter Society* **59**(1), 1–9.

Raffel, M. (2015), 'Background-oriented schlieren (bos) techniques', *Experiments in Fluids* **56**(3), 60.

Raffel, M., Heineck, J., Schairer, E., Leopold, F. and Kindler, K. (2012), Background oriented schlieren techniques for helicopter related large scale and flight testing, pp. 1–9.

Rajshekhar, G. and Ambrosini, D. (2018), 'Multi-scale approach for analyzing convective heat transfer flow in background-oriented schlieren technique', *Optics and Lasers in Engineering* **110**, 415–419.

Ramaiah, J., de Rubeis, T., Gannavarpu, R. and Ambrosini, D. (2023), 'Quantitative flow visualization by hidden grid background oriented schlieren', *Optics and Lasers in Engineering* **160**, 107307.

Raman, G. (1998), 'Advances in understanding supersonic jet screech: Review and perspective', *Progress in Aerospace Sciences* **34**(1), 45–106.

Raman, G. (1999), 'Supersonic jet screech: Half-century from powell to the present', *Journal of Sound and Vibration* **225**(3), 543–571.

Ramanah, D., Raghunath, S., Mee, D. J., Rösgen, T. and Jacobs, P. A. (2007), 'Background oriented schlieren for flow visualisation in hypersonic impulse facilities', *Shock Waves* **17**(1), 65–70.

Reichenzer, F., Schneider, M. and Herkommer, A. (2021), 'Improvement in systematic error in background-oriented schlieren results by using dynamic backgrounds', *Experiments in Fluids* **62**, 1–18.

Rockwell, N. A. (1968), 'A north american rockwell corporation artist's concept depicting the apollo command module (CM), oriented in a blunt-end-forward attitude, re-entering earth's atmosphere after returning from a lunar landing mission'. Accessed: 2024-09-04.

Rosafio, N., Lopes, G., Salvadori, S., Lavagnoli, S. and Misul, D. (2023), 'Rans prediction of losses and transition onset in a high-speed low-pressure turbine cascade', *Energies* **16**(21).

Rossiter, A., Pullan, G. and Melzer, A. (2022), 'The Influence of Boundary Layer State and Trailing Edge Wedge Angle on the Aerodynamic Performance of Transonic Turbine Blades', *Journal of Turbomachinery* **145**(4), 041008.

RSM, T. D. (2023), 'Microwave plasma heater'. Accessed: 2024-08-27.

Sasono, M., Sakti, S. P., Noor, J. E. and Soetedjo, H. (2023), 'Application of checkerboard-based background-oriented schlieren technique for invisible visualization of thermal plumes', *AIP Conference Proceedings* **2720**(1), 040035.

Sattelmayer, T., Felchlin, M. P., Haumann, J., Hellat, J. and Styner, D. (1992), 'Second-generation low-emission combustors for abb gas turbines: Burner development and tests at atmospheric pressure', *Journal of Engineering for Gas Turbines and Power* **114**(1), 118–125.

Scarano, F. and Riethmuller, M. L. (2000), 'Advances in iterative multigrid piv image processing', *Experiments in Fluids* **29**(1), S051–S060.

Schaeffer, S. (2020), 'Heat haze distorts video of semi-trucks driving down a Utah interstate surrounded by mountains on a sunny day'. Accessed: 2024-08-27.

Scharnowski, S. and Kähler, C. J. (2020), 'Particle image velocimetry - classical operating rules from today's perspective', *Optics and Lasers in Engineering* **135**, 106185.

Settles, G. S. (2001), *Basic Concepts*, Springer Berlin Heidelberg, Berlin, Heidelberg, pp. 25–38.

Shimazaki, T., Ichihara, S. and Tagawa, Y. (2022), 'Background oriented schlieren technique with fast Fourier demodulation for measuring large density-gradient fields of fluids', *Experimental Thermal and Fluid Science* **134**, 110598.

Simeonides, G. (1990), The VKI hypersonic wind tunnels and associated measurement techniques, Technical Memorandum VKI TM-46, von Karman Institute for Fluid Dynamics.

Simonassi, L., Lopes, G., Gendebien, S., Torre, A., Patinios, M., Lavagnoli, S., Zeller, N. and Pintat, L. (2022), An experimental test case for transonic low-pressure turbines–part 1: Rig design, instrumentation and experimental methodology, *in* 'Turbo Expo: Power for Land, Sea, and Air', Vol. 86106, American Society of Mechanical Engineers, p. V10BT30A012.

Simonich, J. C., Narayanan, S., Barber, T. J. and Nishimura, M. (2001), 'Aeroacoustic characterization, noise reduction, and dimensional scaling effects of high subsonic jets', *AIAA Journal* **39**(11), 2062–2069.

Sivasubramanian, J. and Fasel, H. F. (2016), Direct numerical simulation of laminar-turbulent transition in a flared cone boundary layer at mach 6, *in* '54th AIAA Aerospace Sciences Meeting, 4-8 January 2016, San Diego, CA'.

Sommersel, O. K., Bjerketvedt, D., Christensen, S. O., Krest, O. and Vaagsaether, K. (2008), 'Application of background oriented schlieren for quantitative measurements of shock waves from explosions', *Shock Waves* **18**(4), 291–297.

Sourgen, F., Haertig, J. and Rey, C. (2004), Comparison between background oriented schlieren measurements (BOS) and numerical simulations, *in* '24th AIAA Aerodynamic Measurement Technology and Ground Testing Conference, 28 June - 01 July 2004, Portland, OR'.

Sourgen, F., Leopold, F. and Klatt, D. (2012), 'Reconstruction of the density field using the colored background oriented schlieren technique (cbos)', *Optics and Lasers in Engineering* **50**(1), 29–38. Advances in Flow Visualization.

Sridhar, V., Kleine, H. and Gai, S. L. (2015), 'Visualization of wave propagation within a supersonic two-dimensional cavity by digital streak schlieren', *Experiments in Fluids* **56**(7), 152.

Stadler, H., Bauknecht, A., Siegrist, S., Flesch, R., Wolf, C. C., van Hinsberg, N. and Jacobs, M. (2017), 'Background-oriented schlieren imaging of flow around a circular cylinder at low mach numbers', *Experiments in Fluids* **58**(9), 114.

Stone, C. and Menon, S. (2001), Combustion instabilities in swirling flows, *in* '37th Joint Propulsion Conference and Exhibit, 08-11 July 2001, Salt Lake City, UT'.

Subash, A. A., Yu, S., Liu, X., Bertsch, M., Szasz, R.-Z., Li, Z., Bai, X.-S., Aldén, M. and Lörstad, D. (2020), 'Flame investigations of a laboratory-scale cecost swirl burner at atmospheric pressure conditions', *Fuel* **279**, 118421.

Sun, D., Roth, S., Lewis, J. P. and Black, M. J. (2008), Learning optical flow, *in* D. Forsyth, P. Torr and A. Zisserman, eds, 'Computer Vision – ECCV 2008', Springer Berlin Heidelberg, Berlin, Heidelberg, pp. 83–97.

Sun, L., Jia, C. and Miao, Y. (2023), 'Visualization of hydrogen leak for electro-hydrogen coupled system based on background oriented schlieren', *Process Safety and Environmental Protection* **175**, 437–446.

Tam, C. K. W. (1995), 'Supersonic jet noise', *Annual Review of Fluid Mechanics* **27**(1), 17–43.

Tanda, G. and Devia, F. (1998), 'Application of a schlieren technique to heat transfer measurements in free-convection', *Experiments in Fluids* **24**(4), 285–290.

Tanda, G., Fossa, M. and Misale, M. (2014), 'Heat transfer measurements in water using a schlieren technique', *International Journal of Heat and Mass Transfer* **71**, 451–458.

Tanimoto, S. and Pavlidis, T. (1975), 'A hierarchical data structure for picture processing', *Computer Graphics and Image Processing* **4**(2), 104–119.

Trolinger, J. D., Buckner, B. and L'Esperance, D. (2015), Background-oriented schlieren for the study of large flow fields, *in* E. Novak and J. D. Trolinger, eds, 'Applied Advanced Optical Metrology Solutions', Vol. 9576, International Society for Optics and Photonics, SPIE, p. 95760E.

Unterberger, A. and Mohri, K. (2022), 'Evolutionary background-oriented schlieren tomography with self-adaptive parameter heuristics', *Opt. Express* **30**(6), 8592–8614.

Van Dyke, M. (1982), *An Album of Fluid Motion*, number pt. 2 *in* 'An Album of Fluid Motion', Parabolic Press.

Vinnichenko, N. A., Pushtaev, A. V., Plaksina, Y. Y. and Uvarov, A. V. (2023), 'Performance of background oriented schlieren with different background patterns and image processing techniques', *Experimental Thermal and Fluid Science* **147**, 110934.

Vinnichenko, N. A., Uvarov, A. V. and Plaksina, Y. Y. (2014), 'Combined study of heat exchange near the liquid–gas interface by means of background oriented schlieren and infrared thermal imaging', *Experimental Thermal and Fluid Science* **59**, 238–245.

Viswanathan, K. (2004), 'Aeroacoustics of hot jets', *Journal of Fluid Mechanics* **516**, 39–82.

Wahls, B. H. and Ekkad, S. V. (2022), 'A new technique using background oriented schlieren for temperature reconstruction of an axisymmetric open reactive flow', *Measurement Science and Technology* **33**(5), 055202.

Wang, B., Sandham, N., Hu, Z. and Liu, W. (2015), 'Numerical study of oblique shock-wave/boundary-layer interaction considering sidewall effects', *Journal of Fluid Mechanics* **767**, 526–561.

Wang, C., Xu, P., Xue, L. and Jiao, Y. (2019), 'Three-dimensional reconstruction of incident shock/boundary layer interaction using background-oriented schlieren', *Acta Astronautica* **157**, 341–349.

Weber, R. and Dugué, J. (1992), 'Combustion accelerated swirling flows in high confinements', *Progress in Energy and Combustion Science* **18**(4), 349–367.

Weilenmann, M., Xiong, Y., Bothien, M. and Noiray, N. (2018), 'Background-oriented schlieren of fuel jet flapping under thermoacoustic oscillations in a sequential combustor', *Journal of Engineering for Gas Turbines and Power* **141**(1), 011030.

Weisberger, J. M. and Bathel, B. F. (2022), 'Projection background-oriented schlieren', *Appl. Opt.* **61**(20), 6006–6015.

Wernet, M. P. (2019), 'Real-time background oriented schlieren with self-illuminated speckle background', *Measurement Science and Technology* **31**(1), 017001.

Wernet, M. P., Georgiadis, N. J. and Locke, R. J. (2021), 'Raman temperature and density measurements in supersonic jets', *Experiments in Fluids* **62**(3), 61.

Westerweel, J. (1997), 'Fundamentals of digital particle image velocimetry', *Measurement Science and Technology* **8**(12), 1379–1392.

Wildeman, S. (2018), 'Real-time quantitative schlieren imaging by fast Fourier demodulation of a checkered backdrop', *Experiments in Fluids* **59**(6), 97.

Willert, C. E., Mitchell, D. M. and Soria, J. (2012), 'An assessment of high-power light-emitting diodes for high frame rate schlieren imaging', *Experiments in Fluids* **53**(2), 413–421.

Wong, M. H., Jordan, P., Maia, I. A. et al. (2021), 'Wavepacket modelling of broadband shock-associated noise in supersonic jets', *Journal of Fluid Mechanics* **918**, A9.

Xiong, Y., Kaufmann, T. and Noiray, N. (2020), 'Towards robust bos measurements for axisymmetric flows', *Experiments in Fluids* **61**(8), 178.

Yang, C., Yao, L., Xu, Z., Chen, X., Liu, J. and Kan, R. (2014), Random dots' parameters optimization study of background for background oriented schlieren (bos) environmental research application, *in* 'Light, Energy and the Environment', Optica Publishing Group, p. EW4A.6.

Zhu, M., Pérez Arroyo, C., Fosso Pouangué, A., Sanjosé, M. and Moreau, S. (2018), 'Isothermal and heated subsonic jet noise using large eddy simulations on unstructured grids', *Computers & Fluids* **171**, 166–192.

Zhu, W., Bons, J. and Gregory, J. (2022), 'Boundary layer and near wake measurements of a two-dimensional airfoil with background-oriented schlieren method', *Experiments in Fluids* **64**(1), 7.

Scientific publications

Author contributions

Paper i: Assessment and Application of Optical Flow in Background-Oriented Schlieren for Compressible Flows

B.O. Cakir conceptualized the study, composed the image processing software, curated the synthetic assessment, built the experimental setup, conducted the experiments with Marc Baise as the facility operator, processed the data, performed the analysis, generated the figures and wrote the manuscript.

Paper ii: Sensitivity and Resolution Response of Optical Flow Based Background Oriented Schlieren to Speckle Patterns

B.O. Cakir conceptualized the study, curated the synthetic assessment, built the experimental setup, conducted the experiments, processed the data, performed the analysis, generated the figures and wrote the manuscript.

Paper iii: Numerical and Experimental Investigations of Flow Features over a Wedge Exposed to Supersonic Flow at High Reynolds Numbers

B.O. Cakir conceptualized the study, performed the computational simulations, built the experimental setup, conducted the experiments with Marc Baise as the facility operator, processed the data, performed the analysis, generated the figures and wrote the manuscript.

Paper iv: Application and Assessment of Background Oriented Schlieren for Laminar Burning Velocity Measurements

B.O. Cakir conceptualized the study, developed the methodology, build the experimental setup with Christian Brackmann, conducted the experiments with David Sanned and Megha Prakash, processed the data, performed the analysis, generated the figures and wrote the manuscript.

Paper v: On the Application of Background Oriented Schlieren to a Transonic Low-Reynolds Turbine Cascade

B.O. Cakir contributed to the conceptualization of the study and the development of the methodology, contributed to the experimental setup configuration, conducted the experiments with the authors, processed the data and analyzed the results with Alexandre Halby, contributed to the generation of the figures and writing the manuscript.

Paper vi: Investigation on Noise and Flow Characteristics of Supersonic Dual-Stream Co-Axial Convergent-Divergent Jets

Alessandro Zarri and Julien de Decker designed and built the facility. **B.O. Cakir** contributed to the conceptualization of the study and the development of the methodology, built the optical measurement setup, conducted the measurements with Alessandro Zarri and Julien de Decker, processed the data, performed the analysis, contributed to the generation of the figures and writing the manuscript.

Printed by Media-Tryck, Lund 2024 NORDIC SWAN ECOLABEL 3041 0903

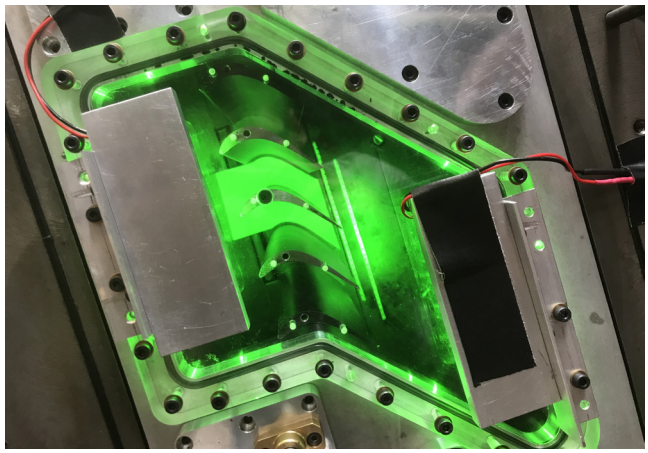

Sustainable Aviation

Achieving a sustainable future in aviation and ensuring the longevity of air mobility require highly adaptable and scalable measurement techniques to address complex flow physics across various phenomena. Background Oriented Schlieren (BOS), a diagnostic technique capable of analyzing flow physics from subsonic to supersonic, as well as non-reactive to reactive flows, is explored and documented. BOS is applied to study flow phenomena over wings, fuselages, inside engines, jet exhausts, and more, offering valuable insights for advancing aviation technologies.

LUND UNIVERSITY

Faculty of Engineering
Department of Energy Sciences

ISBN: 978-91-8104-171-2
ISSN: 0282-1990
ISRN: LUTMDN/TMHP-24/1177-SE